Assessment on the Precision of Total Marrow Irradiation: From Clinical to Preclinical Implementation

A DISSERTATION
SUBMITTED TO THE FACULTY OF THE GRADUATE SCHOOL OF THE
UNIVERSITY OF MINNESOTA
BY

Darren Zuro

IN PARTIAL FULFILMENT OF

THE REQUIREMENTS FOR THE DEGREE OF

DOCTOR OF PHILOSOPHY

Susanta K. Hui, PhD

* June 2021 (Month and year degree requirements were met)

Acknowledgements

I would like to thank my advisor, Susanta Hui, who countless hours of mentoring & guidance have shaped me into an effective scientist. As Dr. Hui would say, “Where is the science?”

I would like to thank Dr. Jerry Froelich for his continued financial support through funding from the Merle and Fern Loken Professorship in Radiologic Sciences and for his mentorship throughout my studies. I would like to thank my advisor Dr. Susanta Hui for financial support through NCI and NIH grants (R01CA154491, P30CA033572) and through ONCOTEST. I would also like to thank him for the extensive amount of time he committed to designing and supporting my studies. Without his funding and support this work would not have been possible.

I would like to thank current and past members of Hui lab, specifically Dr. Jamison Brooks & Dr. Madabushi Srideshikan for assisting me with analysis, experimentation and enduring my presence.

I would like to thank my mother (Karen Zuro), father (Peter Zuro), brother (Adam), and sister (Jenna) for allowing me to pursue my passions and pushing me forward in my life.

Finally, to my muse Johanna, you have been here supporting me as I complete this challenging chapter in my life. Our time together has given me the energy to finish this stage of my career and I look forward to our future together.

Dedication

This dissertation is dedicated to Adam, Jenna, my parents, and Johanna.

Abstract

Total Body irradiation (TBI) has been used for many years as the preconditioning regime before bone marrow transplant. Dose escalation of TBI produced decreased relapse rates in patients with leukemia; however, treatment-related deaths increased because of organ toxicity from TBI negating any potential therapeutic gain. In 2005 a new technique called Total Marrow radiation (TMI) was founded as an alternative to TBI. TMI is a highly conformal treatment of the human skeleton structure requiring a high degree of precision and accuracy for treatment delivery. However, there are several challenges to establish and advance TMI treatment; specifically, 1) the existence of differences in treatment setup between centers which may cause differences in dose delivery and treatment accuracy. 2) the lack of a preclinical model to better understand the biological differences between TMI and TBI. Lack of preclinical TMI model, limits us for in depth understanding of how TMI dose escalation and bone marrow microenvironment plays role in leukemia relapse and whether new therapeutics (e.g. TMI and immune modulation) could be developed to improve treatment outcomes.

In this thesis, I assessed the state of current clinical TMI pre-treatment setup and its effect on dose delivery. Patient setup techniques differed between centers, creating variations in dose delivery. Image fusion accuracy varied by anatomical regions and by imaging technique. This effort allowed us to standardize treatment setup which can be used as reference for all centers.

After creating a multi-center reference for TMI dose distribution, we developed and validated image guided preclinical TMI treatment technique in mice. Dose reduction in preclinical TMI mirrored that in clinical TMI.TMI treated mice showed full long-term donor engraftment after primary bone marrow transplant (BMT) and second serial BMT. Engraftment was similar to TBI. TBI-treated mice showed acute gut damage, which was minimized in mice treated with TMI.

MVCT imaging and whole-body patient immobilization was essential for assessing treatment setup, allowing for the complete analysis of 3D dose distribution in the PTV and lungs. The development of a new 3D targeted preclinical system paves the way for new exploratory studies in the field of bone marrow transplant and radiobiology.

Table of Contents

List of Tables

Figure References

List of Abbreviations

BMT – Bone Marrow Transplant

AML – Acute myeloid leukemia

HCT – Hematopoietic cell transplantation

TBI – Total Body Irradiation

TMI – Total Marrow Irradiation

IMRT – Intensity modulation radiation therapy

GVHD- Graft versus host disease

PTV – Planning Target volume

MVCT- Megavoltage computed tomography

ICTMI - International consortium for Total Marrow Irradiation

WBI – Whole Body Irradiation

PBI – Partial Body Irradiation

IP – Interstitial pneumonitis

RILF – Radiation induced lung fibrosis

DVH – Dose Volume Histogram

EUD - equivalent uniform dose

TCP – Tumor Control Probability

NTCP – Normal Tissue Control Probability

BED – Biological Equivalent dose

TLD - thermolumescent detectors

MLC – Multi-leaf collimator

PTV- Planning Target Volume

CTV – Clinical Target Volume

OAR – Organ at risk

CBCT – Cone Beam Computed Tomography

EUD – Equivalent Uniform Dose

Chapter 1. Introduction

1.1. Rational behind Total Body Irradiation

Bone marrow transplantation (BMT) is a curative treatment option for several malignant and non-malignant hematological diseases. However, without patient preconditioning, donor engraftment would fail. Engraftment failure is a byproduct of immunological response as demonstrated by Medawar et al. (1, 2). Therefore, an immune-suppressant treatment is needed to reduce the risk of donor engraftment rejection. This immune-suppressant treatment for patients with leukemia often takes the forms of Total Body Irradiation (TBI) or more recently Total Marrow Irradiation (TMI). The dose of radiation must be sufficiently large enough to both suppress the recipient's immune system and eliminate the remaining leukemia cells (3-5).

1.2. History of Total Body Irradiation & Bone Marrow Transplant development

TBI has been proven to be an effective radiation treatment for hematological malignancies such as: Hodgkin's and non-Hodgkin's lymphoma, multiple myeloma, chronic leukemia, and a variety of solid tumors (6) with its initial usage dating back to 1927. The use of lethal radiation to suppress immune systems has been the subject of intense research since the late 1940s. Preclinical models of radiation induced immune suppression led to the discovery that bone marrow transplantation which allows for donor bone

marrow engraftment and regeneration of immune system (7, 8). Further preclinical modeling was done where dogs survived lethal exposure of TBI with autologous bone marrow transplant (9). Barnes, et al. was able to apply this method to a leukemia mouse model where mice were rescued from exposure to lethal radiation because of a healthy donor bone marrow transplant (10). This work demonstrated that TBI suppresses the immune system to facilitate long term healthy donor bone marrow engraftment

Study of human bone marrow engraftment after lethal radiation began using hemopoietic tissue from cadavers, fetuses and living donors as far back as 1956 (11). A general lack of success in these earlier studies demonstrated the complexity of the human bone marrow transplant system and required further preclinical investigation. Only after successful experiments on marrow grafting following lethal radiation using outbred dogs (12-14) was there a resurgence of experiments. Successful marrow engraftment after TBI was then achieved using a host of other models such as rodents (15, 16), dogs (17), monkeys (18) and eventually in human patients (19). These studies eventually led to the standardization of marrow engraftment techniques using TBI (20) and clinical trial success (21). Originally published in 1975, the TBI treatment method earned Doctors Donnall Thomas and Joseph E. Murray the Nobel Prize in Medicine in 1990 and since then many studies have been done to determine the most effective treatment regimen for TBI (22-24).

1.3. Current state of TBI and rational behind Total Marrow Irradiation

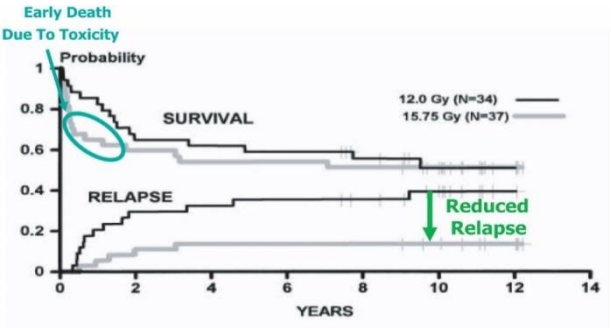

Figure 1-1: Kaplan-Meier estimates of survival and cumulative incidence of relapse for patients conditioned for HLA-identical marrow transplantation by 120 mg/kg cyclophosphamide and 12.0 Gy or 15.75 Gy of fractioned TBI. This figure is taken from the publication reported by Clift et al. in 1998

For over half a century, TBI has been a standard of care as a preconditioning regimen for host immune suppression and reduction of disease burden to allow donor engraftment (4, 5, 25, 26). However, TBI also results in severe toxicities due to large radiation exposure to vital organs. Pulmonary toxicities result in ~50% of transplantation-related deaths (27, 28), and acute graft-vs-host disease (GVHD) is a major post-transplantation complication (29). Additionally, for relapsed/refractory patients with acute myeloid leukemia (AML) who are undergoing hematopoietic cell transplantation (HCT), the TBI conditioning regime is often not sufficient for disease control. Dose escalation of TBI produces decreased relapse rates in patients with leukemia (30-32). However, treatment-related deaths increase because of organ toxicity from TBI (31-34). This outcome negates any potential advantage for survival with escalated doses of TBI as seen in **Figure 1-1**. Numerous techniques have been developed to reduce organ

toxicities associated with TBI (35-39). Low dose fractionation approaches were adopted but toxicities remained high (40). Shielding and compensators were also attempted to reduce organ toxicities but their effectiveness was limited due to the challenge of organ geometry and the precision required for daily patient positioning (41).

Research in total marrow irradiation (TMI) was driven by two primary motivations: 1) 3D assessment of dose inhomogeneities of TBI and 2) a desire to escalate dose to the marrow while minimizing dose to sensitive tissues. In 2004 Hui et al. demonstrated using 3D CT that thermolumescent detectors (TLDs) alone were unable to properly assess large variations in delivered dose for a standard TBI treatment (41). Then in 2005 Hui, et al. introduced a novel way to overcome both the organ toxicity and CT based treatment planning by adopting Helical Tomotherapy (Tomotherapy Inc., Madison, WI) technology (42-48). Unlike TBI, TMI targets the entire skeletal system while sparing sensitive, normal tissues, such as the lungs. Dose to sensitive organs were reduced by 35-70% with accurate dose delivery within ±7% to both target and critical organs a vast improvement over other contemporary radiation techniques at the time. Clinical data shows that dose-escalated TMI (20 Gy) as a preparative regimen prior to allogenic HCT for high-risk refractory leukemia patients was feasible and had therapeutic benefit, conferring an overall survival (OS) rate of 48% at 2 years(49), in contrast to the <10% OS reported for similar patients with active disease given TBI- or busulfan-based myeloablative regimens (50). However, relapse remains a major problem, suggesting more research is needed to

optimize TMI treatment for improving the survival benefit of patients with relapsed/refractory AML and to explore combinatorial therapeutics including TMI together with immunomodulatory drugs for hematological diseases (51). Furthermore, as TMI has become adopted by more centers but there is a wide variation in treatment setup techniques and patient positioning. This creates challenges when attempting center to center treatment outcome comparisons.

1.4. Gap between preclinical and clinical development

Since the development of helical TMI there has been an explosion of feasibility studies and clinical research within the field (43, 44, 46, 47, 52). This technique only made possible by the development of3D imaging with dose modeling and the Multi-leaf collimator (MLC). These leaps forward in technology have further enabled advancements in clinical research (53). However, preclinical modeling has sorely lacked behind. This is largely due to the lack of technological developments for preclinical radiation therapy research. Unlike clinical research, where onboard imaging systems for 3D imaging and MLCs for radiation treatment are relatively common, they have not existed for preclinical systems until recently. Recent developments such as an Intensity Modulated Radiation Treatment (IMRT) (54, 55) and MicroCT treatment systems (56) for preclinical research have closed the technological gap between preclinical and clinical treatments. The introduction of a preclinical 3D CT system has allowed for the study of dose deposition beyond 2D planar film. Preclinical modeling played an integral role in the development of TBI and BMT. This preclinical model furthered the understanding of the complicated biological mechanisms of

immune modulation and bone marrow engraftment. As TMI develops, having a robust preclinical radiobiological model of its own will assist in future progression of clinical treatments.

1.5. Outline of this thesis

Chapter 2 is the evaluation of precision using current clinical TMI treatment techniques and its impact on the dose distribution. TMI is a highly conformal treatment of the human skeleton structure requiring a high degree of precision and accuracy for treatment delivery. There are currently many centers worldwide initiating clinical studies using TMI but there is currently no standard for patient pretreatment setup. To this end, the accuracy of different patient setups was measured using pretreatment imaging and their impact on dose delivery was assessed for multiple institutions.

Chapter 3 transitions to discussing the development and progress of preclinical TMI treatment techniques and their evaluation as effect radiobiological models. A new novel preclinical TMI treatment technique using new microCT technology is reported with an example of a practical application. The model was validated dosimetrically and biologically using bone marrow transplant techniques.

Chapter 4 demonstrates and outlines the details of a perspective radiobiological study for assessing lung toxicities following TMI related treatment. This study is an example of many potential studies and mirrors current clinical works. Chapter 5 is a conclusion with a wrap up outlining future projects that will be developed from the works presented in this thesis.

Chapter 2. Assessment on the Precision of Clinical TMI using Megavoltage computer tomography (MVCT)

2.1. Introduction – Rational behind precision assessment

TMI treatment risks are similar to intensity modulated radiation therapy (IMRT), such as sharp dose gradients near both the planning target volume (PTV) and avoidance structures. The close proximity of dose gradients to these structures increases the risk for detrimental impacts caused by patient positioning and setup uncertainties (57). Reliable pre-treatment patient positioning methods along with accurate and precise verification of patient positioning are therefore crucial to deliver the prescribed dose to the PTV while sparing normal tissues.

Currently, there is a worldwide effort to adopt targeted radiation treatment procedures for hematological malignancies, and the potential for TMI is being studied at multiple centers globally (58, 59). Many of these centers use different pre-treatment position verification techniques. Little is known about how the patient position varies across multiple treatment fractions or how patient positioning impacts TMI dose delivery between different centers. To investigate this unmet clinical need, the international consortium of total marrow irradiation (ICTMI) worked with the six participating institutions to assess the accuracy of patient setup and its impact on dose delivery. Two steps were taken to

accomplish this goal: 1) compare pre-treatment rigid registrations by institution to assess patient setup technique and 2) quantify how pretreatment rigid registration affects the planned dose delivered to the patient. Based on this evaluation, recommendations for improved TMI treatment setup are given.

2.2. Methods

2.2.1. Patient Immobilization

All institutes used whole body immobilization with some minor variations in technique. Institutions 1, 3, 5, and 6 immobilized patients using a Vac-Lok and thermoplastic mask (each from different companies depending on the center) (42, 47). TMI is typically treated in 2 parts: an upper (body) and lower (legs) section. Institution 1 used a breathing motion tracking software to account for chest motion. Institutions 2 and 4 used an all-in-one base plate comprising 2-3 thermoplastic meshes to restrict regions of the head/neck, thorax/arms, and legs (58). For initial setup and verification, a series of tattoos along the head, shoulder, thorax, pelvis, and leg regions were used.

2.2.2. Definition of the CTV and PTV

For TMI, the clinical target volume (CTV) was marrow-containing bony skeleton. Strictly speaking, the entire bony skeleton is more than the marrow-forming tissue and therefore did not need to be entirely included in the CTV. However, for simplicity of contouring, it was easier to use the CT number of bone to define the CTV. For institution 3, instead of a uniformly symmetric margin, the planning target volume (PTV) was created from the CTV using a customized margin and is described as follows. For the areas that have more setup

uncertainty such as shoulders and spinous processes, a 5-10 mm margin was added to CTV to generate PTV. For the arms and thighs, a 10 mm margin was used. For all other bones including skull, anterior spine, and pelvic bones where setup is reproducible, no margin was used because the CTV was the bone, but the biologic target was the marrow. Institutions 1 & 2 used a symmetric 10 mm margin for all target regions. Institutes 4 & 6 used a symmetric 5 mm and 7 mm margin, respectively. Institute 5 had a customized PTV with margins of 5 mm to the long bone of the extremities, 3 mm for pelvis, 2 mm for cranial bones, and 1 mm for all other bones.

2.2.3. Planning Philosophy

We identified two different approaches for TMI treatment planning: conformal avoidance and conformal targeting, as described previously by Hui et al (42). Conformal targeting focuses irradiation on the ribs and spares as much of the non-lung normal tissue as possible. Conformal avoidance irradiates the non-lung normal tissue to the prescribed dose, with a high dose interface at the boundary of the lungs. Institution 1 was the only institution to utilize conformal targeting, whereas the other institutions treated with conformal avoidance. To treat the legs, a second plan was created and the patient rotated to feet first supine and reimaged/treated (60) using the helical Tomotherapy.

2.2.4. Daily MVCT imaging

Daily MVCT images and image registration data from 6 institutions and 68 total patients using different patient immobilizations, megavoltage computed tomography (MVCT) imaging protocols, and TMI treatment plans were acquired

through the International Consortium of TMI (ICTMI) **(Table 2-1)**. The data were collected using the helical Tomotherapy (Accuray Inc., Madison, WI) unit, which has an on-board MVCT detector array to generate volumetric images for patient localization (48). Patient pretreatment setup is defined as the imaging, immobilization, and planning technique used for the delivery of the radiation therapy.

Institution	# of patients	PTV Definition	KVCT data	MVCT data	PTV Planned Dose
1	6	Symmetric 10mm margin	5mm thick slices, 108cm starting from bottom of pelvis	**WBI,** range of 0-6mm with a mean of 3mm thick slices, starting from bottom of pelvis	15-18 Gy in 5 - 6 fractions
2	11	Symmetric 10mm margin	10mm thick slices, 126cm scan length starting from the top of the head	**WBI**, 6mm thick slices, 80cm scan length, starting from top of the head	12Gy in 3 fractions
3	20	Non-symmetric margins variable for target region (see methods for details)	5mm thick slices, 121cm starting from the top of the head	**WBI,** 6mm thick slices, 80cm scan length, starting from top of the head	20Gy in 10 fractions
4	11	Symmetric 5mm margin	10mm thick slices, 134cm scan length starting from the top of the head	**PBI,** two sets of images taken at: 1. center of the pelvis 2. from the neck; 6mm thick slices with a scanning length 30cm each	8-12Gy in 4-7 fractions
5	10	Symmetric margins variable for target regions (see methods for details)	10mm thick slices, 134cm scan length starting from the top of the head	**PBI,** two sets of images taken at: 1. center of the pelvis 2. from the neck; 6mm thick slices with a scanning length 30cm each	13.5Gy in 9 fractions
6	10	Symmetric 7mm margin	2mm thick slices, 185cm scan length starting from the top of the head	**PBI,** two sets of images taken at: 1. iliac crest of the pelvis 2. midline of the eyes; 6mm thick slices with a scanning length 44cm each	12Gy in 3 fractions

Table 2-1: Classification of MVCT protocol, KVCT protocol, dose prescription and PTV definition per institution. Further details of PTV definition for institution 3 and 5 are provided in the methods section.

Two methods of pretreatment imaging were used: Whole body MVCT imaging (WBI) was used in institutions 1, 2, and 3, and partial body MVCT imaging (PBI) was used in institutions 4, 5, and 6 (**Figure 2-1**). Whole body

images were taken from the top of the neck or base of the skull to below the pelvis (**Figure 2-1a**) and registered with the kVCT. Partial body imaging (PBI) techniques typically covered 2-3 regions. The first region started at the base of the skull down to the shoulders (**Figure 2-1b**). The second region covered the abdominal cavity down to the pelvis (**Figure 2-1c**). The third region covered the top of the iliac crest down to the diaphysis of the femur (**Figure 2-1d**). For PBI-based registrations, shifts from both the head and neck (HN) and lower regions were recorded and averaged together. The averaged coordinates were used as the pretreatment shifts for that fraction. Registration of the partial and whole body images and the potential for registration mismatches can be seen in **Figure 2-1e-k** for the different regions. MVCT slices with widths of 6 mm are commonly used to minimize time for patient scanning and post image processing. Before MVCT imaging, alignment with external lasers to fiducial markers on the patient is done by a therapist.

We varied the number of MVCT slices used from whole body images and performed image registrations with the planning kVCT. These registrations were compared with WBI-based registrations in the lung and pelvic bone region for the same patient. PBI slices were determined by initially selecting slices at the iliac crest of the pelvis and cranial half of the lungs, then adding additional inferior slices to both regions. The difference in root-mean-square (RMS) displacement between the WBI registration and PBI registration were calculated with varying image lengths.

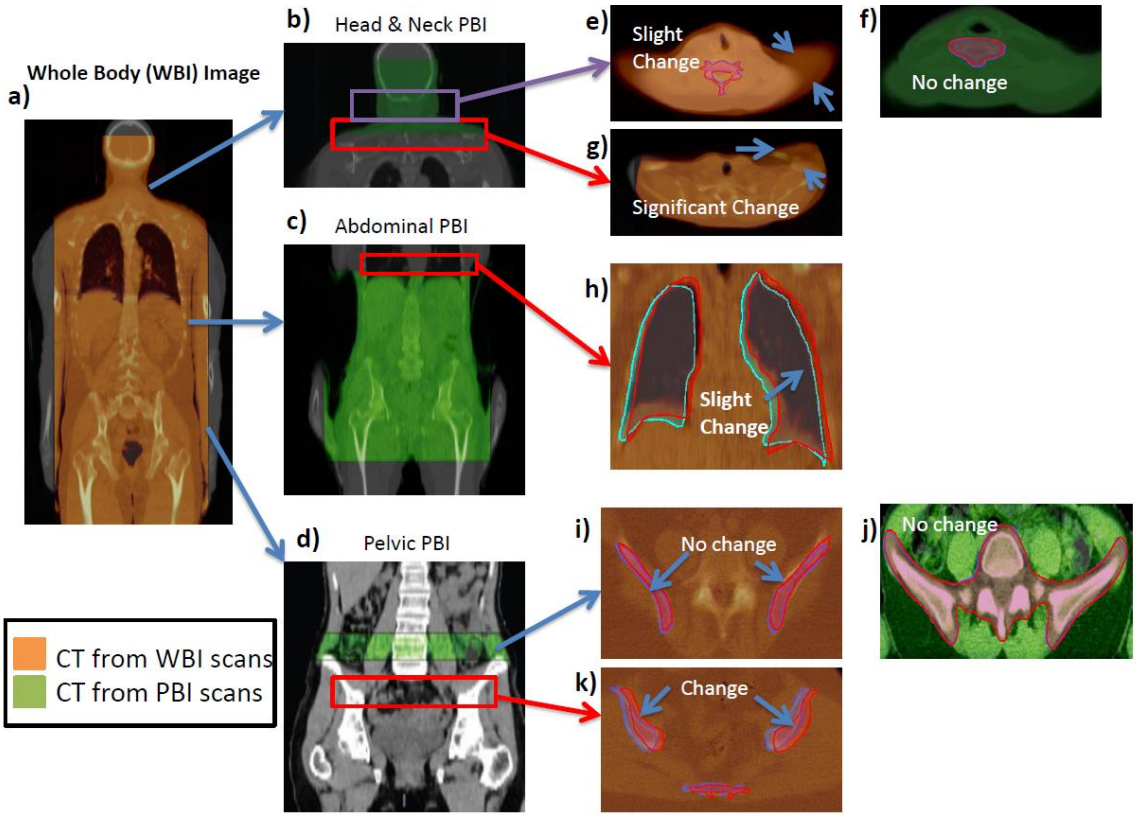

Figure 2-1: Examples of WBI and PBI and their respective registrations. **a)** Whole Body registration with associated kVCT. Three sub-regions commonly imaged in PBI: **b)** head and neck, **c)** abdominal, and **d)** pelvic are shown registering with their kVCTs. Red boxes indicate regions where PBI was not performed but significant mismatches in WBI were found. Slices from WBI and PBI are shown for various regions **(e-k)**. Orange CT scans are from WBI scans. Green CT scans are from PBI scans. Regions outside of PBI imaging show mismatch in WBI while only slight mismatches occur in nearby PBI images regions.

2.2.5. Pretreatment Rigid Registration Assessment and its Effects on Dose Recalculation

Pre-treatment rigid registrations from each institution were evaluated following previously published methods (43, 61, 62). All CT images were down sampled to 256x256 resolution to match Tomotherapy based MVCTs, ensuring that differences in resolution would not affect the dose calculation. Results from

pre-treatment rigid registrations were used to quantify setup errors for each institution, which include global systematic error (2-1), random error (2-2), patient-to-patient variations (2-3), and the overall distribution error (2-4). Equations are derived by Yan, et al (61):

$$M(\mu_i) = \sum_{i=1}^{P} \frac{N_i \mu_i}{N} \; where \; \mu_i = \sum_{k=1}^{N_i} \frac{m_k}{N_i} \qquad (2\text{-}1)$$

$$\sum(\mu_i) = \sqrt{\frac{\sum_{i=1}^{P} N_i(\mu_i - M(\mu_i))^2}{(N-1)}} \qquad (2\text{-}2)$$

$$RMS(\sigma_i) = \sqrt{\sum_{i=1}^{P} \frac{(N_i-1)(\sigma_i)^2}{(N-1)}} \; where \; \sigma_i = \sqrt{\frac{\sum_{k=1}^{N_i}(m_k - \mu_i)^2}{(N_i-1)}} \qquad (2\text{-}3)$$

$$\sum_{overall} = \sqrt{\sum(\mu_i)^2 + RMS^2(\sigma_i)} \qquad (2\text{-}4)$$

μ_i = is the individual systemic error for patient i

P is the total number of patients

N is the total number of treatment fractions

N_i = treatment fractions for patient i

m_k = measured position correction for the k^{th} fraction of patient i

σ_i = individual random error for patient i

Rigid registration dose (or delivered dose) was evaluated using the recorded pre-treatment shifts taken from the Tomotherapy MVCT image guidance system. The reported translational shifts were first applied between the planning KVCT and the daily MVCT, and then the daily fractional dose was calculated using the original DICOM-RT dose files. Since translation shifts were accounted for, we are investigating the residual error from patient setup. All dose

evaluations were performed within the Velocity AI system (Varian Medical Systems, Inc., Palo Alto, CA, USA). The planned dose distribution was compared with the delivered dose (sum of the fractional doses) in terms of a structure's mean dose, 90% (D90), and 10% (D10) isodose line. The relative difference in the planning dose per fraction was evaluated for an overall assessment of treatment delivery accuracy. Both regional dose and overall skeletal dose variations were considered in treatment delivery assessment.

Statistical analyses were performed using GraphPad Prism v 7.04 (GraphPad Software Inc. La Jolla, CA, USA). Data are presented as the mean ± standard deviation. Outliers were identified using a robust nonlinear regression method, ROUT (Q = 1%, "Q" is the maximum desired false discovery rate) and were assessed per institution. Multiple group comparisons were performed with a one-way ANOVA test correcting for multiple comparisons. Group comparisons were performed with an unpaired two-tailed Student's test. A p value of ≤0.05 was considered statistically significant.

2.3. Results

2.3.1. Rigid Registration Errors

Measures of the mean, random, and systematic errors from pre-treatment patient setup are presented in **Figure 2-2** & **Figure 2-3** for each institution, and a detailed chart of the errors is found in **Table 2-2.** As shown in **Figure 2-2**, the highest global error is 8.2 mm, which was significantly different ($p < 0.0001$) from the other institutions. This result is largely due to the y-direction (longitudinal) error of 6.8 mm. Institution 5 was the best overall performing institution, with an

overall distribution error of 4.5 mm compared to 7.3 mm. Results from WBI and PBI institutions for patient to patient and random error can be found in **Figure 2-3**. The imaging techniques were found to be significant from each other ($p < 0.0001$) with WBI having the lower overall distribution error of 3.8 mm compared to PBI's 5.3 mm. Patient roll was small (<1 degree, **Table 2-3**) and therefore it is not included for dose calculation.

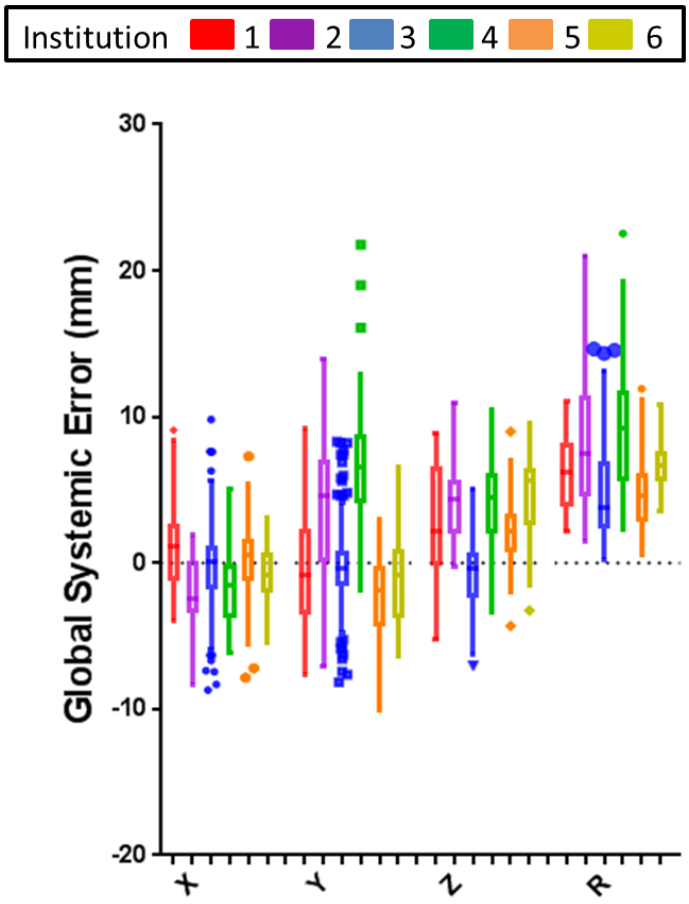

Figure 2-2: Box plot (Tukey) of rigid translations for each institution from pre-treatment rigid registration for each cardinal direction and the R (RMS average:$\sqrt{X^2+Y^2+Z^2}$).

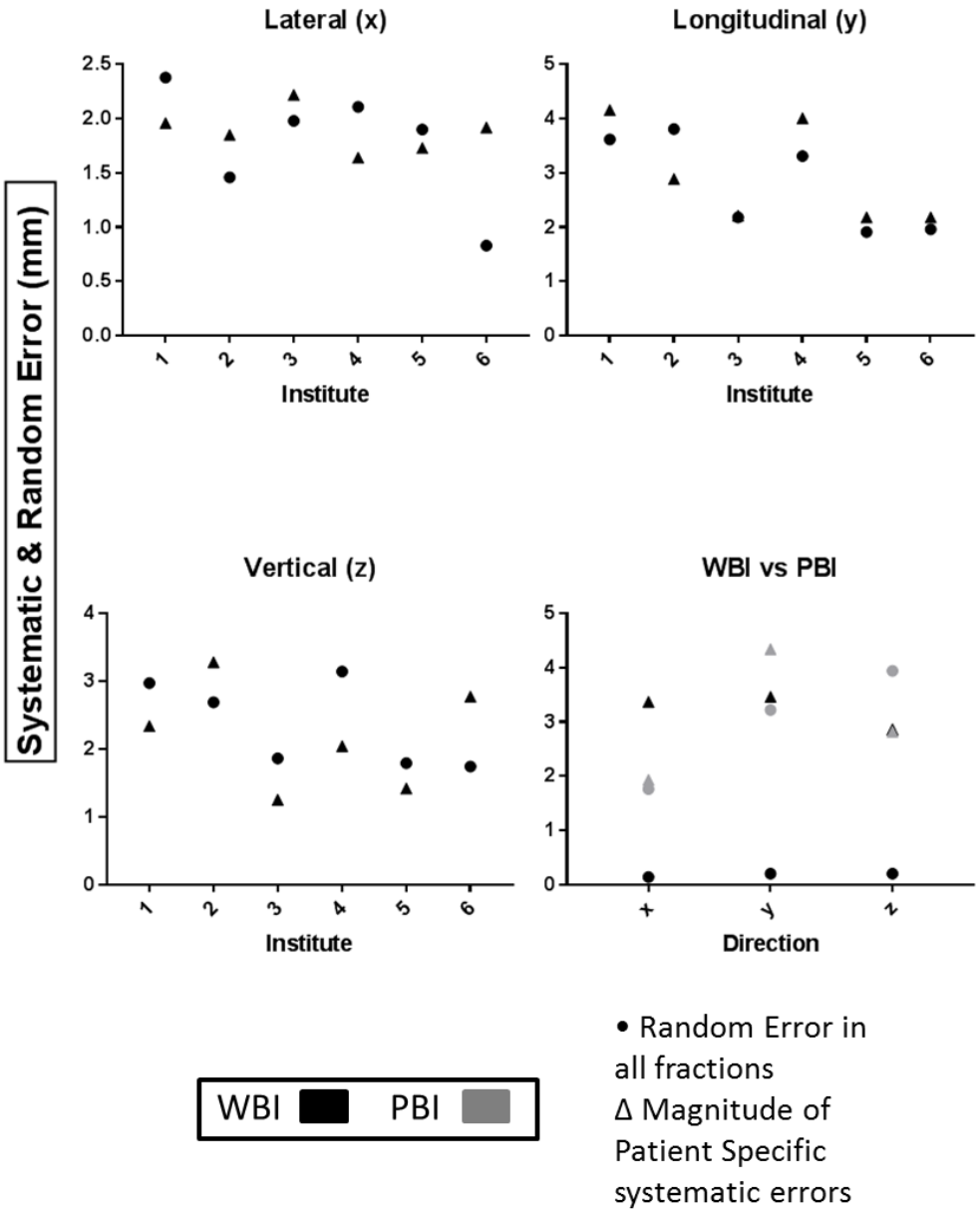

Figure 2-3: Graph of random and systemic errors for each institution (x, y, z) in each cardinal direction (x, y, z). Graph of random and systemic errors for the two primary MVCT imaging techniques: WBI & PBI for each cardinal direction. Numerical results can be found in **Table 2-2 & Table 2-3**. Results were calculated following Yan's methods and detailed in the method section equations (2-1) to (2-4).

Global Systemic Errors					
Institution	X (mm)	Y (mm)	Z (mm)	Average √(X^2 + Y^2 + Z^2)	Roll (degrees)
1	0.95	0.25	2.33	2.53	-0.07
2	-1.78	3.56	4.57	6.06	0.61
3	-0.25	-0.16	-0.57	0.64	-0.04
4	-2.26	6.88	3.76	8.16	0.11
5	0.31	-2.30	2.24	3.22	0.13
6	-0.72	-1.10	4.31	4.51	N/A
Variation in Systemic Error					
Institution	X (mm)	Y (mm)	Z (mm)	Average √(X^2 + Y^2 + Z^2)	Roll (degrees)
1	1.96	3.62	2.34	4.74	0.53
2	1.85	3.81	3.28	5.35	0.53
3	2.22	2.18	1.25	3.36	0.50
4	1.64	3.31	2.04	4.22	0.54
5	1.73	1.91	1.42	2.95	0.21
6	1.92	1.96	2.77	3.90	N/A
Magnitude of Random Error					
Institution	X (mm)	Y (mm)	Z (mm)	Average √(X^2 + Y^2 + Z^2)	Roll (degrees)
1	2.38	4.16	2.97	5.64	0.78
2	1.46	2.89	2.69	4.21	0.40
3	1.98	2.21	1.86	3.50	0.44
4	2.11	4.01	3.14	5.51	0.66
5	1.90	2.18	1.79	3.40	0.28
6	0.83	2.18	1.74	2.91	N/A
Overall Distribution Error					
Institution	X (mm)	Y (mm)	Z (mm)	Average √(X^2 + Y^2 + Z^2)	Roll (degrees)
1	3.09	5.52	3.78	7.36	0.94
2	2.36	4.78	4.24	6.81	0.66
3	2.98	3.10	2.24	4.85	0.67
4	2.67	5.20	3.75	6.94	0.85
5	2.57	2.90	2.29	4.50	0.35
6	2.09	2.93	3.27	4.86	N/A

Table 2-2: Detailed table of global systemic errors for each institution's submitted patient population based on the recorded pretreatment rigid registration.

Global Systemic Errors					
Technique	X (mm)	Y (mm)	Z (mm)	Average √(X^2 + Y^2 + Z^2)	Roll (degrees)
WBI	-0.07	0.60	0.97	5.08	0.04
PBI	-0.68	0.77	3.90	6.60	0.14
Variation in Systemic Error					
Technique	X (mm)	Y (mm)	Z (mm)	Average √(X^2 + Y^2 + Z^2)	Roll (degrees)
WBI	3.37	3.46	2.86	3.36	0.57
PBI	1.93	4.34	2.82	3.16	0.37
Magnitude of Random Error					
Technique	X (mm)	Y (mm)	Z (mm)	Average √(X^2 + Y^2 + Z^2)	Roll (degrees)
WBI	0.14	0.18	0.20	0.21	0.03
PBI	1.76	3.22	3.94	4.27	0.45
Overall Distribution Error					
Technique	X (mm)	Y (mm)	Z (mm)	Average √(X^2 + Y^2 + Z^2)	Roll (degrees)
WBI	3.37	3.47	2.87	3.37	0.57
PBI	2.61	5.40	4.85	5.31	0.59

Table 2-3: Detailed table of global systemic errors for each MVCT imaging technique's patient population based on the recorded pretreatment rigid registration

2.3.2. Effect of MVCT length on patient registration

Because PBI was used by half of the centers covering different anatomical regions with varying number of slices, we investigated whether there was a positive correlation between number of slices used for PBI registration and WBI registrations. The effect of varying the number of MVCT slices used for image registration on registration precision and accuracy are shown in **Figure 2-4**. The

magnitude of RMS displacement between WBI and PBI of varying slices decreased with increasing number of slices for both pelvis and lung regions. Our results indicate a suggested minimal regional coverage of >10 cm in the cranial-caudal direction with a slice thickness of 5-6 mm to minimize spatial error of less than 5% from the overall WBI baseline registration.

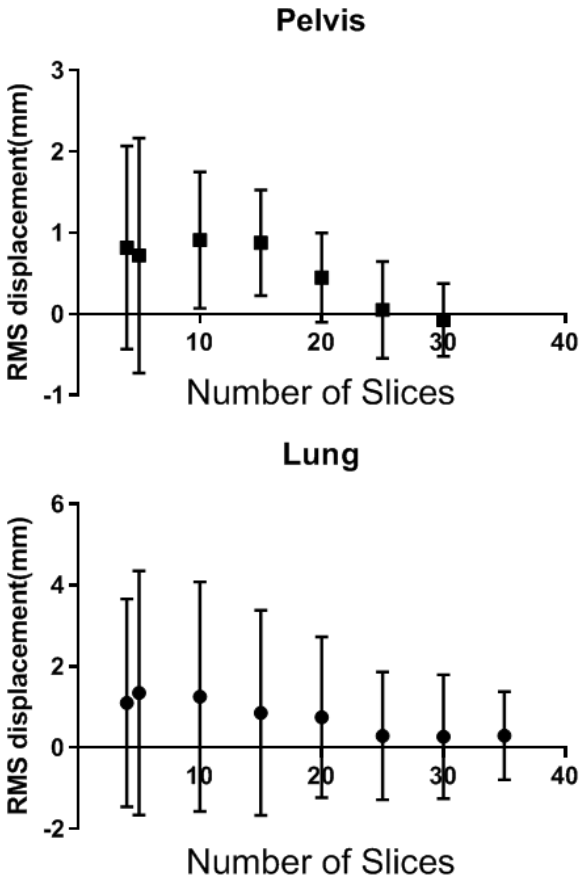

Figure 2-4: Difference between minimal slice registration and WB baseline registration (N=10) for the pelvis and lung regions from the 3 WBI institutions. All images are registered at 256x256 with 6mm slice thickness.

2.3.3. Effects of Rigid registration on dose

Figure 2-5 & Figure 2-6 displays the percentage difference in mean dose for daily treatments for each WBI imaging institution. Percent differences from the planned and delivered doses for the PTV are in **Figure 2-5.** Prescription dose is defined differently for each institution as seen in **Table 2-1. Figure 2-6** displays the percent difference between the regional CTV mean dose and the planned PTV mean dose. **Figure 2-5f** is the 95% Confidence Intervals (CIs) for the PTV and are measured as [-2.8%, -1.3%] in the HN, [-1.3%, -0.4%] in the SC, [-0.9%, -0.3%] in the spine, [-1.2%, -0.6%] in the pelvis, and [-2.0%, -0.6%] for the skeleton. **Figure 2-6f** shows the 95% CIs for the mean CTV dose as compared with the mean PTV dose, measured as [-3.0%, -0.7%] in the HN, [-1.6%, -0.4%] in the SC, [-0.7%, -0.1%] in the spine, [-2.3%, -0.4%] in the pelvis, and [-2.7%, -1.0%] for the skeleton. While institute 1 has higher uncertainty in D90 in skeleton; institutes 2 & 3 have higher uncertainties in the pelvis (**Figure 2-5a**).

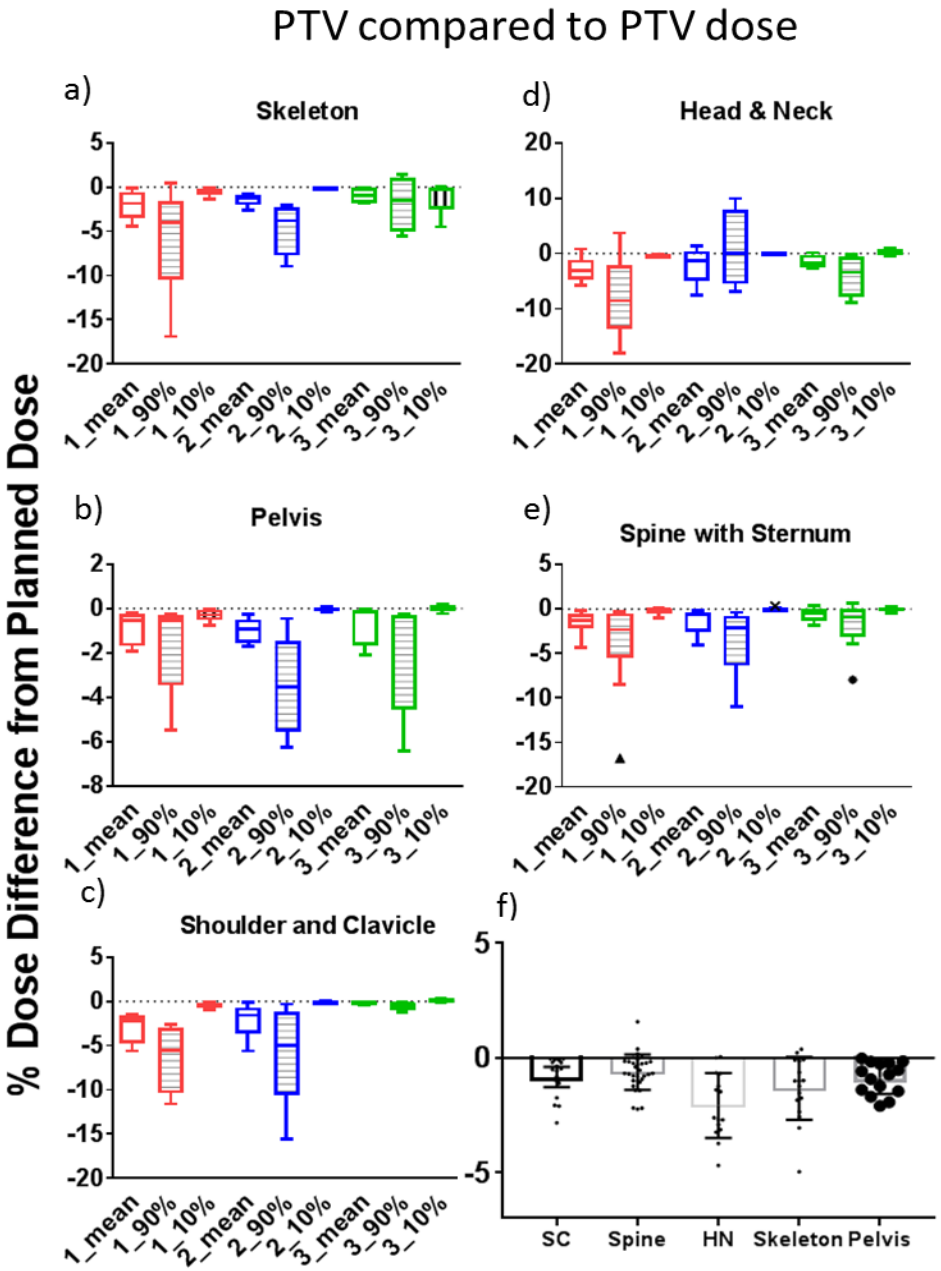

Figure 2-5: a-e) Regional percent dose difference for the PTV between the delivered and the planned mean doses, 90% isodose (D90) and 10% isodose (D10) for the skeleton five sub regions: Head & Neck (HN), Shoulder with Clavicle (SC), Tspine with Sternum, and Lspine, for all Whole Body imaging institutions 1, 2, & 3 (N=5 for each institute). Delivered doses are calculated based on recorded pretreatment shifts before radiation delivery. Regional percent differences in mean dose between **f)** delivered PTV doses from the planned PTV mean dose in the SC, spine, head and neck (HN) based on the number of patients, presented with confidence intervals.

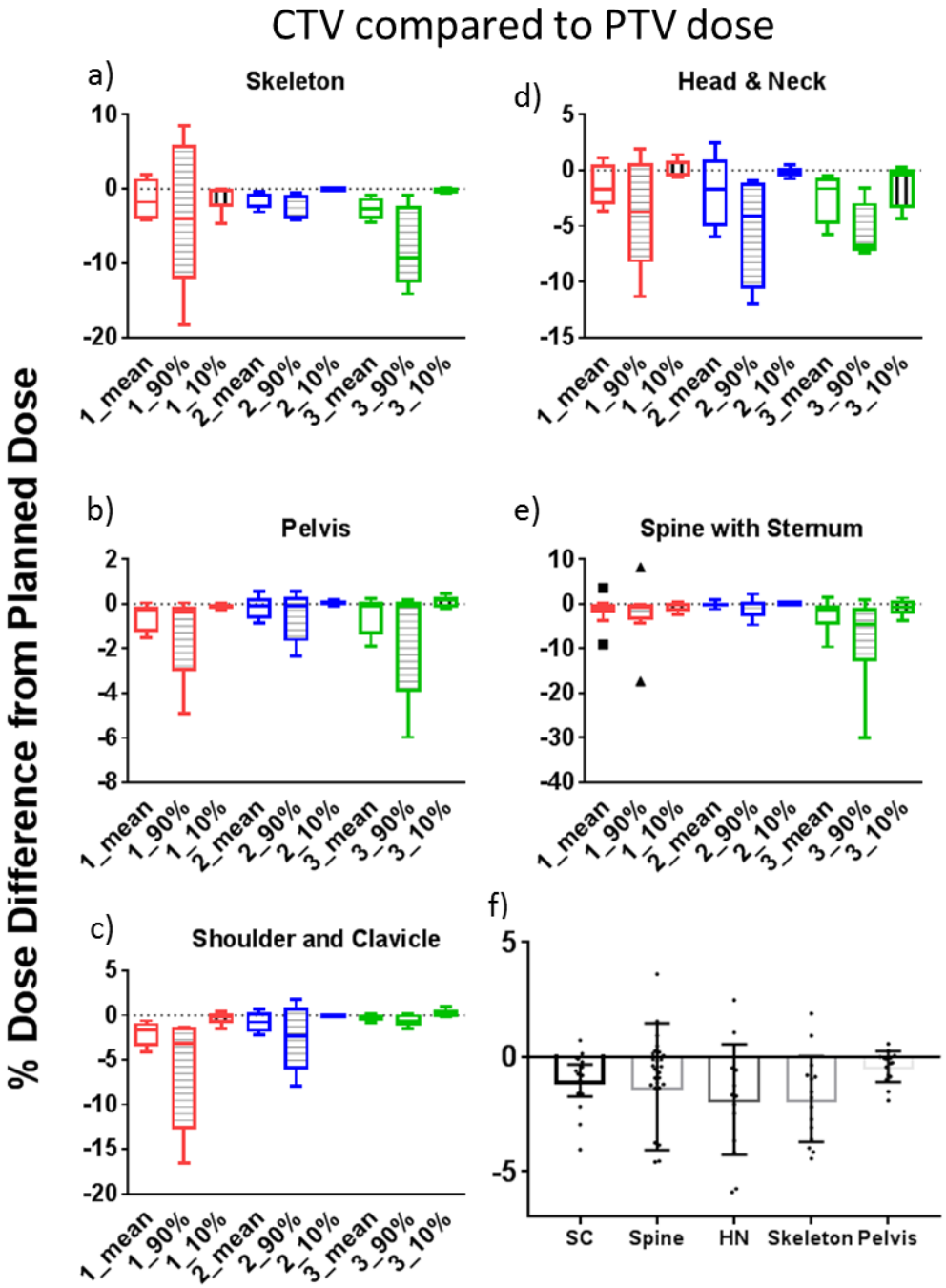

Figure 2-6: **a-e)** Regional percent dose difference for the CTV between the delivered and the planned mean doses, 90% isodose (D90) and 10% isodose (D10) for the skeleton five sub regions: Head & Neck (HN), Shoulder with Clavicle (SC), Tspine with Sternum, and Lspine, for all Whole Body imaging institutions 1, 2, & 3 (N=5 for each institute). Regional percent differences in mean dose between **f)** delivered CTV doses from the planned PTV mean dose in the SC, spine, head and neck (HN) based on the number of patients, presented with confidence intervals.

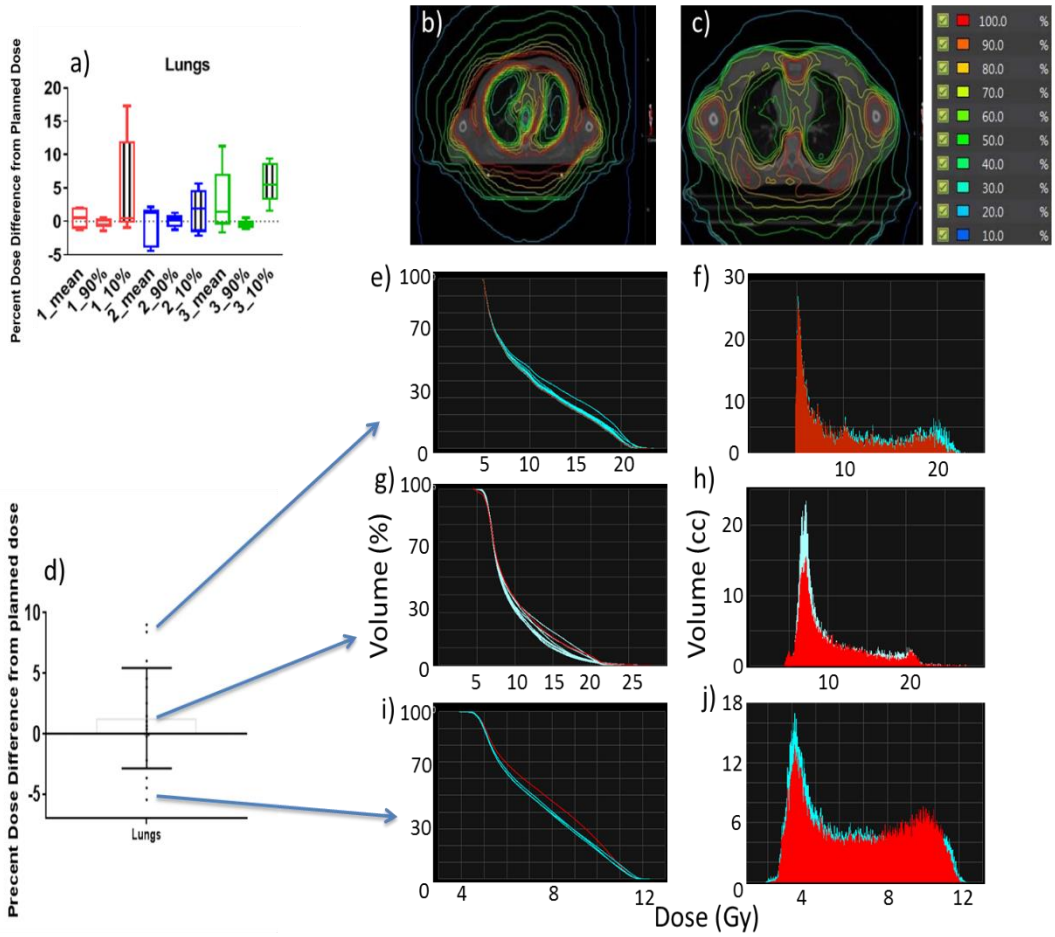

Figure 2-7: **a)** Percent dose difference for the lungs between delivered and planned mean doses, 90% isodose (D90) and 10% isodose (D10). **:** Isodose lines of the thoracic cavity of two different treatment planning methods: **b)** Conformal avoidance and **c)** conformal targeting. **d)** Percent dose difference between expected and delivered dose in the lung for all WBI institutes (N=15) **e-j)** is the resulting DVHs of the lung for 3 different representative cases: overdose, close to expected dose, and under-dosed. Blue represents the resulting fractional dose and red the original planned dose.

Figure 2-7 displays the percentage mean lung dose difference for daily treatments for each WBI imaging institution. The different treatment planning isodose distributions are visualized in **Figure 2-7b & Figure 2-7c.** The 95% CI for lungs from WBI institutes is [-0.8%, 3.4%] as seen in **Figure 2-7d**. **Figure**

2-7e-j are the resulting dose volume histograms (DVHs) of the lungs for 3 different cases: high, close to expected, and low dose. Blue represents the resulting fractional dose and red the original planned dose. A representative fraction with shoulder misalignment and its effect on PTV dose can be seen in **Figure 2-8**.

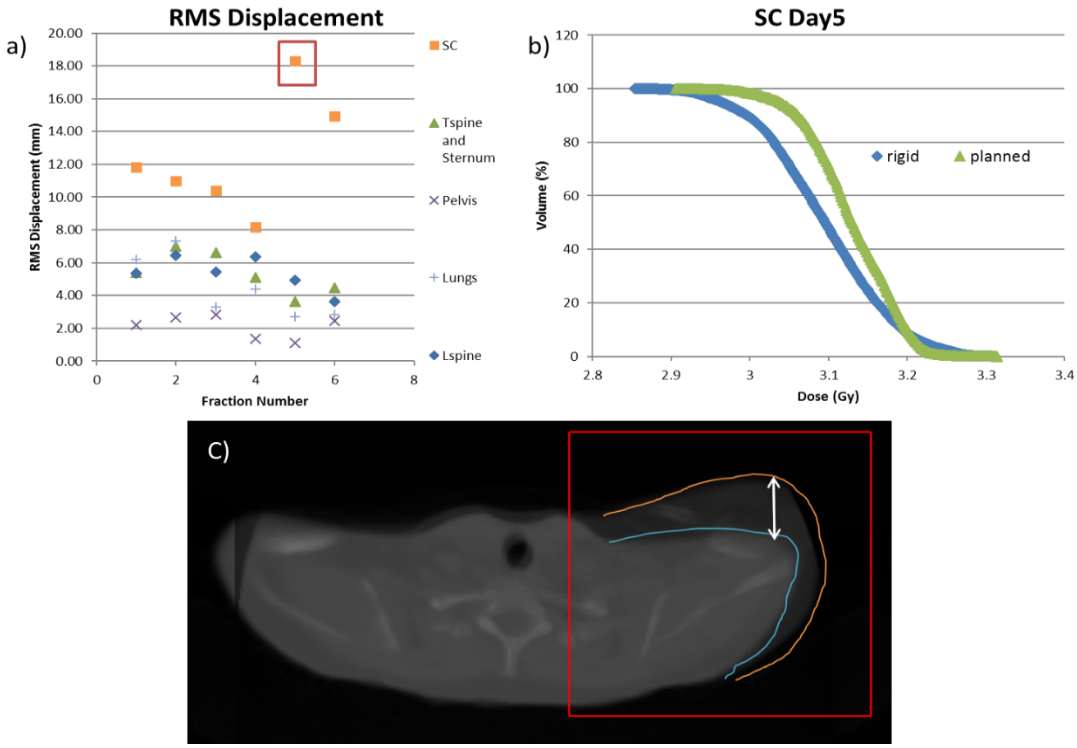

Figure 2-8: Example of misaligned shoulder from TMI treated patient. **a)** root-mean-square (RMS) displacement per fraction showing a large shift in the SC region on days 5 and 6. (RMS = $\sqrt{x2+y2+z2}$)**,** and **b)** dose-volume-histogram (DVH) graph of the rigid and planned dose of the shoulder, for day 5 of treatment **c)** image of misaligned shoulder on day 5 of treatment.

2.4. Discussion

This is the first multicenter investigation of the precision of TMI delivery through the ICTMI consortium. We performed analysis of pretreatment patient setup and its effect on the administered dose between multiple institutions using

different setup methods. MVCT imaging was crucial to assess pretreatment patient setup, dose validation and institutional variations in dosimetric accuracy. Pretreatment WBI MVCT allows for assessment of 3D dose distribution within the skeletal PTV and lungs. Institutional variations in pretreatment patient setup existed with overall distribution errors ranging from 4.5 mm to 7.3 mm.

2.4.1. Pretreatment Rigid Registration and their Effects on Dose Distribution

There are significant differences between institutions for patient pretreatment setup. The longitudinal (y) direction of rigid registration had the highest overall distribution error compared with the lateral (x) and vertical (z) directions (**Table 2-2 and Figure 2-5a)**. These results are different from previous works which indicated greater error in the z direction (43, 62). This difference is likely due to previous studies investigating patient setup for solid tumor treatments rather than whole body skeletal targeting. Most treatment protocols set a threshold for pre-treatment setup. For example, if the shifts are greater than 5 mm, the patient should be moved and reimaged. If pre-alignment is not properly performed, large displacements can be identified with MVCT imaging. In one institution, the vertical direction shifts were far outside expected values [>5 cm]. The pretreatment MVCT allows for detection of these large shifts, suggesting the need for image guidance with conformal radiation delivery.

The D90 had greatest uncertainty in skeletal regions as compared to the mean or D10. On the other hand, the lungs had the greatest uncertainty and dosimetric variation in D10 values. An example of these uncertainties can be

seen in the DVH curves for a single patient treatment (**Figure 2-9**). In TMI studies, the DVH of skeletal target regions at the D90, and the lungs at D10, should be critically evaluated to minimize uncertainties to improve on the overall accuracy and precision of the treatment. Since the CTV is encapsulated within the PTV, the uncertainty in the mean dose is expected to decrease or remain

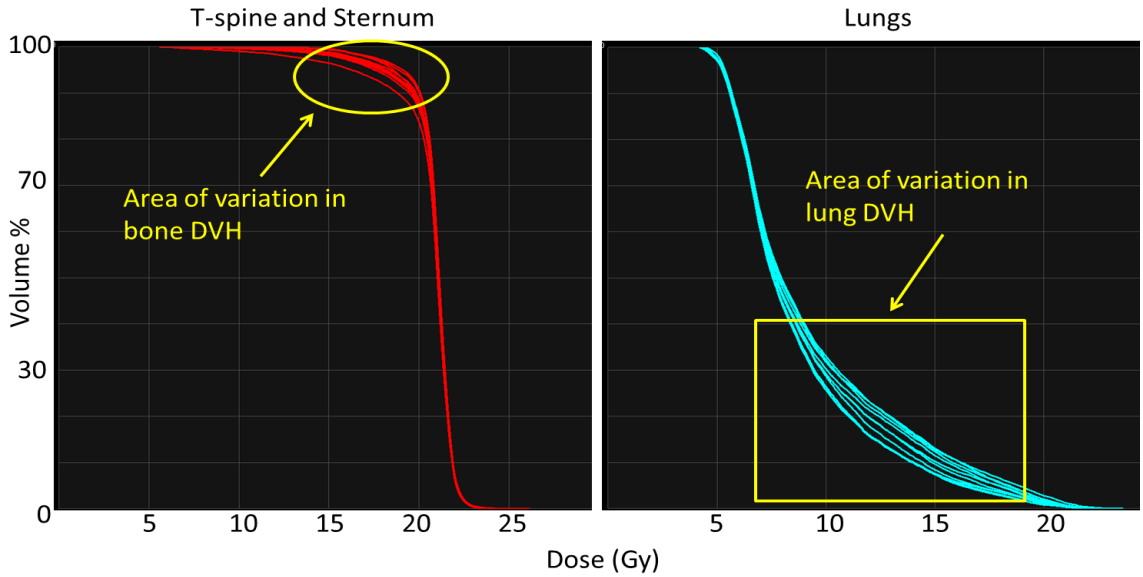

Figure 2-9: Example DVHs of a 10 fraction TMI treatment for: **a)** Tspine and Sternum and **b)** lungs. Variations in the DVH can be seen at the 90-95% line for the bone structure and 10-30% for the lung.

unchanged. Comparing the confidence intervals and dosimetry from **Figure 2-5f & Figure 2-6f** shows that is the case for SC and pelvis; but for the Spine, HN, and skeleton uncertainty increases. Despite differences in dosimetry all regions were still within 5% of expected value. This uncertainty in the mean dose between CTV to PTV and PTV to PTV is most likely inherent (random) error. Sternum was included with the spine which is sensitive to patient's breathing motion therefore can significantly affect the dosimetry. The head and neck dosimetry is not well understood and needs to be investigated further.

Despite regional differences in the delivered dose, the overall PTV mean dose was still within 5% of the planned dose for all institutions. The example in **Figure 2-8** shows the shoulder and clavicle (SC) were misaligned; however, the misalignment had no effect on the overall PTV dose for that day, because the SC only accounts for <2% of the total skeletal volume. However, in the case of non-homogeneous disease distribution (e.g. leukemia), small regions of poor dose coverage could have adverse effects on relapse prevention, demonstrating the importance of 3D DVH calculations of PTV dose (63-65). 3D imaging of target and its localization may be important to avoid the possibility of under-dosing (cold spot) the target regions and to allow accurate dose delivery (63).

2.4.2. The merits of WBI compared to PBI

Among the participating centers, institution 5 had the lowest overall error when compared to the other institutions using PBI imaging. PBI is faster to assess patient positioning than WBI. However, PBI results in incomplete images of certain key regions such as the lung **(Figure 2-1h**), which may result in loss of information that is relevant to assess patient dose delivery. While the variation in systematic error between WBI and PBI is similar, the overall error distribution is less for WBI because of lower random error (**Figure 2-2e & Table 2-3)**. One possibility for higher error in PBI is the averaging of multiple limited body registrations which are then applied as the overall rigid shifts. A limitation of MVCT imaging is poor soft tissue contrast. However, for TMI, MVCT imaging is useful for identifying bony treatment regions. Image resolution and the speed of MVCT imaging for TMI treatments are currently being improved, which has

potential to further reduce image acquisition time, making WBI MVCT scans more feasible (66).

2.4.3. Lung dose and planning philosophy

One of the major goals in TMI planning is to limit the lung dose to reduce risk for interstitial pneumonitis (IP). Previous studies on IP from TBI-related radiation exposure to the lungs is directly associated with mean lung dose, dose per fraction, dose rate, and chemotherapy regimen (67, 68). However, the lung dose measurements from these studies are obtained by single point dosimetry rather than calculated using 3D imaging based dosimetry, which makes variations in dose poorly understood (41). WBI allows for 3D dosimetric analysis, which will enable quantitative associations between 3D dose distribution and IP.

There was greater uncertainty (nearly double) in the D10 for conformal targeting compared with conformal avoidance **(Figure 2-7a)**. Variation in the lung dose is visible fraction to fraction, and often the deviation in the DVH occurs at a high dose as seen in **Figure 2-7e-j**. However, the mean dose for the whole lung was typically higher for conformal avoidance (0.5% from expected) versus conformal targeting (1.2% from expected) planning because of the presence of high dose interfaces near the lung. One of the major goals of TMI clinical trials is to allow for dose escalation, as it has been shown to reduce the relapse rate (52, 69, 70). Increasing accuracy of patient setup will enable further dose sparing to avoidance structures, enabling more reliable treatment delivery and dose escalation. Current prescriptions range from as low as 12Gy to as high as 20 Gy given in 2-4 Gy fractions. In the future, with increasing number of centers

adopting TMI for treating hematological malignancies and experience gained from the current study, we will expand this study to a larger population through the consortium to develop a more robust benchmark on setup and dosimetric tolerance. This approach could help to establish multicenter trials and compare clinical outcomes from different centers.

2.5. Conclusion

This work has shown that center-to-center variations in patient setup and doses delivered are dependent upon patient immobilization, pretreatment imaging protocols and PTV definition for TMI. The whole-body immobilization is generally recommended for patient localization. The WBI MVCT imaging modality is recommended over PBI for monitoring patient setup variation. WBI MVCT imaging is also recommended for monitoring dose delivery. Based upon participating centers, PTV margin can be adjusted depending upon proximity of targets to OARs to improve dosimetric results, furthering the need for WBI before each treatment. Although this study suggests reasonable patient localization and dosimetry, further expansion is under way. As TMI treatment for bone marrow transplantation becomes more mainstream, additional centers can be added globally.

Chapter 3. First Multimodal Image-Guided Total Marrow Irradiation 3D model for Preclinical Studies

3.1. Introduction – Rational behind TMI Preclinical Model development

CT-guided imaging for 3D dose calculation and augmentation of TMI in patients was achieved through a series of developments. Unlike standard TBI treatment, the first CT-guided 3D treatment planning showed a large uncertainty in organ dose coverage (71). The CT-guided TMI development allowed 3D dose calculations and modulation of radiation to desired regions while reducing doses to organs at risk (42). Although clinical TMI technological development has led to a large number of clinical trial investigations worldwide to allow dose escalation and reduction of relapse for patients with high-risk leukemia (53, 72-74), a lack of advanced pre-clinical technology has limited the scope of further scientific advances. Historically, mouse TBI treatment was performed using an X-ray source in which the traditional dose to the object was calculated by measuring the distance between the X-ray source to the object and dose calibration performed as standard (75). This process lacked imaging identifying organs, as well as a 3D dosimetric model to calculate detailed organ dosimetry and ignored the dosimetric effect of tissue heterogeneity. A film-based 2D image guidance identifying organ position and copper compensator allowed us to develop the first-generation TMI. However, it lacks 3D imaging, treatment planning for generating organ dosimetry such as dose volume histograms, and an accurate calculation of the dose to the bone, marrow, lungs and other organs. Therefore,

there is an unmet need for the development of a 3D image guided preclinical TMI model to further our mechanistic understanding of TMI treatment, to test various approaches for advancing TMI in patient care.

Addressing these issues to advance targeted radiation delivery for hematological research, we report here the development of an image-guided, high-precision preclinical TMI mouse model and evaluate its potential for maintaining long-term bone marrow engraftment while reducing organ damage, in comparison to standard TBI. This approach includes the development and characterization of a whole-body, CT-based, 3D image-guidance system identifying target and vital organs, allowing for precise dose calculations and optimization and validation of TMI delivery. Previous efforts to reduce whole-body radiation with the aim of reducing toxicity have resulted in increased relapse potential (reviewed by Sengsayadeth et al.(76)), and reduced engraftment or mixed chimerism(77), which can be overcome by increasing the number of donor cells(78). However, it is unknown how varying radiation exposure to vital organs could affect engraftment dynamics. Since TMI can maintain a high dose of radiation to the bone marrow and spleen, we hypothesized that TMI, along with reduced radiation exposure to body, will allow successful long-term engraftment. We further explored a comparative evaluation of TMI dosimetry between preclinical models and clinical data.

3.2. Methods

All animal experiments were carried out in accordance with the guidelines of the Institutional Animal Care and Use Committee (IACUC). C57BL/6 and

CD45.1 mice were purchased from National Cancer Institute (NCI, Wilmington, MA, USA). Tg(LZG85)Luc-GFP/B6 (B6 luciferase) mice were obtained from Dr. Defu Zheng, City of Hope and maintained by the Animal Resource Center of City of Hope.

3.2.1. Micro Irradiator

The TMI treatment was performed using the Precision X-RAD SMART Plus / 225cx (Precision X-Ray, North Branford, CT, USA), an X-ray irradiator able to image and treat small animals through modulation of its beam filtration, tube current, and potential differences. It had a maximum tube potential of 225 kV. Photons were filtered through a beryllium window with an additional 2.0 mm aluminum filter for imaging and 0.32 mm copper filter for treatment (56).

3.2.2. TMI treatment workflow

A workflow for TMI planning and treatment is represented in **Figure 3-1**. This workflow was performed on a reference planning animal to build a treatment plan for a set of treated animals. The reference planning animal matched the treated animals in species, sex, age (within 2 weeks), and weight (within 4 grams) to ensure treatment accuracy and reproducibility. Further details are provided below.

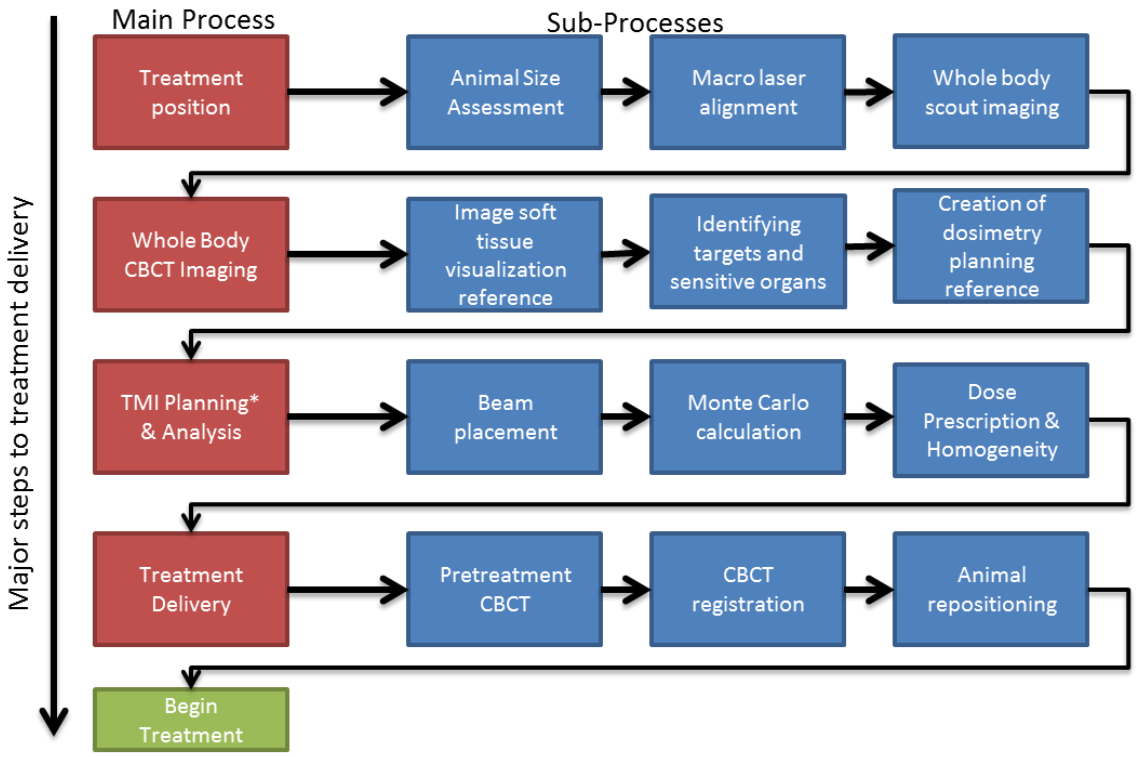

Figure 3-1: The detailed step-by-step process for the TMI treatment is shown. Steps on the left in red are major steps. Steps in blue are sub-steps.

3.2.3. Treatment positioning

An air-tight animal holder (6" long, cylindrical) made primarily of Delrin® and acrylic material was constructed as seen in **Figure 3-2**. The animal was placed in this animal holder to ensure reproducible animal positioning and immobilization. The holder limited animal motion along the longitudinal axis, increasing positioning reproducibility. Two ports from the front of the holder allowed circulation of isoflurane for anesthesia. The holder's effectiveness in stabilizing the mouse in position was tested by acquiring CT images of five female B6 mice (weighing approximately 20g), with both the holder and the flat

standard bed and were used as reference scans for their respective experiments. For simulating treatment conditions, a second set of CT scans for each mouse was then acquired for each setting (holder or standard bed) and registered with the reference scans using the on-board Pilot imaging software. After registration, the absolute displacements (root mean square of changes in sagittal, coronal, and axial directions) were recorded. For imaging and treatment, animals were anesthetized initially with 4% isoflurane at a flow rate of 1.5 liters per minute, then positioned in the animal holder. Isoflurane was then maintained as 2% isoflurane at a flow rate of 1.5 liters.

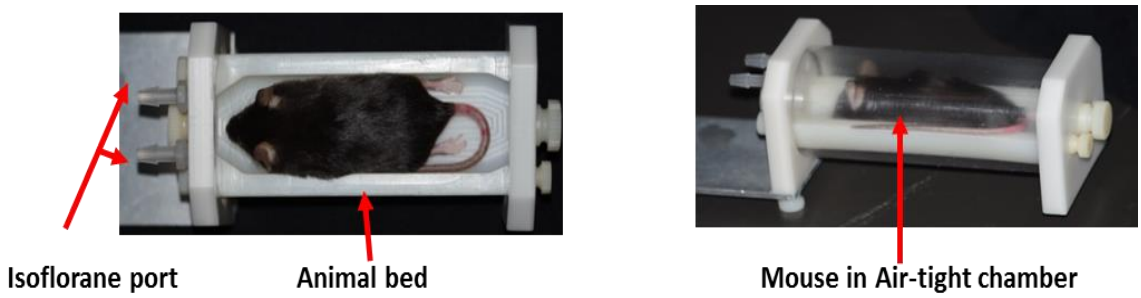

Figure 3-2: Custom-designed mouse holder base used in TMI treatment with a mouse placed in the chamber (base and transparent air-tight cylindrical chamber) to maintain continuous and homogeneous flow of isoflurane during TMI treatment delivery

3.2.4. Whole Body cone-beam computed tomography (CBCT) with contrast

For pre-imaging, the reference animal and holder were aligned using a built-in laser system (macro laser alignment at the isocenter). Scout images (fast partial CBCT) were performed to verify minimal roll or tilt (less than 2 degrees) that may be present after initial laser alignment. CBCT scans of reference animals in the

prone position were acquired using 40 kVp, 3 mA beam settings with a 0.2 mm voxel size. To verify beam coverage of the entire spleen and to provide dose estimations to other soft tissues in the treated mice, a subset of mice were imaged using iodine-based eXIA^{TM} 160 as a soft tissue contrast agent to clearly visualize and contour soft-tissue regions(79, 80). The eXIA^{TM} 160 (Binitio Biomedical Inc, Ottawa, Canada) was injected (5 µl/g of body weight, 100 µl solution) intravenously via the tail vein. Mice were imaged at four different time points; before injection and 1 hour, 4 hours, and 24 hours post injection to measure the temporal pattern of contrast enhancement. Mice images without contrast agents were registered to images of mice with the eXIA^{TM} 160 injections using Velocity AI (Varian Medical Systems, Inc, Palo Alto, CA). Using Velocity, sensitive soft tissue organs were identified and contoured for use in treatment planning. Additionally, in five mice, whole body microMRI (MR solution, Guildford, United Kingdom) was performed and co-registered with a CT scan in Velocity to verify position of organs. A board-certified radiologist evaluated images and contours.

3.2.5. Image registration using the CBCT

Soft tissues were identified using a system of multi-modal images with rigid and deformable image registration. Initially, prior to registration, the contrast and non-contrast cone beam CT (CBCT) scans were registered with rigid registration. Prior to the development of the animal holder, whole-body deformable registration was not possible due to large set up error between planning and contrast images (**Figure 3-3Ai-Figure 3-3Aii)**. Deformable image registration in Velocity AI (Varian Medical Systems, Inc, Palo Alto, CA) was

performed using the Multipass registration setting, an intensity based, modified Basis spline (B-spline) algorithm (81, 82). To improve deformation registration accuracy, deformable image registration was performed in three separate anatomical regions (skull, thoracic cavity, pelvis) (**Figure 3-3Aiii**). However, because of the development of the animal holder, whole body registration became feasible (**Figure 3-31B**) by limiting the initial body positioning.

Because of limitations in CT soft tissue contrast, even with contrast material, whole-body MRI was introduced. We combined multimodal imaging, CT, contrast enhanced CT, and whole-body MRI to identify 3D geometry of vital organs following previously published work (79, 80, 83-85). One week later, mice were scanned with whole body MRI using 7T PET-MRI by MR Solutions^{TM} (vendor's gradient echo sequence with FOV of 80x40x32 mm^3, the matrix of 160x80x64 [RxPxS]; flip angle of 40 deg, TE of 3 ms, and TR of 30 ms). Co-registration of MicroCT and MRI was used to generate a whole-body CT image along with imaging of the organs (**Figure 3-31C**).

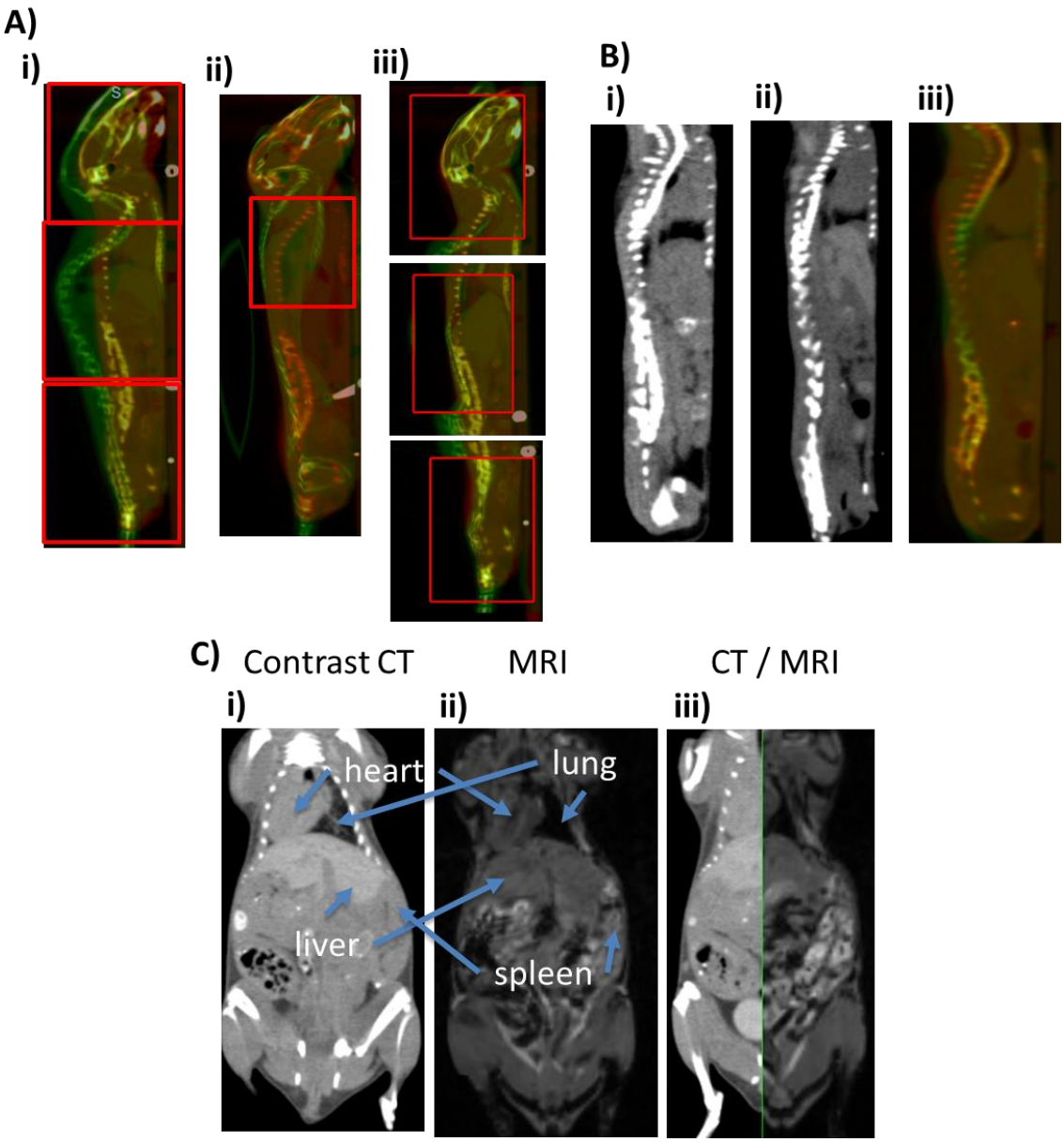

Figure 3-3: **A)** Registration of planning CT to contrast CT for same subject animal without the animal holder. **i)** planning CT (red) displayed over contrast CT (green). **ii)** result of global deformation between planning and contrast CT showing error in certain local regions (e.g., lungs and T spine within defined square box). **iii)** Regional deformation – Body is broken into multiple regions (shown in square red box), each deformed independently of each other between the reference and treated animal. **B)** Registration between **i)** planning and **ii)** contrast CT for the same subject animal with the animal holder. **iii)** whole body registration between planning and contrast CTs. **C)** Deformable registration between **i)** contrast CT and **ii)** MRI. Results of **iii)** deformable registration allowed for identification of soft tissue organs

3.2.6. TMI treatment planning and analysis

Mouse CT scans were divided into 7 regions for treatment optimization. Radiation beam layout by regions (beam size, isocenter location, normalization point) is provided in **Table 3-1.** For each region, parallel opposed beams with varied beam size were used to create a homogenized dose within the center of the beams. Visualization of a projected radiation beam on a 3D CT image allowed for proper beam placement (adjustment of beam size and isocenter) to cover the target and reduce exposure to adjacent critical organs. Beam sizes were varied (40x40mm to 5mm square or circle) in different regions using different collimator settings. During treatment planning, the prescription mean dose was set to cover the target (bone, marrow and spleen). Dose was normalized based on the soft tissue of the marrow within the bone. Treatment for femur and humerus was normalized based on internal bone marrow dose. For regions where the size of the bone marrow compartment was too small, the dose was normalized based on the surrounding soft tissue structures. The spine and pelvis, sternum, and skull were normalized to the spinal cord, local muscle tissue, and brain doses, respectively (details are in **Table 3-1**). For TBI, a CT-guided treatment plan was generated in which the whole-body dose including target and organs was kept at 11 Gy. For initial TMI-based engraftment assessment, 4 separate treatment plans were generated in which target (bone marrow and spleen) dose was kept at 11 Gy in all plans, and dose to organs were kept at 0 Gy (TMI 1), 2 Gy (TMI 1 + 2GY), 4 Gy (TMI 1 + 4GY), and 6 Gy (TMI 1 + 6GY), respectively. This planning and subsequent delivery were performed to evaluate

engraftment differences between different TMI treatments using bioluminescence imaging (BLI). We then selected two TMI treatment groups for long-term studies. In TMI 1, the plan was generated to deliver 11 Gy (5.5 Gy TMI/fraction, 2 fractions) to the target without radiation exposure to the remaining body including vital organs, whereas the TMI 1 + 4GY plan was generated combining TBI and TMI ((2 Gy TBI+3.5 Gy TMI)/fraction in 2 fractions). Both TBI and TMI were delivered at the isocenter with a dose rate of 400 cGy/minute. The treatment planning dose calculation was performed using the small animal radiotherapy planning system SmART-Plan(56) for both soft tissue (gut, lungs, liver) and skeletal structures (skull, femur, pelvis, spine).

Beam layout by region			
Region	Beam Size	Isocenter location	Normalization point
Skull & Cspine	40mm square	center of brain	Center of brain
C to T spine junction	10mm square	above scapula	Above the spine body
Sternum	20mm square	below the sternum enough so edge of beam covers sternum	skin of the sternum
Tpsine & Lspine	20mm square	above the spine so the edge of the beam covers the spine	Above the spine body
Pelvis	20mm square	above the pelvis so the edge of the beam covers the pelvic girdle	above the pelvic crest
Femurs	20mm square	below the femur	BM of femur
Spleen	10mm square	within the spleen	spleen tissue

Table 3-1: Radiation beam layout by regions (beam size, isocenter location, normalization point)

The X-ray tube settings were 225 kVp voltage and 13 mA current. The SmART-Plan employed a Monte Carlo dose engine based on

Monte Carlo Parameters	
Isotropic voxel spacing spacing (mm)	0.4
Variance reduction settings	
N split	200
NRCYCL	0
ihowfarless	off
Electron range rejection	on
ESAVE_GLOBAL (MeV)	1
DOSXYZnrc settings	
Global Ecut (MeV)	0.736
Global Pcut (MeV)	0.01
Zero dose to air	on
EGSnrc settings	
Boundary crossing algorithm	PRESTA-I
Spin effects	off
Brems angular sampling	Simple Koch-Motz
Brems cross sections	NIST
Bound Compton Scattering	Impulse approximation
Radiative Compton corrections	off
Pair angular sampling	off
Pair production cross-sections	Bethe-Heitler
Photoelectron angular sampling	off
Rayleigh scattering	on
Atomic relaxations	off
Electron impact ionization	off
Photon cross sections	xcom

Table 3-2: Parameters used for Monte Carlo simulation of TMI treatment plans is standard, following guideline of Precision Xrad SmART Inc.

EGSnrc/DOSXYZnrc(86, 87) for treatment planning; vendor recommended settings for Monte Carlo simulation can be found in **Table 3-2**: Parameters used

for Monte Carlo simulation of TMI treatment plans is standard, following guideline of Precision Xrad SmART Inc..

The energy spectrum used for the Monte Carlo dose calculation is shown in **Figure 3-4**. To plan the TBI treatments, three regions with parallel opposed beams (40x40 mm^2 square beams size) were used to cover the body, with the dose normalized to the center of the animal's body.

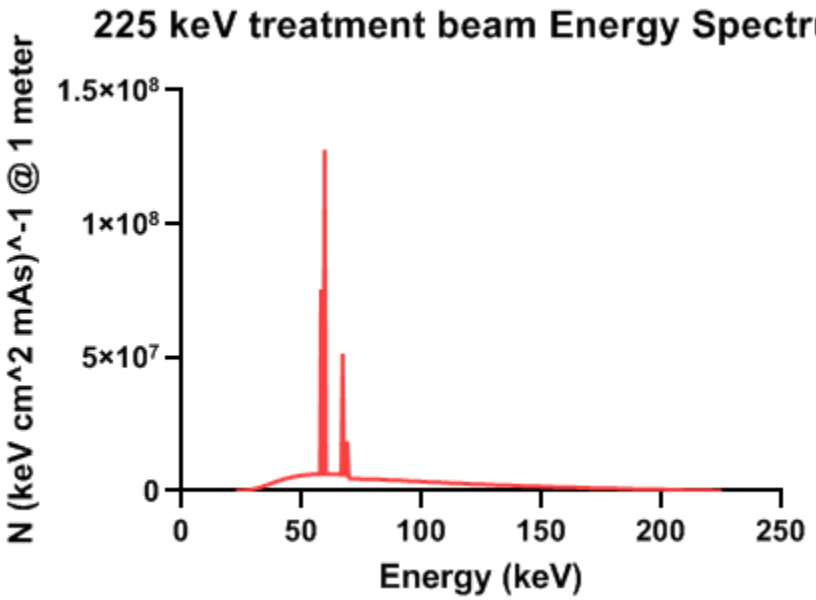

Figure 3-4: Energy spectrum of treatment beam used in Monte Carlo simulations. Generated with SpekCalc[1,2,3] for a 225 keV peak energy beam with 0.32 mm Cu & 0.8 mm Be filter. Assuming air thickness of 300 mm at angle of 20 degrees from the normal. The energy spectrum used to simulate TMI is given with a mean energy of 86.1 keV and effective energy of 78.8 keV.

3.2.7. TMI treatment delivery

Mice were treated in the prone position for all sessions. After creation of the TMI treatment plan, an individual mouse (placed in mouse holder under anesthesia) was repositioned on the center of table, guided by laser alignment as

described earlier for image scanning, to match the planning reference animal. CBCT or scout images of the treated mice were acquired and co-registered to the reference planning mouse using linear registration with the onboard registration software in the Precision X-ray system. The total treatment time for an 11 Gy TMI treatment was approximately 60 minutes. As a secondary goal, we further measured the effect of (a) mouse positioning on TMI dosimetry using female B6 mice aged 8 to 10 weeks with weights of ~20g, with TMI planning done in both prone and supine positions, and (b) animal size upon dose delivery using three sets of female B6 mice aged 6-15 weeks weighing 16-18g, 19-22g, and 29-31g, respectively, simulated in the prone position with TMI.

3.2.8. Dosimetric validation

Detail validation of Monte Carlo-based treatment planning system (TPS) including calculation of dose-to-medium were previously published (56, 88). Additional dosimetric validation was performed using the following steps: **(i) Film and dosimeter-based dosimetry:** A modified TMI treatment plan (quality assurance TMI) was made to verify the dose delivery. The mouse was placed along its side, and radiation was delivered perpendicularly to the sagittal plane to allow the use of Gafchromic^{TM} EBT3 films (Ashland Specialty Ingredients, Bridgewater, NJ, USA) (89). Prior to film calibration, dose output was verified with an ion chamber (PTW TN30013 Farmer Chamber, Freiburg, Germany) following TG-61, TRS-398 standard protocol. All dosimetric output measurements are performed semi-annually based on the advice of the manufacturer (90). Briefly, the film was calibrated for treatment settings at the isocenter up to 5 Gy. After

calibration, the film was placed under the mouse, and a tissue prescription dose of 2 Gy was delivered. Afterwards, different regions of interest were outlined on the film identifying the exit dose through spine, lungs, and gut to accommodate density variation in the path of the X ray. The mean dose measurement was compared with the treatment planning system at the film location to establish agreement. The film was included in the QA simulation and treated as water. We used 2 Gy for film validation so that the dose response was in the linear region of the EBT3 film. As a second form of dosimetric validation, optically stimulated luminescent dosimeters (OSLDs, Landauer, Inc, Greenwood, IL, USA) (91) were measured with a tissue prescription dose of 5 Gy. Two film profiles of a 2 Gy TMI QA can be seen in **Figure 3-5.** Here dose from the overlap regions can be observed as ~50% of the prescription dose. A higher dose of 5 Gy was used for verification to demonstrate the robustness of the TMI treatment delivery. OSLDs were calibrated with the treatment settings (225kVp, 13mA) and then placed underneath the animal along the gut and spine. As with the film, OSLDs were included in the simulation with the measurement point treated as a medium of water.

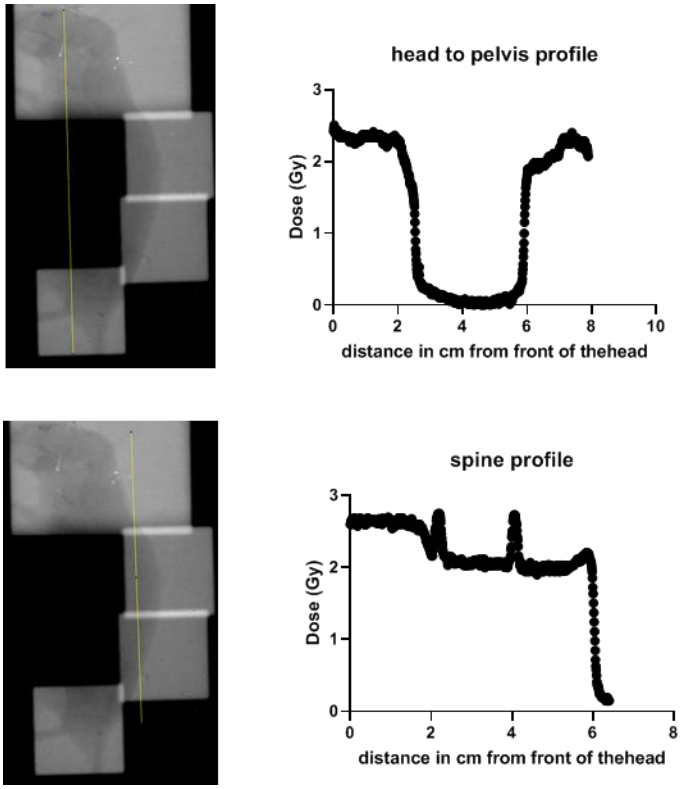

Figure 3-5: Film profiles of TMI QA treatment plan

(ii) Bone and marrow dosimetry: To the best of our knowledge, there is no currently available method in a preclinical system to directly measure dose deposition within the bone and marrow regions with consideration of heterogeneous tissue material for low-energy radiation beams. Overcoming the limitation of assessing dosimetry in bone and marrow regions, a 3D bone and marrow mimetic phantom was developed to study the dosimetric profile between bone and marrow. It was made with polycaprolactone (PCL), β-tri-calcium phosphate and poly (lactic-co-glycolic acid) (PLGA*)* -hydroxyapatite (HA) composite materials. These materials are biocompatible and osteoconductive (92, 93). The outer wall of the bone phantom is made of PCL polymer for providing rigidity (with high tensile strength of 16 MPa and tensile modulus of

0.4 GPa) to the bone phantom. PCL is highly hydrophobic and has longer degradation times than PLGA. β-tricalcium phosphate was added to PCL for alveolar bone augmentation and architectural stability. These materials were carefully heated to a molten solution, cast into desired molds, and characterized using a scanning electron microscope. The inner wall of the bone phantoms was coated with a 1 mm thick layer of PLGA-HA composite material. The fabricated BM phantom average Hounsfield unit (HU) was measured (996 ±130) and found to be within the range of normal bone density values. BM dose *in vivo* was evaluated by imaging the mouse pelvis and spine region with 0.1 mm voxel CT scans and planned with 150 µm dose grids. For the BM cylindrical phantom, a parallel opposed beam (20x20 mm^2) was used from the side, and dose was normalized (11 Gy) at the center (bone marrow) of the phantom.

3.2.9. Survival Study

Mice were randomly distributed to different groups and exposed to different regimens and followed for survival. TBI (11 Gy), TMI 1 (11 Gy), TMI 12 Gy and TMI 14 Gy were delivered in single fraction, while TBI, TMI _0, TMI 1 + 4GY, TMI 1 + 6GY and TMI 14 Gy were delivered in two fractions at 6h difference. Mice were then followed for survival.

3.2.10. TMI treatment plans used for assessment of engraftment in a congenic BMT model

A congenic BMT model was carried out by transplanting donor C57BL/6 (CD45.2) BM cells in irradiated recipient CD45.1 B6 mice. For initial TMI-based engraftment assessment, 4 separate treatment plans (TMI 1, TMI 1 + 2GY, TMI 1

+ 4GY, and TMI 1 + 6GY) were generated. TMI 1 is the treatment plan where the bones receive the prescription dose (11 Gy) while the rest of the body receives as low as reasonably achievable dose (this dose is due to their proximity to the beams placed in TMI plan). TMI 1 + 2GY, TMI 1 + 4GY and TMI 1 + 6GY are treatment plan where mice are deliberately treated with 2 Gy, 4 Gy and 6 Gy TBI respectively, and TMI doses were varied to maintain 11 Gy prescription dose to the bones. Alternative simplified description is following, (TMI 1: TMI 11 Gy + TBI 0 Gy); (TMI 1 + 2GY: TMI 9 Gy + TBI 2 Gy); (TMI 1 + 4GY: TMI 7 Gy + TBI 4 Gy) and (TMI 1 + 6GY: TMI 5 Gy + TBI 6 Gy). Subsequently, treatment was delivered (in two fractions, 6h difference) and engraftment differences was evaluated between different TMI treatments using bioluminescence imaging (BLI) and compared it with TBI (11 Gy). We selected two TMI treatment groups TMI 1 and TMI 1 + 4GY for long-term engraftment and secondary bone marrow transplant studies. Three days post BMT, small intestines were harvested, and histological analysis was carried out. For non-invasive assessments of BM cells engraftment, whole body BLI imaging was performed. The details are in the supplement.

3.2.11. Comparative evaluation of dose coverage between preclinical and clinical TMI

To compare preclinical dosimetry with clinical systems, we reviewed ten published articles in which patients with leukemia were treated with TMI techniques using either helical tomotherapy (Tomotherapy Inc, Madison, WI, USA) or volumetric arc therapy (VMAT) linear accelerators. Among the available literature, we selected 10 previously published papers on TMI to obtain

dosimetric coverage to various organs such as the skeleton, gut, lungs, kidneys, liver, and spleen (73, 94-100). Among these centers, some centers recruited patients for dose escalation studies with the goal of reducing relapse, whereas other centers used the technique to reduce organ exposure but to maintain the same prescription dose. Since prescription dose varies across centers, we tabulated the relative dose exposure to organs with respect to the prescribed dose and compared with the relative dose exposure obtained in our preclinical TMI model.

Statistical analysis was performed using the 2-tailed unpaired *t* test, and multiple group comparisons were performed with a one-way ANOVA test correcting for multiple comparisons. Data are presented as the mean ± standard deviation or standard error measurement. The difference was considered significant when the p value was <0.05. Statistical analyses were generated using GraphPad Prism software (GraphPad Software Inc. La Jolla, CA, USA). ns=not significant, *=$p<0.05$, **=$p<0.01$, ***=$p<0.0005$, ****=$p<0.00005$.

3.3. Results

3.3.1. Pre-imaging setup and identification of sensitive organs

Images of the custom-made treatment bed are presented in **Figure 3-2**: Custom-designed mouse holder base used in TMI treatment with a mouse placed in the chamber (base and transparent air-tight cylindrical chamber) to maintain continuous and homogeneous flow of isoflurane during TMI treatment delivery. The absolute displacement was reduced from 2.8 ± 1.1 mm using the standard bed to 1.5 ± 0.7 mm using the customized holder (n = 5). Reducing

displacements would reduce dose delivery uncertainty as the dose volume histogram (DVH) showed a high radiation dose gradient for the target. The holder allowed for less position verification imaging and repositioning compared to that in the standard bed, which reduced set up time between treated animals to about 10 minutes.

Although CBCT provided a suitable contrast for skeletal tissue, there was limited contrast for soft tissue in the CBCT, thereby limiting the ability to visualize the spleen, an extramedullary hematopoietic organ, which was part of the target. To accurately identify the spleen, we used the eXIA^{TM} 160 on a subset of mice to observe the spleen for the planning target volume. Visualization of the the eXIA^{TM} 160 contrast on whole body CT images scanned at four different time points are shown in **Figure 3-6**. **Figure 3-6** showed contrast uptake by different organs over a 24 hour period, suggesting that a CT image, one hour post contrast injection, will provide maximum contrast for organ delineation. Accordingly, 3D organs were contoured for treatment planning as shown in **Figure 3-8.**

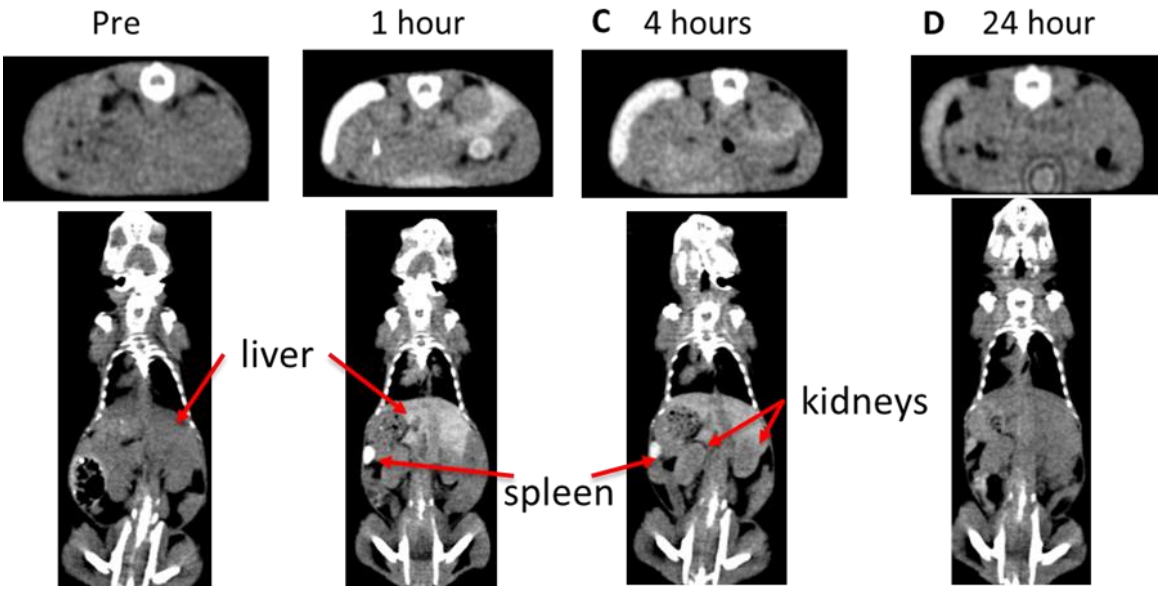

Figure 3-6: **A-D)** The contrast agent eXIA^{TM} 160 was injected via tail vein, and in vivo time-lapse CT imaging was carried out at different time points. Representative CT images taken at different time points are shown: **A)** prior to injection, **B)** 1h, **C)** 4h **E)** 24h after injection.

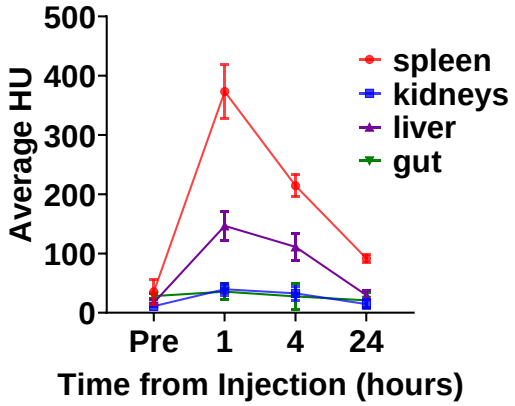

Figure 3-7: The change in Hounsfield Units over the course of 24h after injection is shown (n=5)

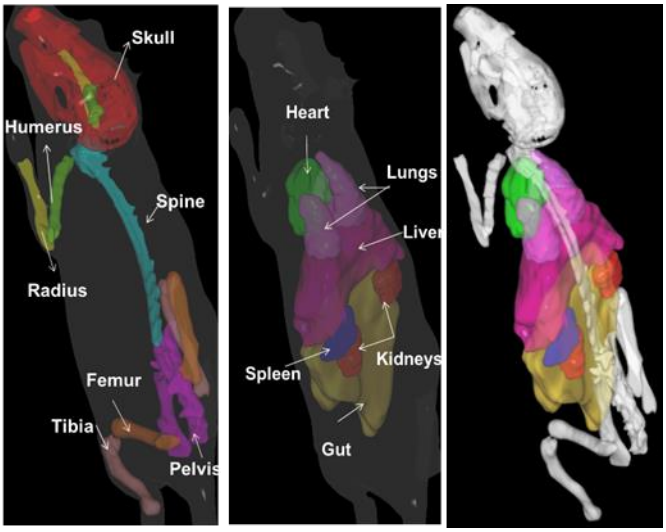

Figure 3-8: Mouse contour (3D) showing skeletal tissue and vital organs, used in developing the TMI treatment plan

3.3.2. Dosimetric validation of TMI

Figure 3-9 displays a fluoroscopic image of a mouse with beam layout for TMI quality assurance testing with the 3 regions (spine, lungs, gut) used for measuring agreement between Monte Carlo simulation and film dosimetry. As an alternative method, dose measured using OSLD detectors at the aforementioned locations were compared with the simulated dose as shown in **Figure 3-9F**. Film

and OSLD measurements were within ±5% accuracy of the simulated TMI dose calculation.

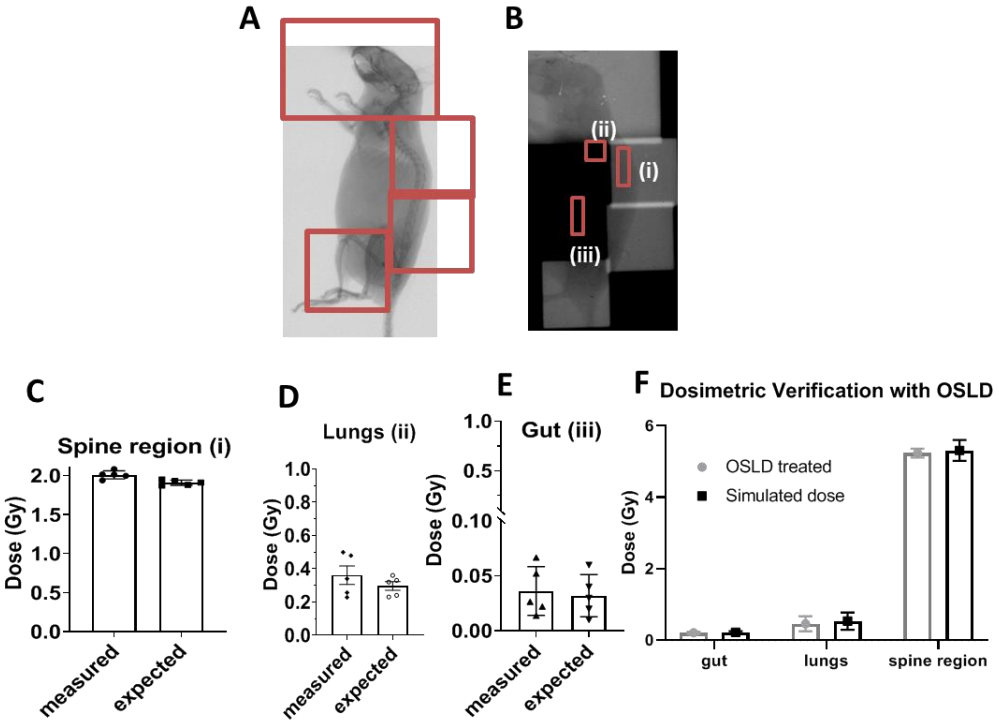

Figure 3-9: **A)** Fluorographic image displaying the animal position used for dosimetric verification with beam layout displayed in red. **B)** Gafchromic film used for dose verification (TMI dose delivered with 2 Gy) at three regions: **C)** spine, **D)** lungs and **E)** gut regions. Bar graphs displaying differences between measured and delivered dose to the Gafchromic film in spine, lungs and gut as identified in red in B. **F)** Bar graphs displaying differences between measured and delivered dose to the OSLD in same regions as described in B and C, delivered with 5 Gy

In vivo, dose profiles of bone and marrow at two regions, femur and spine, are shown in **Figure 3-10 A&B**. The dose profile for the BM phantom is shown in **Figure 3-11 A-C**. Both phantom and *in vivo* dose profile assessments revealed that the relative dose to the bone was 2.5 times higher than to the marrow dose (37 ± 3% n=5 mice, measured from contours of femoral bone and bone marrow). When the BM received an 11 Gy prescription dose, the mean dose absorption to

the bone was approximately 27.5 Gy. For in vivo biological dosimetry assessment, 2 days post TBI and TMI, mice BM cellularity was reduced by 86.9 ± 1.5% and 88.1 ± 0.7%, respectively, compared to unirradiated control mice (**Figure 3-12**). This result suggested that TMI delivery caused similar BM cytotoxicity when compared to TBI in the short term.

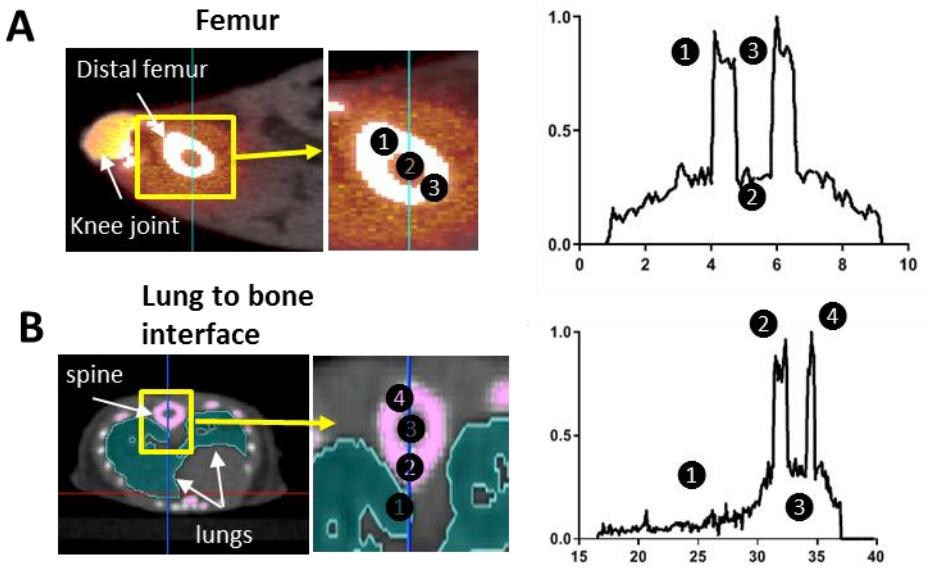

Figure 3-10: Dose painting location and corresponding dose profile across bone, marrow, and surrounding tissue regions in femur (**A**) and spine (**B**) region are shown. The dose calculation was measured using Monte Carlo planning system with grid size of 150 μm

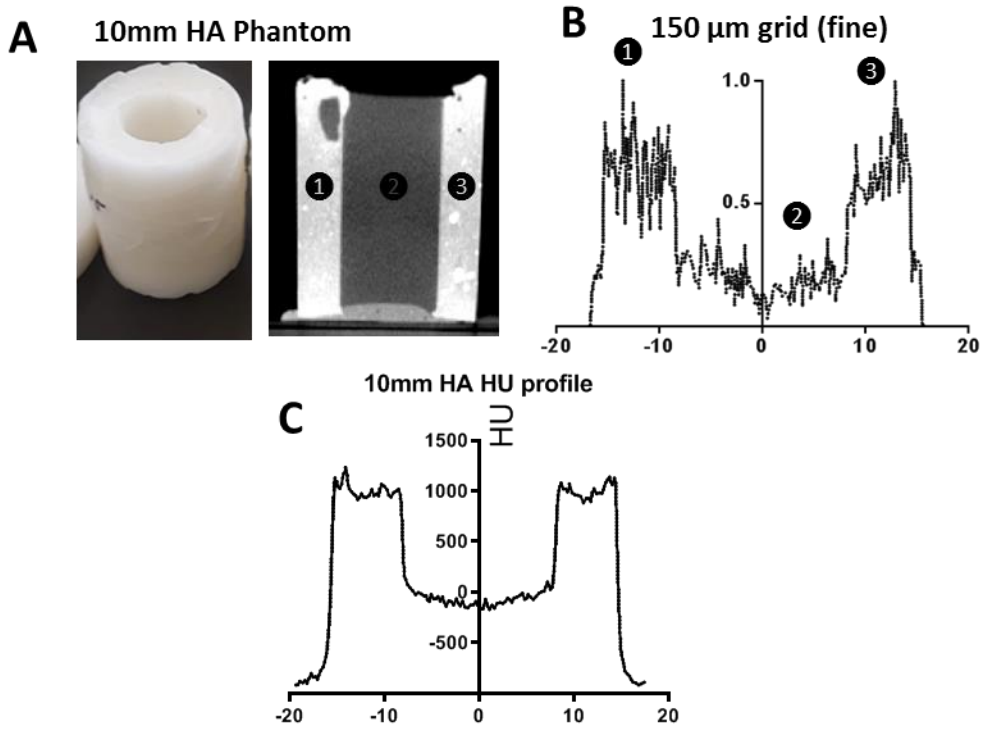

Figure 3-11: **A)** Bone and marrow mimetic phantom and **B)** dose profiles of this phantom filled with distilled water was measured using Monte Carlo planning system with dose calculation grid size of 150 µm. **C)** Hounsfield unit profile included

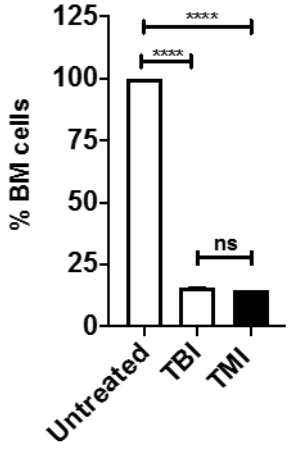

Figure 3-12: BM cellularity 40±4 h post TMI and TBI showed very similar reduction of BM cells in comparison to untreated mice BM, indicating similar BM damage.

3.3.3. TMI treatment planning and dosimetry

Schematics with demonstrations for parallel opposed beams in coronal view (**Figure 3-13A**), sagittal view (**Figure 3-13B**) and in a representative two cross-sectional views (**Figure 3-13 C&D**) presented the beam layout for a TMI treatment. Parallel opposed beams were used to create a homogenous dose toward the beam's overlapping center (bone marrow). The 3D dose distributions represented by the DVHs are shown for TMI 1, TMI 1 + 4GY, and TBI treatments (**Figure 3-13 E&F).** The dose statistics are shown in **Table 3-3** for 11 Gy TMI 1, TMI 1 + 4GY (TMI 7Gy + TBI 4Gy) and TBI treatment plans calculated on the same mice (n=5). The mean dose to the bone was within ±5% between TBI, TMI 1 and TMI 1 + 4GY. Spleen dose was 11 Gy, kept at the prescription dose. The lung mean dose was reduced by 57% for TMI 1 and 31% for TMI 1 + 4GY. The gut mean dose was reduced by 67% for TMI 1 and 43% for TMI 1 + 4GY. Finally, the liver mean dose was reduced by 65% for TMI 1 and 41% for TMI 1 + 4GY. About 40-60% of the volume of vital organs received less than 10% of the prescription (11 Gy) dose; however, the part of organs close to the placed beams in TMI 1 received a higher dose, thereby increasing the mean delivered dose to 30-40%. In TMI 1 + 4GY, roughly 40% of the vital organs received at least 50% of the prescription dose. Therefore, the mean dose value needs to be cautiously considered for TMI planning. The simulated TBI and TMI 1 treatment plans in the color wash are shown in **Figure 3-13G**. Mice position and weight had no impact on TMI dosimetry (**Table 3-4**).

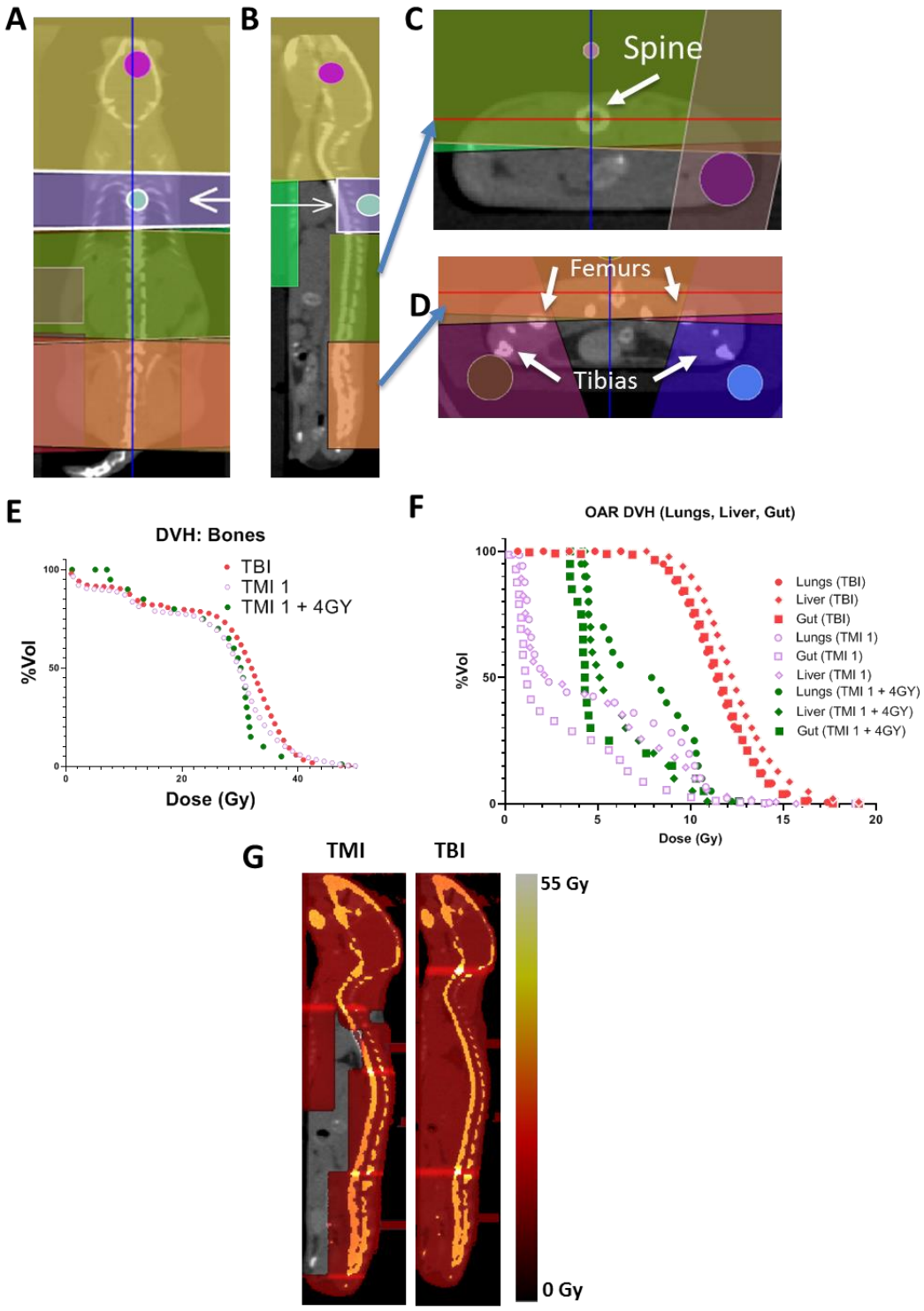

Figure 3-13: Beam arrangement for parallel opposed beams in coronal view **(A)**, sagittal view **(B)**, axial view at spine **(C)** and axial view at pelvis **(D)**. A representative DVH comparing TMI 1 and TBI plan for major organs viz., **(E)**, bones **(F)** gut, liver, and lung. **G)** Dose painting of TMI and TBI plan.

A

Organ	TBI	TMI 1		TMI 1 + 4GY	
	Dmean (Gy)	Dmean (Gy)	% Dose difference from TBI	Dmean (Gy)	% Dose difference from TBI
Bone (PTV)	27.5 ± 1.2	27.8 ± 1.6	1.1	26.5 ± 1.5	-3.6
Lungs	12.0 ± 0.7	5.1 ± 0.9	-57.5	7.5 ± 0.8	-37.5
Gut	11.5 ± 0.1	3.8 ± 0.9	-67.0	5.4 ± 0.1	-53.1
Liver	12.6 ± 0.2	4.4 ± 0.5	-65.1	6.0 ± 0.8	-52.4

B

Organ	TBI	TMI 1		TMI 1 + 4GY	
	D95 (Gy)	D95 (Gy)	% Dose difference from TBI	D95 (Gy)	% Dose difference from TBI
Bone (PTV)	1.4 ± 0.7	2.6 ± 3.4	85.7	7.6 ± 3.7	442.8
Lungs	8.8 ± 0.4	1.0 ± 0.1	-88.6	4.1 ± 0.3	-60.0
Gut	8.6 ± 0.1	0.7 ± 0.1	-91.9	3.5 ± 0.1	-59.5
Liver	9.4 ± 0.1	0.9 ± 0.1	-90.4	4.3 ± 0.1	-53.8

C

Organ	TBI	TMI 1		TMI 1 + 4GY	
	D80 (Gy)	D80 (Gy)	% Dose difference from TBI	D80 (Gy)	% Dose difference from TBI
Bone (PTV)	15.2 ± 3.1	19.6 ± 5.8	28.9	18.6 ± 4.3	22.4
Lungs	10.2 ± 0.5	1.5 ± 0.3	-85.3	4.5 ± 0.2	-55.9
Gut	10.0 ± 0.1	0.9 ± 0.1	-91.0	3.9 ± 0.2	-61.0
Liver	10.8 ± 0.1	1.3 ± 0.1	-88.0	4.4 ± 0.2	-58.3

D

Organ	TBI	TMI 1		TMI 1 + 4GY	
	D5 (Gy)	D5 (Gy)	% Dose difference from TBI	D5 (Gy)	% Dose difference from TBI
Bone (PTV)	40.2 ± 1.1	40.7 ± 2.9	1.2	37.1 ± 5.2	-7.7
Lungs	15.7 ± 1.3	11.3 ± 0.6	-28.0	11.1 ± 0.7	-29.3
Gut	14.6 ± 0.1	10.8 ± 0.9	-26.0	10.7 ± 0.2	-26.7
Liver	17.6 ± 1.3	11.3 ± 1.4	-35.8	10.1 ± 0.6	-42.6

Table 3-3: **A)** The mean delivered dose to target (bone marrow, spleen) and organs (lungs, gut and liver) was determined for the TBI, TMI 1 and TMI 1 + 4GY treatment plans. The % reduction in dose delivered was calculated using the TBI-delivered dose to the respective organs as reference. There was a significant reduction of dose delivered to lung, liver, and gut; however, dose delivered to bone marrow was similar between TBI, TMI 1 and TMI 1 + 4GY plans. **B-D**) The D95 (**B**), D80 (**C**), and D5 (**D**) for bones and other vital organs for TBI, TMI 1 and TMI 1 + 4GY plans. The dose values ± standard deviation was calculated for n=5 mice/group.

A

n=5	Dmean (Gy)			D95 (Gy)			D5 (Gy)		
	Prone	Supine	Signif?	Prone	Supine	Signif?	Prone	Supine	Signif?
Bone (PTV)	26.2 ± 1.5	26.2 ± 1.5	no	3.5 ± 4.2	3.5 ± 4.2	no	40.7 ± 2.9	40.7 ± 2.9	no
Lungs	5.1 ±0.8	5.6 ± 0.2	no	1.0 ± 0.1	1.1 ± 0.1	no	11.6 ± 0.4	11.2 ± 0.2	no
Gut	3.7 ± 0.7	3.3 ± 0.4	no	0.7 ± 0.1	0.7 ± 0.1	no	10.1 ± 0.7	10.7 ± 1.1	no
Liver	4.4 ± 0.5	4.5 ± 1.4	no	11.4 ± 1.3	1.0 ± 0.1	no	4.8 ± 3.9	12.7 ± 3.2	no

B

n=5	Dmean (Gy)			D95 (Gy)			D5 (Gy)		
	16-18g (4-6 weeks)	29g-31g (14+ weeks)	20g (8-10 weeks)	16-18g (4-6 weeks)	29g-31g (14+ weeks)	20g (8-10 weeks)	16-18g (4-6 weeks)	29g-31g (14+ weeks)	20g (8-10 weeks)
Bone (PTV)	28.5 ± 0.3	27.4 ± 0.6	26.2 ± 1.5	3.8 ± 3.2	1.3 ± 0.1	3.6 ± 4.2	42.2 ± 1.3	51.3 ± 4.6	40.7 ± 2.9
Lungs	5.2 ± 1.0	3.9 ± 1.0	5.1 ± 0.8	1.1 ± 0.2	1.1 ± 0.1	5.1 ± 0.8	12.0 ± 1.4	10.6 ± 1.5	11.6 ± 0.5
Gut	3.4 ± 0.6	2.7 ± 0.4	3.7 ± 0.7	0.6 ± 0.1	0.2 ± 0.4	0.7 ± 0.1	10.4 ± 0.3	10.4 ± 1.4	10.2 ± 0.7
Liver	5.1 ± 0.1	3.8 ± 0.5	4.4 ± 0.5	0.9 ± 0.1	0.8 ± 0.1	0.8 ± 0.1	12.1 ± 1.4	12.7 ± 0.8	11.4 ± 1.3

Table 3-4: For an 11 Gy reference plan **A**) Table comparing prone and supine position effect on TMI planning, **B)** Table comparing age and weight effect on TMI planning

3.3.4. Comparative evaluation of preclinical to clinical TMI

Comparison of preclinical TMI plan dosimetry to clinical results is shown in

Figure 3-14. Mean dose reductions were observed for many sensitive organs

(heart, lungs, liver, and gut), while a similar dose was maintained for the spleen and skeleton. The exception were the kidneys, which showed a relatively higher dose in preclinical model, because kidneys fell within the primary radiation beam due to their proximity to the spine. Future development toward a multi-leaf collimator in preclinical treatment is expected to reduce radiation exposure to organs by considering their size, shape, and proximity to the target. **Figure 3-15** displays a region by region breakdown between preclinical and clinical TMI with their respective DVHs for comparison.

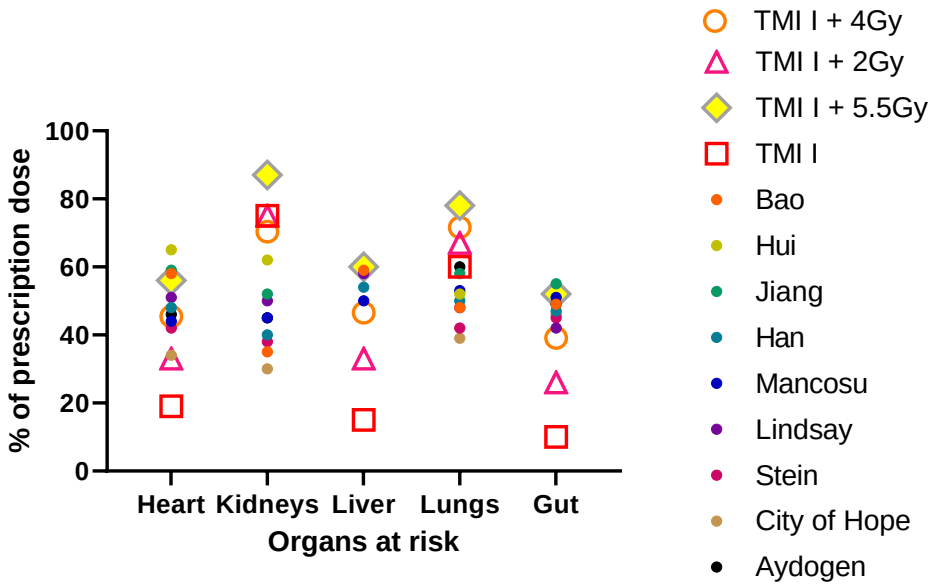

Figure 3-14: Preclinical and clinical dosimetric comparisons**:** Dosimetric comparison between 10 preclinical and 10 clinical TMI cases. Median dose difference represented as a percentage of the prescription dose. Regions of interest are the heart, lungs, liver, spleen, gut, kidneys

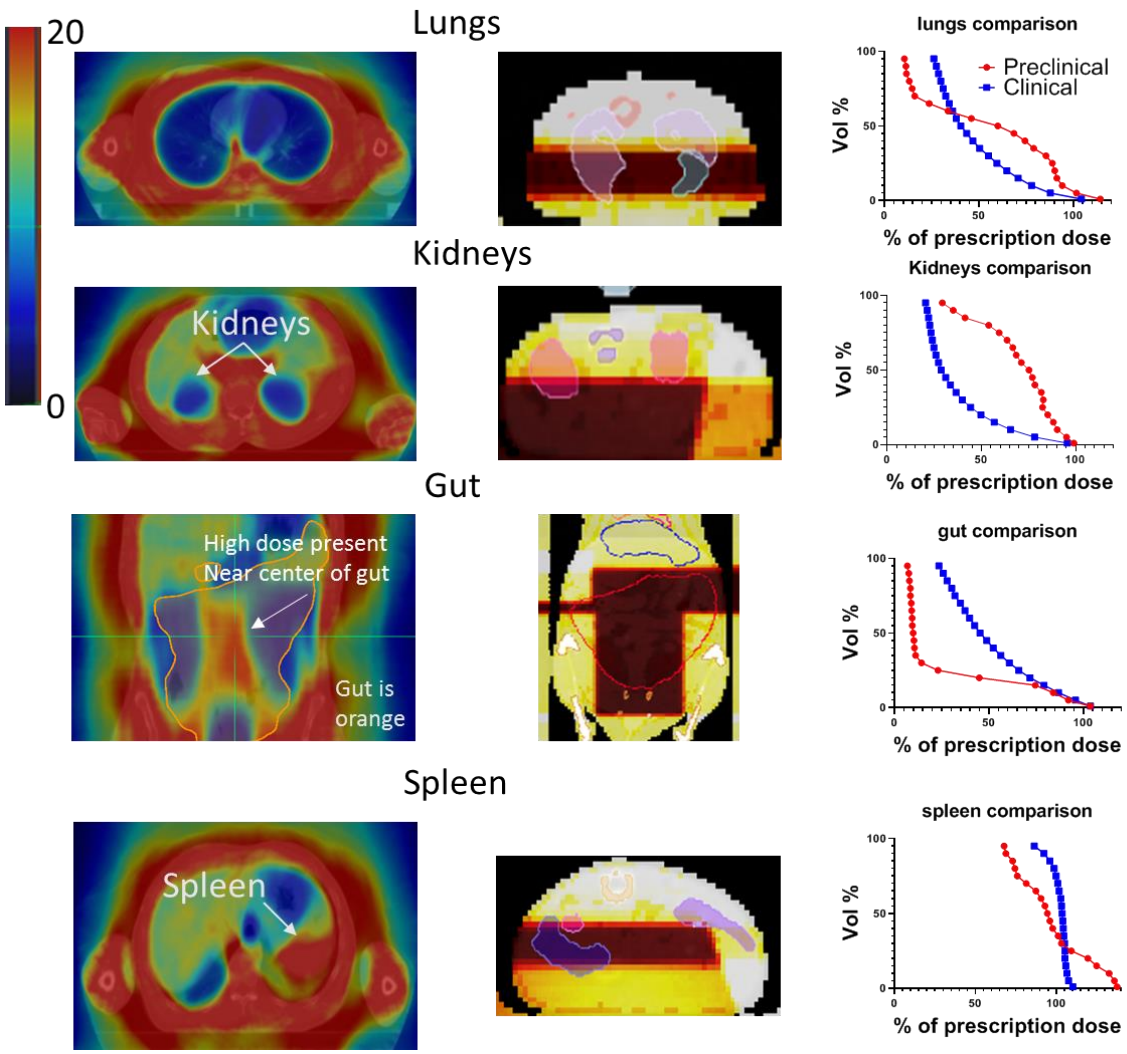

Figure 3-15: Regional analysis of clinical to preclinical TMI 1 with resulting DVHs for: lungs, kidneys, gut, and spleen. Red is preclinical and blue it clinical on the DVH.

3.3.4.1. Lungs

The mean dose of the lungs is higher in preclinical compared to the clinical by 7-8%. This higher dose can be seen in the DVH with the preclinical treatment depositing more dose in the lungs at 60% of the organ volume. This higher dose is deposited in the posterior part of the lungs i.e. region close to the

spine. Most of this dose is secondary scatter but there is some primary beam “clipping” causing the mean dose to rise.

3.3.4.2. Kidneys

Mean dose in the kidneys for preclinical TMI is 32% higher when compared with clinical. 50% of the organ volume is on average 75% of the prescription dose. The location of the kidneys close of the lumbar spine target means a portion of the kidneys fall within the primary beam. The isocenter is moved to a virtual isocenter above the spine to minimize kidneys dose while still maintain at 80% of prescription dose to the spine. Kidneys will remain problematic for 3D TMI treatments until the development of more precise radiation delivery tools.

3.3.4.3. Gut

The mean preclinical gut dose is half of the mean clinical gut dose. From the DVH, 75% of the organ is receiving as little as 10% of the prescription dose. This contrasts with the clinic where 50% of the organ is receiving 50% of the prescription dose. There are differences in gut dose distribution, most of the clinical gut hotspot is located within the organ center in the large intestine. For preclinical most of the prescription dose lies away from the midline of the gut with a portion of the small intestine receiving damage.

3.3.4.4. Spleen

There are several reasons to target spleen as it a large reserve of Hemopoietic stem cells (HSC). Spleen treatment in clinical TMI is conformal with

the D90 hitting 90% of the organ volume. Preclinical spleen dose however dose not achieve a D90 dose coverage till 60% of the organ volume. In addition, 35% of the organ is receiving over 100% of the intended dose. This is due to the beam location for the spine intersecting the spleen. For preclinical treatment a second boost beam is applied tangent of the animal body to ensure at least 50% of the organ is receiving 90% of the dose. TMI maintains long-term engraftment with reduced organ damage.

TMI maintains long-term engraftment with reduced organ damage

We asked whether the commonly known myeloablative TBI dose (~11 Gy in C57BL/6) was similar to TMI for survival. Surprisingly, unlike TBI (14 days) where 11 Gy was completely lethal, TMI with a 11 Gy prescribed dose to the target and avoidance of dose to the rest of the body (TMI 1) was well tolerated and conferred survival for more than 100 days, indicating autologous recovery of BM. Therefore, we increased the dose of TMI and found that TMI 14 Gy (15 days) was lethal while TMI 12 Gy (79 days) was sublethal **(Figure 3-16A**). However, TMI (11 Gy) with a reduced body dose (4-6 Gy) was lethal (12 days) (**Figure 3-16A**). The survival of the mouse was similar whether the radiation was given in one single dose or in 2 factions 6h apart. The two-fraction regime was considered for rest of the study.

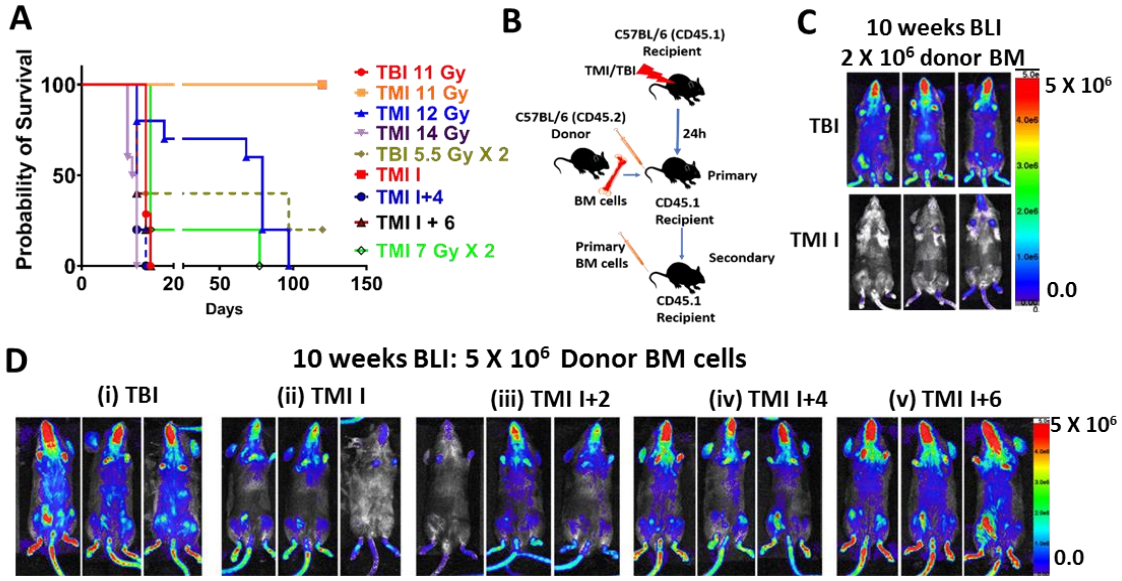

Figure 3-16: **A)** Survival curve showing that myeloablative dose of radiation for B6 mice was higher when radiation was delivered by TMI (14 Gy) than TBI (11 Gy). **B**) Schema of congenic primary and secondary bone marrow transplant (BMT) study. **C**) CD45.2 B6-Luciferase+ donor BM cells (2 million) engraftment 10 weeks post BMT by BLI. **D**) Donor cell engraftment in mice treated using different forms of TMI by varying doses to body (TMI I:0 Gy body; TMI I + 2: 2 Gy body; TMI I + 4; 4 Gy body; TMI I + 6: 6 Gy body). CD45.2 B6-Luciferase+ donor BM cell (5 million) engraftment 10 weeks post BMT by BLI.

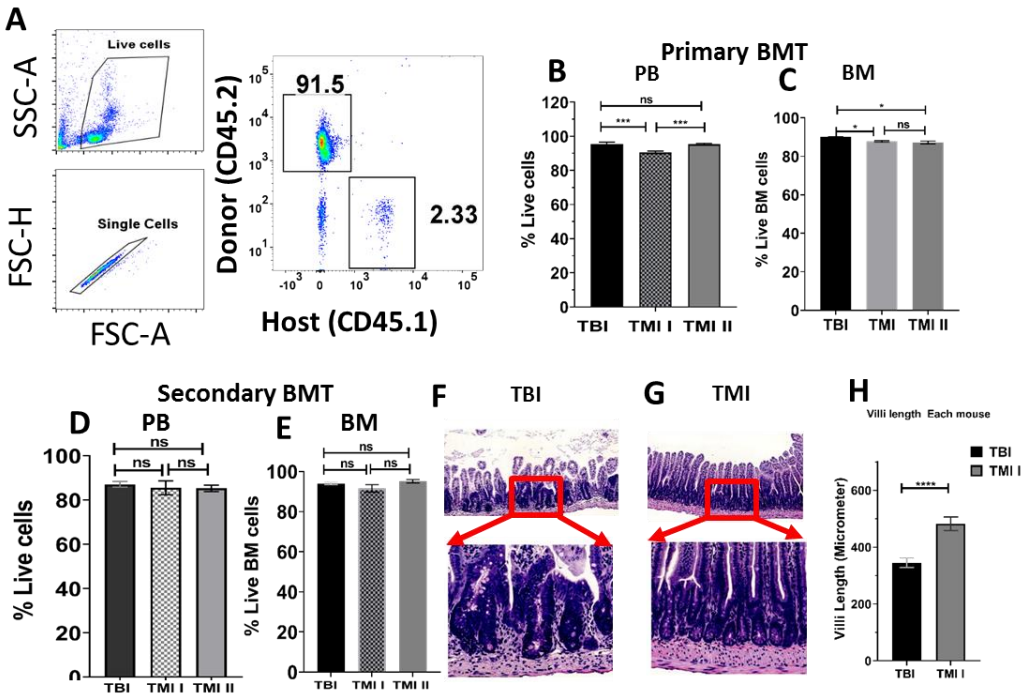

Figure 3-17: **A**) Flow cytometry analysis and donor cell gating in TBI and TMI treated mice. **B)** The donor cell engraftment in peripheral blood (PB); 10 weeks post BMT and **C)** BM 25 weeks post BMT. Secondary BMT mouse showed similar donor engraftment in **D)** PB and **E)** BM between mice transplanted with primary BM cells from TBI, TMI I and TMI I + 4 treated mice (n=5). Representative images of H&E-stained small intestine sections 3 days post BMT from TBI (**F**) and TMI I (**G**) treated mice. Enlarged portion of the small intestine showing blunting of villi and crypts hyperplasia in TBI treated mice while TMI treated mice showed normal gut morphology. **H**) Average villi length (micrometer) for TBI and TMI treated mice (n≥3 mice)

Next, we evaluated the effect of TMI on long-term engraftment in the congenic mouse BMT mouse model. The recipient mice (CD45.1; C57BL/6) were transplanted with donor marrow cells (CD45.2) 24h post radiation as shown in the schema (**Figure 3-16B)**. BLI based non-invasive assessment of donor cell engraftment shows that TMI I treated mice failed to engraft when 2 million donor BM cells was given, whereas TBI-treated mice engrafted successfully (**Figure 3-16C**). We hypothesized that since TMI 11 Gy dose to the bone marrow was not

myeloablative more donor cells may be required to ensure engraftment. Increasing the donor BM cells to 5 million cells improved BM engraftment; however, engraftment was relatively lower than in TBI-treated mice (**Figure 3-16 D (ii)**). We also analyzed engraftment in mice treated with TMI and with a partial body dose. TMI with a body dose of 0 and 2 Gy (TMI I and TMI I+2) (**Figure 3-16D ii, iii**) had slightly reduced engraftment. However, a body dose of 4 Gy and 6 Gy (TMI I+4 and TMI I+6, respectively) ensured engraftment similar to TBI (**Figure 3-16D (i, iv, v)**). Therefore, we chose TMI I+4 for further study. Additionally, a further increase in the number of donor BM cells to 10 million showed ~90% engraftment in the peripheral blood of TMI I, TMI I + 4 and TBI treated mice by ~10-12 weeks post BMT (**Figure 3-17A-C**). The long-term engraftment analysis in the BM at 25 weeks post BMT showed that all mice groups engrafted donor BM cells similarly (**Figure 3-17C**). A secondary BMT, using BM cells from the primary TBI, TMI I and TMI I + 4 treated mice showed similar donor cell engraftment in PB and BM (**Figure 3-17D-E**) in the secondary recipient mouse, suggesting similar long-term repopulating ability for all three groups.

In assessing post BMT acute gut damage, three days post BMT, TMI-treated mice gut showed mostly normal mucosal lining. The TBI treated mice mucosa shows villous blunting and crypt hyperplasia, as well as glandular drop out (**Figure 3-17F-G**). The height of the villi is shorter in the TBI setting (blunting) (**Figure 3-17H**) and there are fewer villi per area (drop out), relative to TMI. At the higher magnification (H&E, 200X magnification), the crypt in the TBI sample

shows crowding of the crypt lining cells (**Figure 3-17H**). This result clearly indicates that TMI, similarly to TBI, maintains suitable engraftment post BMT, however with the added advantage of reduced organ damage.

3.4. Discussion

Innovations of image-guided TMI and its translation from the bench to bedside have facilitated the exploration of precision radiation treatment as a conditioning regimen for bone marrow transplantation in hematological malignancies (42, 47, 53, 73, 74, 94, 101) . However, a lack of a preclinical high-precision TMI model impedes mechanistic understanding and investigation of experimental therapeutics. We developed and comprehensively characterized a novel multimodal image guided preclinical TMI 3D model, which can deliver precise radiation to the mouse skeletal system while reducing dose exposure to vital organs, an approach not achievable in standard TBI. Furthermore, we evaluated the impact of TMI with varying radiation dose exposures to the body in a congenic BMT model.

3.4.1. Scientific and dosimetric development of Preclinical TMI

The described preclinical TMI development overcame several limitations by integrating several technological and computational advancements. The contrast enhanced whole body CT imaging and whole body MRI were employed to obtain 3D anatomical details of target and vital organs. The CT-guided Monte Carlo dose calculations accounted for tissue heterogeneity, enhancing accuracy of organ dose evaluation. Furthermore, onboard CT imaging allowed geometric verification and adjustment of mice prior to treatment delivery to ensure accurate

dose delivery. The 3D dose painting in a color map used in our model allowed visualization and inspection of dose coverage to targets and vital organs, as well as identifying locations of higher dose or hot spots due to overlap of the beam and underdoses due to gaps in beam placement. Hotspot management (in vital organs like the lungs) was essential for TMI treatment delivery. Furthermore, anatomically specific volumetric information allowed generating organ-specific DVHs, a quantitative radiation parameter that could be experimentally varied to measure treatment response, organ-specific toxicities, and immune modulation. This factor could also be exploited for inhomogeneous distribution and tumor heterogeneity (102). Taken together, overall, our preclinical TMI model allowed a high-precision dose optimization for targets such as bone, bone marrow, and spleen and non-target vital organs including lungs, liver, and gut. Lastly, dosimetric similarities and equivalence of our preclinical model to the clinical studies suggested that our model may be used for future clinically relevant investigations.

Although the TBI mouse model has been used for over 6 decades for biological investigations, the dose has not been calculated with consideration of tissue heterogeneity. In addition, TBI dose calculations for human studies have been performed without tissue heterogeneity. In human TBI treatment, a high energy (6 MeV linear accelerator, effective X ray energy ~ 1300 KeV) X-ray beam is used, whereas in mouse TBI, the commonly used method is a low-energy X-ray irradiator. However, there is a relatively high dose to bone medium in mice during exposure to low energy, which is due to the following two reasons

(103, 104): a) The characteristic energy spectrum used for TMI or TBI treatment has a mean energy of 86.1 keV and effective energy of 78.8 keV (Supplementary Fig. S1),(105, 106) and b) the photoelectric absorption for this energy in bone medium is high (88), as the photoelectric mass coefficient is proportional to atomic number and energy:

$$\frac{\tau}{\rho} \propto \left(\frac{Z}{h\nu}\right)^3$$

where $\frac{\tau}{\rho}$ is the photoelectric mass attenuation coefficient, Z is the atomic composition of the medium, and hv is the energy of the incident photon. To the best of our knowledge, there is no currently available method in a preclinical system to directly measure dose deposition within the bone and marrow regions with consideration of heterogeneous tissue material for low-energy radiation beams. In our model, a sharp dose variation in the BM junction was evident from our BM mimetic phantom and was corroborated with the dose profile generated from treatment across the femoral cross section (**Figure 3-10 & Figure 3-11**). Therefore, when the mouse BM received 11 Gy in our study, the dose to bone was much higher (~27.5 Gy) using an X-ray irradiator. However, 11 Gy TBI has been commonly used in preclinical studies, without the realization that bone dose was much higher. The results from our preclinical model indicated the potential for inadvertent bone damage from TBI treatment. Therefore, caution should be taken when we use TMI to escalate BM dose to complement our clinical dose escalation studies and/or to eliminate remaining BM cells; bone damage should be carefully monitored.

3.4.2. Role of Preclinical TMI in future biological studies

During survival assessment, we found that mice treated with TMI 11 Gy survived for more than 100 days, implying autologous BM recovery, while TBI 11 Gy was lethal. Among several reasons, one possible explanation is that unexposed lymph nodes, liver, and other organs provide a supportive environment to BM cells for autologous transplant after application of 11 Gy TMI. Therefore, we used different TMI doses and found that a TMI dose of up to 14 Gy was needed to ensure lethality in mice. How organ damage plays a role in engraftment will require future thorough investigation. However, 48h post 11 Gy, both TMI and TBI treated mice showed significantly reduced BM cellularity (~10%) (**Figure 3-12**), suggesting early damage to BM was very similar. Furthermore, as shown in the DVH (**Figure 3-13F**), the dose given for vital organs (gut, liver, lung, etc.) in the TMI model was significantly reduced from that in TBI, suggesting that the lethality may be a compound effect of BM failure and organ damage.

Additionally, increased donor BM cells (up to 10 million cells) was required for successful donor engraftment in TMI I treatment. However, a partial body dose of 4-6 Gy in addition to 11 Gy to the BM ensured better engraftment. Therefore, these results warrant more studies to understand the role of various organs in BM recovery and long-term engraftment post BMT. Our TMI model will provide an opportunity to decipher the individual organ role in autologous BM recovery/graft rejection, and effects of BM-specific dose escalation. Furthermore, TMI showed similar long-term engraftment as compared to TBI (**Figure 3-17B-**

E), and temporal profiling indicated donor engraftment was complete by 8 weeks and was stable over the long term (25 weeks). Therefore, the TMI model may be an alternative preclinical transplantation conditioning approach to TBI.

3.4.3. Technical limitations of current preclinical TMI model

Clinical TMI went through several developments, making the system user friendly, and exploration of appropriate applications to show its benefit led to more centers adopting this technology. At the same time, there are several limitations to our first preclinical TMI 3D model. It requires technical expertise to utilize whole body CT and MR imaging, identify and contour organs, and perform treatment planning and delivery. Moreover, treatment time is significantly longer than with TBI. We expect to adopt several technological developments to make the system robust, user friendly, and reduced in overall treatment time (54, 55). Among several approaches, custom-built mouse holders, atlas-based automated contouring of target and organs, automated selection of the radiation field, and multi-leaf collimator based intensity modulated radiation would help to reduce the time needed for the treatment and would enhance precision dosimetry, which will be incorporated to the preclinical platform over time.

3.5. Conclusion

In conclusion, our novel preclinical image-guided 3D TMI model could be used as a new method for delivering radiation with high accuracy to geometrically and functionally complex targets, while reducing or sparing radiation to vital organs to preserve their functions. The model provides robust evidence of long-term engrafted BM and reconstitution ability. Thus, our new high-precision TMI

preclinical model potentially enables the reverse translation of clinical data to improve mechanistic studies, ultimately leading to clinical development of potentially safe, effective, and durable therapeutic interventions for malignant and non-malignant hematological disorders.

Chapter 4. Preliminary radiobiological assessment of lung toxicities following Preclinical TMI treatment

4.1. Introduction

Normal lung tissue tolerance constitutes a limiting factor in TMI. Interstitial pneumonitis (IP) and radiation-induced lung fibrosis (RILF) are critical determinant for acute and late normal tissue complications. An estimated 25% of all BMT patients will die of IP (107). One of major goals of TMI planning is limiting the risk of lung damage. Previously we have investigated this from a clinical perspective by single point dosimetry and mean lung dose (67, 68). Computed tomography (CT) based treatment planning can provide a detailed calculation of dose delivery to the lung. However, a lack of advanced pre-clinical technology regulated the TMI animal model to film-based 2D organ dosimetry. As outlined in Chapter 3, recent developments in preclinical technologies have allowed for the 3D imaging of animal organs with Monte Carlo based radiation treatment planning. This allows for 3D organ dosimetry with the generation of a dose volume histogram (DVH), a necessary component of radiobiological modeling. Using this new platform can enhance the understanding of complex biological systems as well as perform detailed organ dosimetry. With this platform, we assessed the lung potential lung toxicities of the preclinical platform using a series of established models for both mice and humans.

Due to the 3D CT images used in planning we can access lung dose risk using modern dosimetric analysis such as the concept of equivalent uniform dose

(EUD) (108). The concept of equivalent uniform dose (EUD) assumes that any two dose distributions are equivalent if they cause the same biological effect. Based on the 3D dose distribution or DVH the EUD can be calculated and used to estimate the tumor control probability (TCP) and normal tissue control probability (NTCP) (109). Through the assessment of the TCP/NTCP preclinical treatment plans can be optimized to better improve the therapeutic window (difference between TCP & NTCP).

Currently, there is a worldwide effort to adopt TMI. However, many of these centers use different treatment setups with a wide range of fractionated schemes and prescription doses (110). Investigating these differences in a preclinical model can assist in the standardization of TMI. In addition, one of the major goals of clinical TMI treatment development is escalating the prescription dose. Initial clinical trials have demonstrated that dose escalation has an overall improvement of the survival rate (69). Additional, previous work on radiation treatment of Acute myeloblastic leukemia (AML), on the most common forms of leukemia, has demonstrated large variations in cell sensitivity (111). Given all these varying factors and the desire to use the preclinical TMI platform for a variety of biological work there exists a need for a robust risk assessment radiobiological model for preclinical TMI.

4.2. Methods

4.2.1. Using Equivalent Uniform dose for TCP / NTCP calculations

The EUD is a mathematical model derived based on a mechanistic formulation using a linear-quadratic cell survival model (108).

$$EUD = (\sum_{i=1}(v_i D_i^a))^{\frac{1}{a}}$$

The EUD can be used for both tumors and normal tissues, where a is a unitless model parameters that is specific to the normal structure or tumor of interest, and v_i is unitless and represents the i^{th} partial volume of the whole structure of interest corresponds to 1, the sum of all partial volumes v_i will equal 1. D_i represents the dose of the i^{th} partial volume. The parameter a will determine the behavior of the EUD-based model. Typically, the local control for tumors will depend on the volume that received the minimum dose. For normal tissues that exhibit a large volume effect the dose response may be closer to the average dose.

To calculate the EUD based NTCP, Niemierko proposed using the logistic function (112):

$$NTCP = \frac{1}{1+\left(\frac{TD_{50}}{EUD}\right)^{4\gamma_{50}}}$$

TD_{50} is the tolerance dose for 50% complication rate at a specific time interval. γ_{50} is a unitless model parameter that is specific to the normal structure or tumor of interest and describes the slope of the dose-response curve. γ_{50} has a value of 4 for late effects and a value of 2 for tumors. The parameters of a and γ_{50} are obtained by experimental result by fitting dose response data to the EUD TCP/NTCP results.

To calculate the EUD based TCP:

$$TCP = \frac{1}{1+\left(\frac{TCD_{50}}{EUD}\right)^{4\gamma_{50}}}$$

The TCD_{50} is the tumor dose to control 50% of the tumors when the tumor is homogeneously irradiated.

4.2.2. Interstitial pneumonitis model in humans

Interstitial pneumonitis modeling	
Model used	Safwat
a	1
γ50	2
TCD50	12
# of fractions	single
alpha / beta ratio	2.8

Table 4-1: Settings used for three different Pneumonitis models

We applied the concept of EUD to calculate TCP and NTCP on 5 TMI treated mice to observe the changes in lung dose as a function of NTCP using a free software developed by Niemierko, et al. (112). Given are 3 cases of TBI/TMI treatment: 1) standard TBI, 2) TMI1 (100% TMI), 3) TMI2 (50% TMI, 50% TBI). Each case was simulated with prescriptions of 11Gy and 22Gy to simulate risk with dose escalation. The mice used where female Jackson B6 aged 8-12 weeks weighing approximately 20g. **Table 4-1** lists the parameters used for interstitial

pneumonitis endpoint simulation which are based on the work by Safwat, et al. (113) . The single fraction animal TBI model and a non-chemo model are used for the purposes of lung NTCP modeling. A gamma of 2 is used for all modeling as is recommend from Emami (114) and Niemierko (108). Safwat does not report an alpha-beta in his work so the reported alpha-beta from Sampath (2.8) is used.

4.2.3. Lung fibrosis model in mice

Lung fibrosis calculations were done using work established by Zhou (115). Setting used for simulation are given in **Table 4-2**.

Lung Fibrosis		
Model used	Zhou - 1	Zhou - 5
a	1	1
γ50	4	4
TCD50	14.55	27.7
# of fractions	single	5
alpha / beta ratio	4.4879	3.9474

Table 4-2: Table of modeling parameters used for fibrosis outcome

4.3. Results

4.3.1. Effect on complications from single verse multiple fractionation

Results of single and five fraction treatments with dose ranging from 11Gy to 22Gy total dose from radiobiological modeling using the free software from Niemieko using Zhou and normal tissue responses is given in **Table 4-3.**

Sawfat single fx - NTCP (%)			
Physical dose (Gy)	TBI	TMI1	TMI2
11	15.06	0.13	1.56
22	99.97	89.29	99.35

Sawfat 5 fx - NTCP (%)			
Physical dose (Gy)	TBI	TMI1	TMI2
11	0.0	0.0	0.0
22	20.65	0.24	2.65

Zhou single fx - NTCP (%)			
Physical dose (Gy)	TBI	TMI1	TMI2
11	0.49	0	0
22	99.6	2.1	43.6

Zhou 5 fx - NTCP (%)			
Physical dose (Gy)	TBI	TMI1	TMI2
11	0.00	0	0
22	1.15	0	0.02

Table 4-3: Results of single and five fraction treatments with dose ranging from 11Gy to 22Gy using Zhou fibrosis model & Safwat pneumonitis model

From **Table 4-3** fractionation can reduce the complication factor for adverse radiation induced effects. Complications for pneumonitis were reduced from 15.06% in the TBI to below 0.01% for 11Gy by introducing a fractionation regime. For dose escalation fractionation managed to reduce the complication to 20.65%. Complication probability for fibrosis was reduced from 99.6% to 1.15% in TBI for TMI2 complication was also reduced from 43.6% to 0.02%.

4.3.2. NTCP of fibrosis & pneumonitis models

Figure 4-1 displays the dose response model using Zhou single fraction parameters. NTCP curves are described by their physical dose to have 50% complication and complication at a fixed dose. TBI 50% complication has the lowest dose at 15.5Gy, TMI II 50% complication is reached at 23Gy, and TMI I

50% complication is reached at 31Gy. At 50% TBI complication (15.5Gy), TMI I is under 1% and TMI II is around 2.5%.

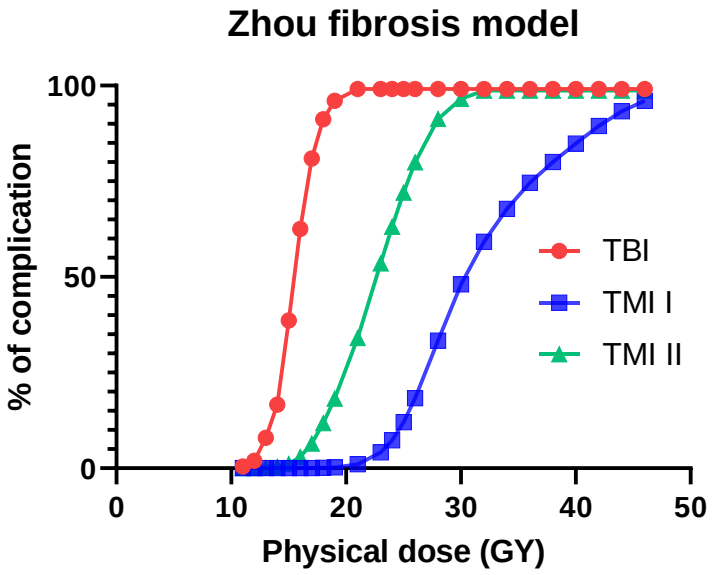

Figure 4-1: NTCP curves of TBI, TMI I, & TMI II using Zhou fibrosis parameters for single fraction

As outlined in Chapter 3 TMI body dose can be altered based on the needs of the project. To demonstrate the effect this can have on the lungs we varied TMI body dose from 0% (TMI) to 100% (TBI) of the prescription dose and calculated the NTCP based on a non-chemotherapy Safwat model which can be seen in **Figure 4-2**. 12Gy was chosen as it was the reported TCD_{50} from Safwat's study.

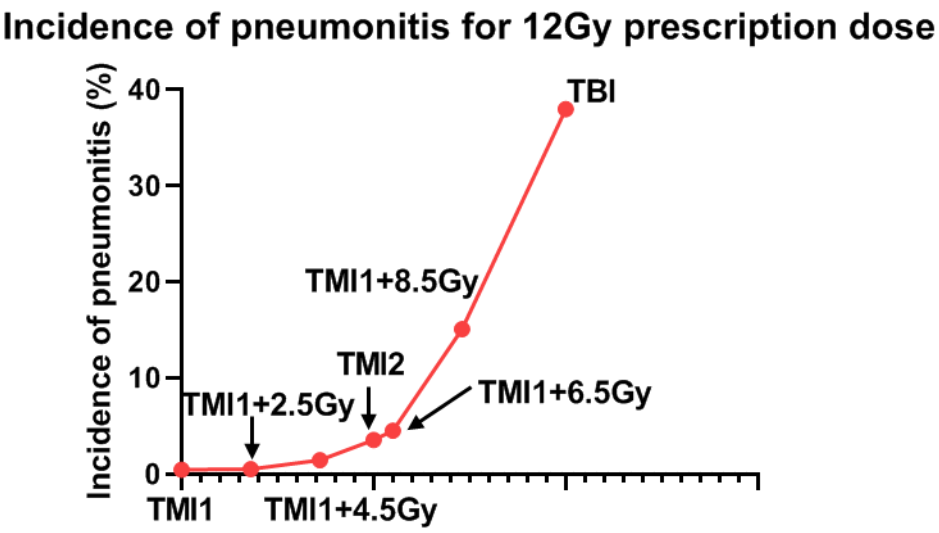

Figure 4-2: Application of mouse pneumonitis model following Safwat for single fraction

TBI has the highest complication with 38% and TMI1 has the lowest complication with 0.44% for an 12Gy single fraction treatment plan. TMI1+8.5Gy has a complication of 15.1% demonstrating that reduction a 10% reduction in the mean dose can have a significant reduction in pneumonitis incidence.

4.4. Discussion

With the recent development of a 3D conformal imaging system for preclinical TMI treatment there exists the possibility of developing a radiobiological model for predicting the risk of radiation induced lung abnormalities.

4.4.1. Dose escalation in the TMI model

The results show that dose escalation in the TMI preclinical model is possible as lung pneumonitis risk remains low in TMI1 (0.13%) and TMI2 (1.56%) when compared with TBI (15.06%) in dose escalation following Safwat modeling. Using the Zhou single fraction dose escalated fibrosis model TMI2 had a significantly increased risk of 43.6% when compared with TMI1 at 2.16%. Additionally, TBI fibrosis risk remains high at 99.6% indicating TBI mouse model will experience long term health problems post radiation. Unsurprisingly, fibrosis risk decreased with fractionation in the TBI, TMI1 and TMI2 to 1.15%, 0.000185%, and 0.0277% respectively for 22Gy dose treatment. These results imply that fractionation should be considered when investigating dose escalation as long-term negative biological minimizes negative health related effects.

It should be noted that pneumonitis simulations used an alpha-beta of 2.8 reported from Sampath (67). Sampath was selected since the work was exclusively based on TBI and Safwat did not report on an alpha-beta. However, Sampath's modeling was with humans instead of the mice. The difference in biological response can be seen in the TCD_{50}. Human non-chemo models reported a dose of 10.6Gy verse the animal Safwat model of 12Gy. It can be deduced that since modeling factors are different between human and animal then alpha-beta could be as well.

4.4.2. Complications with radiobiological model

Beyond just radiation there are additional non-radiation variables could influence lung complications. Tait reported an influence of graft versus host

diseases in the occurrence of lung complication due to infectious pneumonitis and cytomegalovirus (116). Chemotherapy may also be responsible for lung toxicity (117). This is important as often TMI is performed in combination with bone marrow transplant and/or chemotherapy. Safwat did modeling with chemo and non-chemo models using cyclophosphamide (250mg/kg). The results show and reduction in TCD_{50} from 12Gy to 5.3Gy. This effect can be seen in human modeling from Sampath's work were the difference between the TCD_{50} with (8.8Gy) and without (10.6Gy) chemotherapy. For the purposes of biological modeling, additional models should be created based on the chemotherapy doses and radiation fractionation combinations to account for these varying risks.

One major complication of TCP/NTCP modeling is the EUD interpatient inhomogeneity. The EUD interpatient inhomogeneity remains relatively robust so long as the D50 for each subject remain within 30% of the prescribed dose (108). For TMI1 had variations of 32%, TMI2 variations of 30%, and TBI variations of 1% in the D50. These results imply inhomogeneity in TMI1 & TMI2 most like caused by the placement of the thoracic spine treatment beams. In future studies this inhomogeneity must be carefully consider during TMI treatment planning and delivery.

As mentioned in previous discussions preclinical technological advancements can be assessed using a preclinical radiobiological model (55). Minimizing lung exposure will reduce the risk of complications and allow for further dose escalation that will be the subject of future studies. Another potential limitation of this study is the treatment time and anesthesia exposure. Preliminary

data has demonstrated that prolonged exposure to anesthesia can cause biological complications in the mice. Long recovery times post radiation and enhanced GVHD symptoms. This is preliminary observation and will be the subject of further investigations.

Another avenue of further study will be the dose rate effect on TMI lung biology. Experimental studies have shown a relationship between dose rate and cell killing with lower dose rates leading to less cell death (118, 119). Whether this effect translates to improved bone marrow cell engraftment has not yet been investigated. However, it has been demonstrated to be a factor for lung pneumonitis complication. Safwat et al (113) reported a 3.8Gy decrease in the TCD_{50} between mice receiving a lower dose rate. For simulation, the higher dose rate was chosen. Once a preclinical lung toxicity model has been established experiments comparing variable dose rates can be performed.

This work represents a simulation of preclinical lung complications following TMI treatment using work based on human clinical trial outcomes. There is currently no established radiobiological model done with the mouse model. With the establishment of a TMI animal treatment platform TCP/NTCP modeling can be investigated further and become standardized for a preclinical system.

Chapter 5. Conclusion

5.1. Summary and general conclusions

TMI continues to be demonstrated as a viable alternative to TBI. Early feasibilities studies have produced positive results in the clinic (53). However, if clinical development is to continue then further investigation into the methodology behind TMI treatment and into its biological effect are needed. In this thesis, the current state of clinical TMI pre-treatment set up was assessed, the development of a new investigative preclinical platform was established and finally a demonstratable use of this platform outlining beginning a new era in radiobiological research.

5.2. Future work

5.2.1. Clinical TMI

With increasing number of centers adopting there exists a need for the establishment of a standardized clinical procedure. From previous work the WBI MVCT imaging modality is recommended over PBI for monitoring patient setup variation (110). WBI MVCT imaging is also recommended for monitoring dose delivery. Based upon participating centers, PTV margin can be adjusted depending upon proximity of targets to OARs to improve dosimetric results, furthering the need for WBI before each treatment. However, WBI prior to every treatment fraction is time consuming and difficult for the patient. Implementation of a fast MVCT imaging system can make the prospect of WBI more appealing to physicians and patients (66). Currently, there is an effort to create an AAPM

(American Association of Physicist in Medicine) task group for clinical TMI to establish benchmarks and recommendations for treatment.

The study of the bone marrow environment using Dual Energy Computed Tomography (DECT) has demonstrated its feasibility for clinical use (120, 121). Additionally, work has been done demonstrating the effectiveness in tracking AML disease in patients using F-18 fluorothymidine (FLT) (65). Currently there is a clinical study implementing these different modalities with TBI/TMI treatment patients to assess their Marrow Adipose Tissue (MAT) before and after treatment. In the future these modalities can be used to target high disease sites creating a new form of TMI, Functional TMI. However, for functional TMI to be implemented the precision of TMI treatment must be carefully considered.

5.2.2. Preclinical Model

A major strength of the preclinical treatment platform is the 3D Cone Beam CT. The 3D system allows for the creation of DVHs which are needed for radiobiological assessment of a treatment plan. Current clinical radiobiological work relies on clumping data from a variety of treatments. Since we have established our own treatment model TCP/NTCP plan optimization can be done. These studies can provide further insight into the function of TMI lung resiliency from radiation damage. The majority of the interstitial pneumonitis NTCP data is based off of human data from previous work by Emami, et al. and Sampath et al (67) (114). A significant influence on NTCP is the TCD_{50}. Sampath reports a lower TCD_{50} of 8.8 – 10.6Gy compared with Emami's TCD_{50} of 14.55Gy. The majority of Emami's data is clubbed together from patients with Hodgkin's

disease, localized lung carcinomas, hemibody or TBI with only the most serious of complications (pneumonitis) taken into consideration. Sampath's data is based entirely upon TBI treatments. This could imply that radiation of the total body is increasing the complication probability of pneumonitis beyond just total lung treatments Given that in TMI treatments the gut and lungs are spared more radiation damage than in TBI, it is possible the TCD_{50} for preclinical TMI could be higher than Sampath's clinically reported values. Such experimental studies investigating the role of gut in lung complication can be performed.

In clinical TMI the dose rate is set to around 400 cGy/min, a significant increase from the 15-20 cGy/min found in clinical TBI (53). Several publications have shown that high dose rate has no effect in TBI (122, 123). However, other sources have suggested that high dose rate may have adverse effects on normal organs in particular the lungs (124, 125). Safwat, et al. (113) The preclinical platform is capable studying such radiobiological effects in a controlled environment. Future studies will include testing a variable dose rate against our TCP/NTCP model and observe how dose rate can affect the bone marrow engraftment.

Our image guided TMI model could be potentially used for a range of scientific investigations: (i) RT dose escalation, complementing our ongoing clinical dose escalation strategy to study therapeutic benefit/survival toxcities of using chemotherapy before or after TMI. (ii) Biological investigation of radiation effects on hematopoietic stems cells between TMI and TBI-treated mice. (iii) radiation induced Lung injury (pneumonitis & fibrosis) and gut graft versus host

disease (GVHD) are often associated with high radiation exposure(27, 126). TMI reduced organ damage, particularly acute gut damage post BMT. Previous study suggests that an increased gut dose increases the severity of GVHD (126). Therefore, the GVHD mouse model in allogeneic BMT settings using TMI would enable us to further understand the role of radiation-induced gut damage in GVHD. (iv) A recent study using an anti-CD33-PET imaging modality showed that AML disease localizes mostly in the skeletal system and is highly heterogeneous (127). This disease heterogeneity has also been observed using F-18 fluorothymidine (FLT) PET imaging in patients (65, 128). Thus, PET-guided functional TMI (fTMI) could allow localized radiation boosts to sites of high disease burden to enhance increased tumor cell killing without damaging the entire skeletal system (51, 128). (v) T-regulatory and T-conventional (Tregs/Tcon) based adoptive immunotherapy in conjunction with the TBI conditioning regimen has been optimized in patients with leukemia (129). However, relapse rates have remained unacceptably high in the setting of haploidentical HCT. The major advantage of BM-targeted TMI is to be able to treat with dose-escalated TMI to offer a strong antileukemic conditioning for patients who cannot tolerate TBI because of older age, or for younger patient populations with comorbidities (130). Additionally, it is also possible that TMI may reduce the rate of transplant related mortality (TRM) in younger patients while maintaining the antileukemic activity of TBI. This outcome has led to the initiation of Treg/Tcon together with TMI conditioning to enhance the antileukemic effect (131). Our preclinical model will enable in-depth understanding of how TMI

conditioning in combination with adoptive immunotherapy reduces GVHD as well as maintaining a strong graft versus leukemia (GVL) effect. (vi) Furthermore, non-malignant hematological disorders (thalassemia and sickle cell disorders), are responsible for significant morbidity and mortality, representing a major global health problem. About 40-50% of patients have graft failure after allogeneic HCT (132), and increasing TBI conditioning from 2 Gy to 4 Gy significantly reduced graft failure (133). Multiple forms of organ damage are reported in adult patients with SCD (134). Therefore, it is anticipated that the TMI technology could adequately deliver high doses to the BM to improve engraftment, but with reduced radiation exposure to vital organs to decrease comorbidities associated with SCD.

Citations

1. Medawar PB. Tests by tissue culture methods on the nature of immunity to transplanted skin. The Quarterly journal of microscopical science. 1948;89(Pt 3):239-52. PubMed PMID: 18888181.
2. Medawar PB. Immunity to homologous grafted skin; the fate of skin homografts transplanted to the brain, to subcutaneous tissue, and to the anterior chamber of the eye. British journal of experimental pathology. 1948;29(1):58-69. PubMed PMID: 18865105; PubMed Central PMCID: PMC2073079.
3. Thomas ED. Bone marrow transplantation: prospects for leukemia and other conditions. The Proceedings of the Institute of Medicine of Chicago. 1975;30(8):256-8. PubMed PMID: 1103123.
4. Thomas ED, Storb R, Clift RA, Fefer A, Johnson L, Neiman PE, et al. Bone-marrow transplantation (second of two parts). The New England journal of medicine. 1975;292(17):895-902. doi: 10.1056/NEJM197504242921706. PubMed PMID: 235092.
5. Thomas E, Storb R, Clift RA, Fefer A, Johnson FL, Neiman PE, et al. Bone-marrow transplantation (first of two parts). The New England journal of medicine. 1975;292(16):832-43. doi: 10.1056/NEJM197504172921605. PubMed PMID: 234595.
6. Jacobs ML, Marasso FJ. A Four-Year Experience with Total-Body Irradiation. Radiology. 1965;84:452-6. doi: 10.1148/84.3.452. PubMed PMID: 14280717.
7. Lorenz E, Uphoff D, Reid TR, Shelton E. Modification of irradiation injury in mice and guinea pigs by bone marrow injections. Journal of the National Cancer Institute. 1951;12(1):197-201. PubMed PMID: 14874130.
8. Jacobson LO, Marks EK, et al. The role of the spleen in radiation injury. Proceedings of the Society for Experimental Biology and Medicine Society for Experimental Biology and Medicine. 1949;70(4):740-2. doi: 10.3181/00379727-70-17053. PubMed PMID: 18149489.
9. Cavins JA, Kasakura S, Thomas ED, Ferrebee JW. Recovery of lethally irradiated dogs following infusion of autologous marrow stored at low temperature in dimethylsulphoxide. Blood. 1962;20:730-4. PubMed PMID: 14019494.
10. Barnes DW, Corp MJ, Loutit JF, Neal FE. Treatment of murine leukaemia with X rays and homologous bone marrow; preliminary communication. British medical journal. 1956;2(4993):626-7. doi: 10.1136/bmj.2.4993.626. PubMed PMID: 13356034; PubMed Central PMCID: PMC2035298.
11. Bortin MM. A compendium of reported human bone marrow transplants. Transplantation. 1970;9(6):571-87. doi: 10.1097/00007890-197006000-00006. PubMed PMID: 4911417.
12. Storb R, Epstein RB, Bryant J, Ragde H, Thomas ED. Marrow grafts by combined marrow and leukocyte infusions in unrelated dogs selected by histocompatibility typing. Transplantation. 1968;6(4):587-93. doi: 10.1097/00007890-196807000-00011. PubMed PMID: 4876499.
13. Epstein RB, Storb R, Clift RA, Thomas ED. Transplantation of stored allogeneic bone marrow in dogs selected by histocompatibility typing. Transplantation. 1969;8(4):496-501. doi: 10.1097/00007890-196910000-00022. PubMed PMID: 4911249.
14. Epstein RB, Storb R, Ragde H, Thomas ED. Cytotoxic typing antisera for marrow grafting in littermate dogs. Transplantation. 1968;6(1):45-58. doi: 10.1097/00007890-196801000-00005. PubMed PMID: 4866738.
15. Santos GW, Owens AH, Jr. Allogeneic marrow transplants in cyclophosphamide treated mice. Transplantation proceedings. 1969;1(1):44-6. PubMed PMID: 4400067.
16. Glynn JP, Fefer A, Halpern BL. Cyclophosphamide-induced chimerism. Cancer research. 1968;28(1):41-3. PubMed PMID: 4169583.
17. Storb R, Epstein RB, Rudolph RH, Thomas ED. Allogeneic canine bone marrow transplantation following cyclophosphamide. Transplantation. 1969;7(5):378-86. doi: 10.1097/00007890-196905000-00007. PubMed PMID: 4890905.

18. Storb R, Buckner CD, Dillingham LA, Thomas ED. Cyclophosphamide regimens in rhesus monkey with and without marrow infusion. Cancer research. 1970;30(8):2195-203. PubMed PMID: 4990004.
19. Buckner CD, Epstein RB, Rudolph RH, Clift RA, Storb R, Thomas ED. Allogeneic marrow engraftment following whole body irradiation in a patient with leukemia. Blood. 1970;35(6):741-50. PubMed PMID: 4913404.
20. Thomas ED, Storb R. Technique for human marrow grafting. Blood. 1970;36(4):507-15. PubMed PMID: 4916999.
21. Thomas ED, Buckner CD, Banaji M, Clift RA, Fefer A, Flournoy N, et al. One hundred patients with acute leukemia treated by chemotherapy, total body irradiation, and allogeneic marrow transplantation. Blood. 1977;49(4):511-33. PubMed PMID: 14751.
22. Bieri S, Helg C, Chapuis B, Miralbell R. Total body irradiation before allogeneic bone marrow transplantation: Is more dose better? Int J Radiat Oncol. 2001;49(4):1071-7. doi: Doi 10.1016/S0360-3016(00)01491-7. PubMed PMID: WOS:000167327200019.
23. Socie G, Devergie A, Girinsky T, Reiffers J, Vernant JP, Le Bourgeois JP, et al. Influence of the fractionation of total body irradiation on complications and relapse rate for chronic myelogenous leukemia. The Groupe d'Etude des greffes de moelle osseuse (GEGMO). International journal of radiation oncology, biology, physics. 1991;20(3):397-404. doi: 10.1016/0360-3016(91)90048-9. PubMed PMID: 1995523.
24. Thomas ED, Clift RA, Hersman J, Sanders JE, Stewart P, Buckner CD, et al. Marrow transplantation for acute nonlymphoblastic leukemic in first remission using fractionated or single-dose irradiation. International journal of radiation oncology, biology, physics. 1982;8(5):817-21. doi: 10.1016/0360-3016(82)90083-9. PubMed PMID: 7050046.
25. Copelan EA. Hematopoietic stem-cell transplantation. New England Journal of Medicine. 2006;354(17):1813-26.
26. Thomas ED, Lochte HL, Cannon JH, Sahler OD, Ferrebee JW. Supralethal whole body irradiation and isologous marrow transplantation in man. The Journal of clinical investigation. 1959;38(10):1709-16.
27. Abugideiri M, Nanda RH, Butker C, Zhang C, Kim S, Chiang KY, et al. Factors Influencing Pulmonary Toxicity in Children Undergoing Allogeneic Hematopoietic Stem Cell Transplantation in the Setting of Total Body Irradiation-Based Myeloablative Conditioning. International journal of radiation oncology, biology, physics. 2016;94(2):349-59. Epub 2016/02/09. doi: 10.1016/j.ijrobp.2015.10.054. PubMed PMID: 26853343.
28. Ho VT, Weller E, Lee SJ, Alyea EP, Antin JH, Soiffer RJ. Prognostic factors for early severe pulmonary complications after hematopoietic stem cell transplantation. Biology of blood and marrow transplantation : journal of the American Society for Blood and Marrow Transplantation. 2001;7(4):223-9. Epub 2001/05/15. doi: 10.1053/bbmt.2001.v7.pm11349809. PubMed PMID: 11349809.
29. Salhotra A, Hui S, Yang D, Mokhtari S, Mei M, Al Malki MM, et al. Long-Term Outcomes of Patients with Acute Myelogenous Leukemia Treated with Myeloablative Fractionated Total Body Irradiation TBI-Based Conditioning with a Tacrolimus- and Sirolimus-Based Graft-versus-Host Disease Prophylaxis Regimen: 6-Year Follow-Up from a Single Center. Biology of blood and marrow transplantation : journal of the American Society for Blood and Marrow Transplantation. 2020;26(2):292-9. Epub 2019/09/20. doi: 10.1016/j.bbmt.2019.09.017. PubMed PMID: 31536825.
30. Kal HB, Loes van Kempen-Harteveld M, Heijenbrok-Kal MH, Struikmans H. Biologically effective dose in total-body irradiation and hematopoietic stem cell transplantation. Strahlentherapie und Onkologie : Organ der Deutschen Rontgengesellschaft [et al]. 2006;182(11):672-9. doi: 10.1007/s00066-006-1528-6. PubMed PMID: 17072526.
31. Esiashvili N, Lu X, Ulin K, Laurie F, Kessel S, Kalapurakal JA, et al. Higher Reported Lung Dose Received During Total Body Irradiation for Allogeneic Hematopoietic Stem Cell Transplantation in Children With Acute Lymphoblastic Leukemia Is Associated With Inferior Survival: A Report from the Children's Oncology Group. International journal of radiation oncology, biology, physics. 2019. doi: 10.1016/j.ijrobp.2019.02.034. PubMed PMID: 30807822.
32. Clift RA, Buckner CD, Appelbaum FR, Sullivan KM, Storb R, Thomas ED. Long-term follow-Up of a randomized trial of two irradiation regimens for patients receiving allogeneic marrow transplants during first remission of acute myeloid leukemia. Blood. 1998;92(4):1455-6. PubMed PMID: 9694737.
33. Clift RA, Buckner CD, Appelbaum FR, Bearman SI, Petersen FB, Fisher LD, et al. Allogeneic marrow transplantation in patients with acute myeloid leukemia in first remission: a randomized trial of two irradiation regimens. Blood. 1990;76(9):1867-71. PubMed PMID: 2224134.

34. Morgan TL, Falk PM, Kogut N, Shah KH, Tome M, Kagan AR. A comparison of single-dose and fractionated total-body irradiation on the development of pneumonitis following bone marrow transplantation. Int J Radiat Oncol. 1996;36(1):61-6. doi: Doi 10.1016/S0360-3016(96)00246-5. PubMed PMID: WOS:A1996VH84000007.
35. Gerbi BJ, Dusenbery KE. Design specifications for a treatment stand used for total body photon irradiation with patients in a standing position. Medical dosimetry : official journal of the American Association of Medical Dosimetrists. 1995;20(1):25-30. doi: 10.1016/0958-3947(94)00047-m. PubMed PMID: 7794487.
36. Roth J. Physical aspects of total body irradiation in Basel. Strahlentherapie und Onkologie : Organ der Deutschen Rontgengesellschaft [et al]. 1986;162(4):237-9. PubMed PMID: 3518101.
37. Pla M, Chenery SG, Podgorsak EB. Total body irradiation with a sweeping beam. International journal of radiation oncology, biology, physics. 1983;9(1):83-9. doi: 10.1016/0360-3016(83)90214-6. PubMed PMID: 6341334.
38. Chui CS, Fontenla DP, Mullokandov E, Kapulsky A, Lo YC, Lo CJ. Total body irradiation with an arc and a gravity-oriented compensator. International journal of radiation oncology, biology, physics. 1997;39(5):1191-5. doi: 10.1016/s0360-3016(97)00498-7. PubMed PMID: 9392562.
39. Cunningham JR, Wright DJ. A simple facility for wholebody irradiation. Radiology. 1962;78:941-9. doi: 10.1148/78.6.941. PubMed PMID: 13882648.
40. Wheldon TE. The radiobiological basis of total body irradiation. The British journal of radiology. 1997;70(840):1204-7. doi: 10.1259/bjr.70.840.9505837. PubMed PMID: 9505837.
41. Hui SK, Das RK, Thomadsen B, Henderson D. CT-based analysis of dose homogeneity in total body irradiation using lateral beam. Journal of applied clinical medical physics. 2004;5(4):71-9. PubMed PMID: 15738922.
42. Hui SK, Kapatoes J, Fowler J, Henderson D, Olivera G, Manon RR, et al. Feasibility study of helical tomotherapy for total body or total marrow irradiation. Med Phys. 2005;32(10):3214-24. doi: 10.1118/1.2044428. PubMed PMID: WOS:000232755900018.
43. Hui SK, Lusczek E, DeFor T, Dusenbery K, Levitt S. Three-dimensional patient setup errors at different treatment sites measured by the Tomotherapy megavoltage CT. Strahlentherapie und Onkologie : Organ der Deutschen Rontgengesellschaft [et al]. 2012;188(4):346-52. doi: 10.1007/s00066-011-0066-z. PubMed PMID: 22398931.
44. Schultheiss TE, Wong J, Liu A, Olivera G, Somlo G. Image-guided total marrow and total lymphatic irradiation using helical tomotherapy. Int J Radiat Oncol. 2007;67(4):1259-67. doi: 10.1016/j.ijrobp.2006.10.047. PubMed PMID: WOS:000245021100037.
45. Han C, Schultheisss TE, Wong JY. Dosimetric study of volumetric modulated arc therapy fields for total marrow irradiation. Radiotherapy and oncology : journal of the European Society for Therapeutic Radiology and Oncology. 2012;102(2):315-20. doi: 10.1016/j.radonc.2011.06.005. PubMed PMID: 21724284.
46. Wong JY, Rosenthal J, Liu A, Schultheiss T, Forman S, Somlo G. Image-guided total-marrow irradiation using helical tomotherapy in patients with multiple myeloma and acute leukemia undergoing hematopoietic cell transplantation. International journal of radiation oncology, biology, physics. 2009;73(1):273-9. doi: 10.1016/j.ijrobp.2008.04.071. PubMed PMID: 18786784; PubMed Central PMCID: PMC3896447.
47. Wong JYC, Liu A, Schultheiss T, Popplewell L, Stein A, Rosenthal J, et al. Targeted total marrow irradiation using three-dimensional image-guided tomographic intensity-modulated radiation therapy: An alternative to standard total body irradiation. Biol Blood Marrow Tr. 2006;12(3):306-15. doi: 10.1016/j.bbmt.2005.10.026. PubMed PMID: WOS:000236190600008.
48. Ruchala KJ, Olivera GH, Kapatoes JM, Schloesser EA, Reckwerdt PJ, Mackie TR. Megavoltage CT image reconstruction during tomotherapy treatments. Physics in medicine and biology. 2000;45(12):3545-62. PubMed PMID: 11131183.
49. Stein A, Tsai N-C, Palmer J, Al Malki MM, Aldoss I, Ali H, et al. Total Marrow and Lymphoid Irradiation (TMLI) in Combination with Cyclophosphamide and Etoposide in Patients with Relapsed/Refractory Acute Leukemia Undergoing Allogeneic Hematopoietic Cell Transplantation. European Society for Blood and Marrow Transplantation, accepted abstract. 2019.
50. Duval M, Klein J, He W, Cahn J, Cairo M, Camitta B, et al. Hematopoietic Stem-Cell Transplantation for Acute Leukemia in Relapse or Primary Induction Failure. Journal of clinical oncology. 2010;28(23):3730.

51. Sargur Madabushi S, Zuro D, SU Y-L, Vishwasrao P, Brooks J, E Parra L, et al. Targeted Marrow Radiation (TMI) Improves Therapeutic Efficacy of STAT3 Decoy Molecules By Augmenting Its Delivery and Immune Modulation in an AML Mouse Model. Blood. 2019;134(Supplement_1):3929-. doi: 10.1182/blood-2019-127470.
52. Wong JY, Forman S, Somlo G, Rosenthal J, Liu A, Schultheiss T, et al. Dose escalation of total marrow irradiation with concurrent chemotherapy in patients with advanced acute leukemia undergoing allogeneic hematopoietic cell transplantation. International journal of radiation oncology, biology, physics. 2013;85(1):148-56. doi: 10.1016/j.ijrobp.2012.03.033. PubMed PMID: 22592050; PubMed Central PMCID: PMC4312108.
53. Hui S, Brunstein C, Takahashi Y, DeFor T, Holtan SG, Bachanova V, et al. Dose Escalation of Total Marrow Irradiation in High-Risk Patients Undergoing Allogeneic Hematopoietic Stem Cell Transplantation. Biology of Blood and Marrow Transplantation. 2017.
54. Woods K, Neph R, Nguyen D, Sheng K. A sparse orthogonal collimator for small animal intensity-modulated radiation therapy. Part II: hardware development and commissioning. Med Phys. 2019;46(12):5733-47. doi: 10.1002/mp.13870. PubMed PMID: 31621091.
55. Woods K, Nguyen D, Neph R, Ruan D, O'Connor D, Sheng K. A sparse orthogonal collimator for small animal intensity-modulated radiation therapy part I: Planning system development and commissioning. Med Phys. 2019;46(12):5703-13. doi: 10.1002/mp.13872. PubMed PMID: 31621920; PubMed Central PMCID: PMC6899210.
56. van Hoof SJ, Granton PV, Verhaegen F. Development and validation of a treatment planning system for small animal radiotherapy: SmART-Plan. Radiotherapy and oncology : journal of the European Society for Therapeutic Radiology and Oncology. 2013;109(3):361-6. doi: 10.1016/j.radonc.2013.10.003. PubMed PMID: 24183860.
57. Manning MA, Wu QW, Cardinale RM, Mohan R, Lauve AD, Kavanagh BD, et al. The effect of setup uncertainty on normal tissue sparing with IMRT for head-and-neck cancer. Int J Radiat Oncol. 2001;51(5):1400-9. doi: Doi 10.1016/S0360-3016(01)01740-0. PubMed PMID: WOS:000172495200027.
58. Corvo R, Zeverino M, Vagge S, Agostinelli S, Barra S, Taccini G, et al. Helical tomotherapy targeting total bone marrow after total body irradiation for patients with relapsed acute leukemia undergoing an allogeneic stem cell transplant. Radiotherapy and Oncology. 2011;98(3):382-6. doi: 10.1016/j.radonc.2011.01.016. PubMed PMID: WOS:000289022800018.
59. Engellau J, Haraldsson A, Engstrom P, Lenhoff S. Implementation of Total Marrow Irradiation With Helical Tomotherapy; Clinical Experiences and Report on Organ Sparing in Pediatric Patients. Int J Radiat Oncol. 2018;101(4):1006-7. doi: DOI 10.1016/j.ijrobp.2018.01.080. PubMed PMID: WOS:000436809700050.
60. Zeverino M, Agostinelli S, Taccini G, Cavagnetto F, Garelli S, Gusinu M, et al. Advances in the implementation of helical tomotherapy-based total marrow irradiation with a novel field junction technique. Medical dosimetry : official journal of the American Association of Medical Dosimetrists. 2012;37(3):314-20. doi: 10.1016/j.meddos.2011.12.001. PubMed PMID: 22326734.
61. Yan D, Wong J, Vicini F, Michalski J, Pan C, Frazier A, et al. Adaptive modification of treatment planning to minimize the deleterious effects of treatment setup errors. International journal of radiation oncology, biology, physics. 1997;38(1):197-206. PubMed PMID: 9212024.
62. Schubert LK, Westerly DC, Tome WA, Mehta MP, Soisson ET, Mackie TR, et al. A comprehensive assessment by tumor site of patient setup using daily MVCT imaging from more than 3,800 helical tomotherapy treatments. International journal of radiation oncology, biology, physics. 2009;73(4):1260-9. doi: 10.1016/j.ijrobp.2008.11.054. PubMed PMID: 19251098; PubMed Central PMCID: PMC2749998.
63. Tome WA, Fowler JF. On cold spots in tumor subvolumes. Med Phys. 2002;29(7):1590-8. doi: 10.1118/1.1485060. PubMed PMID: WOS:000176930900025.
64. Mackie TR, Kapatoes J, Ruchala K, Lu WG, Wu C, Olivera G, et al. Image guidance for precise conformal radiotherapy. Int J Radiat Oncol. 2003;56(1):89-105. doi: 10.1016/S0360-3016(03)00090-7. PubMed PMID: WOS:000182309800012.
65. Vanderhoek M, Juckett MB, Perlman SB, Nickles RJ, Jeraj R. Early assessment of treatment response in patients with AML using [(18)F]FLT PET imaging. Leukemia research. 2011;35(3):310-6. doi: 10.1016/j.leukres.2010.06.010. PubMed PMID: 20832860; PubMed Central PMCID: PMC3319294.
66. Magome T, Haga A, Takahashi Y, Nakagawa K, Dusenbery KE, Hui SK. Fast Megavoltage Computed Tomography: A Rapid Imaging Method for Total Body or Marrow Irradiation in Helical

Tomotherapy. International journal of radiation oncology, biology, physics. 2016;96(3):688-95. doi: 10.1016/j.ijrobp.2016.06.2458. PubMed PMID: 27681766; PubMed Central PMCID: PMC5081222.
67. Sampath S, Schultheiss TE, Wong J. Dose response and factors related to interstitial pneumonitis after bone marrow transplant. International journal of radiation oncology, biology, physics. 2005;63(3):876-84. doi: 10.1016/j.ijrobp.2005.02.032. PubMed PMID: 16199317.
68. Gao RW, Weisdorf DJ, DeFor TE, Ehler E, Dusenbery KE. Influence of Total Body Irradiation Dose Rate on Idiopathic Pneumonia Syndrome in Acute Leukemia Patients Undergoing Allogeneic Hematopoietic Cell Transplantation. International journal of radiation oncology, biology, physics. 2019;103(1):180-9. doi: 10.1016/j.ijrobp.2018.09.002. PubMed PMID: 30205123.
69. Stein A, Palmer J, Tsai NC, Al Malki MM, Aldoss I, Ali H, et al. Phase I Trial of Total Marrow and Lymphoid Irradiation Transplantation Conditioning in Patients with Relapsed/Refractory Acute Leukemia. Biology of blood and marrow transplantation : journal of the American Society for Blood and Marrow Transplantation. 2017;23(4):618-24. doi: 10.1016/j.bbmt.2017.01.067. PubMed PMID: 28087456; PubMed Central PMCID: PMC5382014.
70. Hui S, Brunstein C, Takahashi Y, DeFor T, Holtan SG, Bachanova V, et al. Dose Escalation of Total Marrow Irradiation in High-Risk Patients Undergoing Allogeneic Hematopoietic Stem Cell Transplantation. Biology of blood and marrow transplantation : journal of the American Society for Blood and Marrow Transplantation. 2017;23(7):1110-6. doi: 10.1016/j.bbmt.2017.04.002. PubMed PMID: 28396164; PubMed Central PMCID: PMC5531195.
71. Hui SK, Das RK, Thomadsen B, Henderson D. CT-based analysis of dose homogeneity in total body irradiation using lateral beam. Journal of applied clinical medical physics / American College of Medical Physics. 2004;5(4):71-9. PubMed PMID: 16.
72. Patel PR, Rondelli D. Total Marrow and Lymphoid Irradiation to Rescue Refractory Leukemia. Biology of Blood and Marrow Transplantation. 2017;23(4):536-7.
73. Stein A, Palmer J, Tsai N-C, Al Malki MM, Aldoss I, Ali H, et al. Phase I Trial of Total Marrow and Lymphoid Irradiation Transplant Conditioning in Patients with Relapsed/Refractory Acute Leukemia. Biology of Blood and Marrow Transplantation. 2017.
74. Rosenthal J, Wong J, Stein A, Qian D, Hitt D, Naeem H, et al. Phase 1/2 trial of total marrow and lymph node irradiation to augment reduced-intensity transplantation for advanced hematologic malignancies. Blood. 2011;117(1):309-15.
75. Ma CM, Coffey CW, DeWerd LA, Liu C, Nath R, Seltzer SM, et al. AAPM protocol for 40-300 kV x-ray beam dosimetry in radiotherapy and radiobiology. Med Phys. 2001;28(6):868-93. Epub 2001/07/07. doi: 10.1118/1.1374247. PubMed PMID: 11439485.
76. Sengsayadeth S, Savani BN, Blaise D, Malard F, Nagler A, Mohty M. Reduced intensity conditioning allogeneic hematopoietic cell transplantation for adult acute myeloid leukemia in complete remission - a review from the Acute Leukemia Working Party of the EBMT. Haematologica. 2015;100(7):859-69. Epub 2015/07/02. doi: 10.3324/haematol.2015.123331. PubMed PMID: 26130513; PubMed Central PMCID: PMCPMC4486220.
77. Andrade J, Ge S, Symbatyan G, Rosol MS, Olch AJ, Crooks GM. Effects of sublethal irradiation on patterns of engraftment after murine bone marrow transplantation. Biology of blood and marrow transplantation : journal of the American Society for Blood and Marrow Transplantation. 2011;17(5):608-19. Epub 2010/12/24. doi: 10.1016/j.bbmt.2010.12.697. PubMed PMID: 21176787; PubMed Central PMCID: PMCPMC3086732.
78. Bachar-Lustig E, Rachamim N, Li H-W, Lan F, Reisner Y. Megadose of T cell-depleted bone marrow overcomes MHC barriers in sublethally irradiated mice. Nature Medicine. 1995;1(12):1268-73. doi: 10.1038/nm1295-1268.
79. Willekens I, Buls N, De Maeseneer M, Lahoutte T, de Mey J. Use of eXIA 160 XL for contrast studies in micro-computed tomography: experimental observations. Molecular imaging. 2013;12(6):349-56. PubMed PMID: 23981780.
80. Willekens I, Lahoutte T, Buls N, Vanhove C, Deklerck R, Bossuyt A, et al. Time-course of contrast enhancement in spleen and liver with Exia 160, Fenestra LC, and VC. Molecular imaging and biology : MIB : the official publication of the Academy of Molecular Imaging. 2009;11(2):128-35. doi: 10.1007/s11307-008-0186-8. PubMed PMID: 19067081.
81. Lin H, Ayan A, Zhai H, Zhu T, Both S. SU-GG-I-109: a quantitative evaluation of velocity AI deformable image registration. Med Phys. 2010;37(6Part4):3126-.

82. Kirby N, Chuang C, Ueda U, Pouliot J. The need for application-based adaptation of deformable image registration. Med Phys. 2013;40(1):011702.
83. Akselrod-Ballin A, Dafni H, Addadi Y, Biton I, Avni R, Brenner Y, et al. Multimodal correlative preclinical whole body imaging and segmentation. Scientific reports. 2016;6:27940.
84. Baiker M, Milles J, Dijkstra J, Henning TD, Weber AW, Que I, et al. Atlas-based whole-body segmentation of mice from low-contrast Micro-CT data. Med Image Anal. 2010;14(6):723-37. Epub 2010/06/26. doi: 10.1016/j.media.2010.04.008. PubMed PMID: 20576463.
85. Rosenhain S, Magnuska ZA, Yamoah GG, Rawashdeh WA, Kiessling F, Gremse F. A preclinical micro-computed tomography database including 3D whole body organ segmentations. Sci Data. 2018;5:180294. Epub 2018/12/19. doi: 10.1038/sdata.2018.294. PubMed PMID: 30561432; PubMed Central PMCID: PMCPMC6298256.
86. Downes P, Jarvis R, Radu E, Kawrakow I, Spezi E. Monte Carlo simulation and patient dosimetry for a kilovoltage cone-beam CT unit. Med Phys. 2009;36(9):4156-67. Epub 2009/10/09. doi: 10.1118/1.3196182. PubMed PMID: 19810489.
87. Faddegon BA, Kawrakow I, Kubyshin Y, Perl J, Sempau J, Urban L. The accuracy of EGSnrc, Geant4 and PENELOPE Monte Carlo systems for the simulation of electron scatter in external beam radiotherapy. Physics in medicine and biology. 2009;54(20):6151-63. Epub 2009/09/26. doi: 10.1088/0031-9155/54/20/008. PubMed PMID: 19779217; PubMed Central PMCID: PMCPMC3462739.
88. Verhaegen F, van Hoof S, Granton PV, Trani D. A review of treatment planning for precision image-guided photon beam pre-clinical animal radiation studies. Zeitschrift fur medizinische Physik. 2014;24(4):323-34. doi: 10.1016/j.zemedi.2014.02.004. PubMed PMID: 24629309.
89. Hui S, Takahashi Y, Holtan SG, Azimi R, Seelig D, Yagi M, et al. Early assessment of dosimetric and biological differences of total marrow irradiation versus total body irradiation in rodents. Radiother Oncol. 2017;124(3):468-74. doi: 10.1016/j.radonc.2017.07.018. PubMed PMID: WOS:000413383700018.
90. Verhaegen F, Dubois L, Gianolini S, Hill MA, Karger CP, Lauber K, et al. ESTRO ACROP: Technology for precision small animal radiotherapy research: Optimal use and challenges. Radiotherapy and oncology : journal of the European Society for Therapeutic Radiology and Oncology. 2018;126(3):471-8. doi: 10.1016/j.radonc.2017.11.016. PubMed PMID: 29269093.
91. Scarboro SB, Cody D, Alvarez P, Followill D, Court L, Stingo FC, et al. Characterization of the nanoDot OSLD dosimeter in CT. Med Phys. 2015;42(4):1797-807. doi: 10.1118/1.4914398. PubMed PMID: WOS:000352273200034.
92. Matsumine A, Myoui A, Kusuzaki K, Araki N, Seto M, Yoshikawa H, et al. Calcium hydroxyapatite ceramic implants in bone tumour surgery. A long-term follow-up study. J Bone Joint Surg Br. 2004;86(5):719-25. Epub 2004/07/28. doi: 10.1302/0301-620x.86b5.14242. PubMed PMID: 15274270.
93. Jarcho M. Calcium phosphate ceramics as hard tissue prosthetics. Clin Orthop Relat Res. 1981(157):259-78. Epub 1981/06/01. PubMed PMID: 7018783.
94. Aydogan B, Yeginer M, Kavak GO, Fan J, Radosevich JA, Gwe-Ya K. Total marrow irradiation with RapidArc volumetric arc therapy. International Journal of Radiation Oncology* Biology* Physics. 2011;81(2):592-9.
95. Bao Z, Zhao H, Wang D, Gong J, Zhong Y, Xiong Y, et al. Feasibility of a novel dose fractionation strategy in TMI/TMLI. Radiat Oncol. 2018;13(1):248. Epub 2018/12/19. doi: 10.1186/s13014-018-1201-0. PubMed PMID: 30558631; PubMed Central PMCID: PMCPMC6296054.
96. Han C, Schultheisss TE, Wong JY. Dosimetric study of volumetric modulated arc therapy fields for total marrow irradiation. Radiotherapy and Oncology. 2012;102(2):315-20.
97. Hui SK, Verneris MR, Higgins P, Gerbi B, Weigel B, Baker SK, et al. Helical tomotherapy targeting total bone marrow - first clinical experience at the University of Minnesota. Acta Oncol. 2007;46(2):250-5. Epub 2007/04/25. doi: 10.1080/02841860601042449. PubMed PMID: 17453378.
98. Jensen LG, Stiller T, Wong JY, Palmer J, Stein A, Rosenthal J. Total marrow lymphoid irradiation/fludarabine/melphalan conditioning for allogeneic hematopoietic cell transplantation. Biology of Blood and Marrow Transplantation. 2018;24(2):301-7.
99. Mancosu P, Navarria P, Castagna L, Reggiori G, Sarina B, Tomatis S, et al. Interplay effects between dose distribution quality and positioning accuracy in total marrow irradiation with volumetric modulated arc therapy. Med Phys. 2013;40(11):111713. Epub 2013/12/11. doi: 10.1118/1.4823767. PubMed PMID: 24320421.

100. McCutchen KW, Watkins JM, Eberts P, Terwilliger LE, Ashenafi MS, Jenrette JM, 3rd. Helical tomotherapy for total lymphoid irradiation. Radiat Med. 2008;26(10):622-6. Epub 2009/01/10. doi: 10.1007/s11604-008-0281-4. PubMed PMID: 19132495.
101. Fogliata A, Cozzi L, Clivio A, Ibatici A, Mancosu P, Navarria P, et al. Preclinical assessment of volumetric modulated arc therapy for total marrow irradiation. International Journal of Radiation Oncology* Biology* Physics. 2011;80(2):628-36.
102. Galvin JM, De Neve W. Intensity modulating and other radiation therapy devices for dose painting. Journal of clinical oncology. 2007;25(8):924-30.
103. Chow J, Owrangi A. SU-E-T-142: Effect of the Bone Heterogeneity On the Unflattened and Flattened Photon Beam Dosimetry: A Monte Carlo Comparison. Med Phys. 2014;41(6Part13):255-. doi: 10.1118/1.4888472.
104. Bazalova M, Carrier JF, Beaulieu L, Verhaegen F. Dual-energy CT-based material extraction for tissue segmentation in Monte Carlo dose calculations. Physics in medicine and biology. 2008;53(9):2439-56. doi: 10.1088/0031-9155/53/9/015. PubMed PMID: 18421124.
105. Poludniowski GG, Evans PM. Calculation of x-ray spectra emerging from an x-ray tube. Part I. electron penetration characteristics in x-ray targets. Med Phys. 2007;34(6):2164-74. Epub 2007/07/28. doi: 10.1118/1.2734725. PubMed PMID: 17654919.
106. Poludniowski G, Landry G, DeBlois F, Evans PM, Verhaegen F. SpekCalc: a program to calculate photon spectra from tungsten anode x-ray tubes. Physics in medicine and biology. 2009;54(19):N433-8. Epub 2009/09/03. doi: 10.1088/0031-9155/54/19/n01. PubMed PMID: 19724100.
107. Cardozo BL, Zoetelief H, van Bekkum DW, Zurcher C, Hagenbeek A. Lung damage following bone marrow transplantation: I. The contribution of irradiation. International journal of radiation oncology, biology, physics. 1985;11(5):907-14. doi: 10.1016/0360-3016(85)90112-9. PubMed PMID: 3886609.
108. Niemierko A. Reporting and analyzing dose distributions: a concept of equivalent uniform dose. Med Phys. 1997;24(1):103-10. doi: 10.1118/1.598063. PubMed PMID: 9029544.
109. Chaikh A, Balosso J. The use of TCP based EUD to rank and compare lung radiotherapy plans: in-silico study to evaluate the correlation between TCP with physical quality indices. Translational lung cancer research. 2017;6(3):366-72. doi: 10.21037/tlcr.2017.04.07. PubMed PMID: 28713681; PubMed Central PMCID: PMC5504110.
110. Zuro D, Vagge S, Broggi S, Agostinelli S, Takahashi Y, Brooks J, et al. Multi-institutional evaluation of MVCT guided patient registration and dosimetric precision in total marrow irradiation: A global health initiative by the international consortium of total marrow irradiation. Radiotherapy and oncology : journal of the European Society for Therapeutic Radiology and Oncology. 2019;141:275-82. Epub 2019/08/20. doi: 10.1016/j.radonc.2019.07.010. PubMed PMID: 31421913.
111. Cowen D, Richaud P, Landriau S, Lagarde P, Mahon FX, Baudet JJ, et al. Radiobiological features of acute myeloblastic leukemia: comparison of self-renewal versus terminally differentiated populations. International journal of radiation oncology, biology, physics. 1994;30(5):1133-40. doi: 10.1016/0360-3016(94)90320-4. PubMed PMID: 7961022.
112. Gay HA, Niemierko A. A free program for calculating EUD-based NTCP and TCP in external beam radiotherapy. Physica medica : PM : an international journal devoted to the applications of physics to medicine and biology : official journal of the Italian Association of Biomedical Physics. 2007;23(3-4):115-25. doi: 10.1016/j.ejmp.2007.07.001. PubMed PMID: 17825595.
113. Safwat A, Nielsen OS, El-Badawy S, Overgaard J. Effect of radiation dose rate and cyclophosphamide on pulmonary toxicity after total body irradiation in a mouse model. International journal of radiation oncology, biology, physics. 1996;34(1):85-91. doi: 10.1016/0360-3016(95)02078-0. PubMed PMID: 12118569.
114. Emami B, Lyman J, Brown A, Coia L, Goitein M, Munzenrider JE, et al. Tolerance of normal tissue to therapeutic irradiation. International journal of radiation oncology, biology, physics. 1991;21(1):109-22. doi: 10.1016/0360-3016(91)90171-y. PubMed PMID: 2032882.
115. Zhou C, Jones B, Moustafa M, Schwager C, Bauer J, Yang B, et al. Quantitative assessment of radiation dose and fractionation effects on normal tissue by utilizing a novel lung fibrosis index model. Radiation oncology. 2017;12(1):172. doi: 10.1186/s13014-017-0912-y. PubMed PMID: 29116014; PubMed Central PMCID: PMC5678815.
116. Tait RC, Burnett AK, Robertson AG, McNee S, Riyami BM, Carter R, et al. Subclinical pulmonary function defects following autologous and allogeneic bone marrow transplantation: relationship

to total body irradiation and graft-versus-host disease. International journal of radiation oncology, biology, physics. 1991;20(6):1219-27. doi: 10.1016/0360-3016(91)90231-r. PubMed PMID: 2045296.
117. Down JD, Berman AJ, Warhol M, Van Dijken PJ, Ferrara JL, Yeap B, et al. Late tissue-specific toxicity of total body irradiation and busulfan in a murine bone marrow transplant model. International journal of radiation oncology, biology, physics. 1989;17(1):109-16. doi: 10.1016/0360-3016(89)90377-5. PubMed PMID: 2663795.
118. Hall EJ, Bedford JS. Dose Rate: Its Effect on the Survival of Hela Cells Irradiated with Gamma Rays. Radiat Res. 1964;22:305-15. PubMed PMID: 14168892.
119. Hall EJ, Brenner DJ. The dose-rate effect revisited: radiobiological considerations of importance in radiotherapy. International journal of radiation oncology, biology, physics. 1991;21(6):1403-14. doi: 10.1016/0360-3016(91)90314-t. PubMed PMID: 1938548.
120. Arentsen L, Yagi M, Takahashi Y, Bolan PJ, White M, Yee D, et al. Validation of marrow fat assessment using noninvasive imaging with histologic examination of human bone samples. Bone. 2015;72:118-22. doi: 10.1016/j.bone.2014.11.002. PubMed PMID: 25460181; PubMed Central PMCID: PMC4282942.
121. Magome T, Froelich J, Takahashi Y, Arentsen L, Holtan S, Verneris MR, et al. Evaluation of Functional Marrow Irradiation Based on Skeletal Marrow Composition Obtained Using Dual-Energy Computed Tomography. International journal of radiation oncology, biology, physics. 2016;96(3):679-87. doi: 10.1016/j.ijrobp.2016.06.2459. PubMed PMID: 27681765; PubMed Central PMCID: PMC5081224.
122. Tarbell NJ, Amato DA, Down JD, Mauch P, Hellman S. Fractionation and dose rate effects in mice: a model for bone marrow transplantation in man. International journal of radiation oncology, biology, physics. 1987;13(7):1065-9. doi: 10.1016/0360-3016(87)90046-0. PubMed PMID: 3298176.
123. FitzGerald TJ, McKenna M, Kase K, Daugherty C, Rothstein L, Greenberger JS. Effect of X-irradiation dose rate on the clonagenic survival of human and experimental animal hematopoietic tumor cell lines: evidence for heterogeneity. International journal of radiation oncology, biology, physics. 1986;12(1):69-73. doi: 10.1016/0360-3016(86)90417-7. PubMed PMID: 3943994.
124. Beyzadeoglu M, Oysul K, Dirican B, Arpaci F, Balkan A, Surenkok S, et al. Effect of dose-rate and lung dose in total body irradiation on interstitial pneumonitis after bone marrow transplantation. The Tohoku journal of experimental medicine. 2004;202(4):255-63. doi: 10.1620/tjem.202.255. PubMed PMID: 15109123.
125. Carruthers SA, Wallington MM. Total body irradiation and pneumonitis risk: a review of outcomes. British journal of cancer. 2004;90(11):2080-4. doi: 10.1038/sj.bjc.6601751. PubMed PMID: 15150598; PubMed Central PMCID: PMC2409505.
126. Hill GR, Crawford JM, Cooke KR, Brinson YS, Pan L, Ferrara JL. Total body irradiation and acute graft-versus-host disease: the role of gastrointestinal damage and inflammatory cytokines. Blood. 1997;90(8):3204-13. Epub 1997/10/24. PubMed PMID: 9376604.
127. Srideshikan SM, Brooks J, Zuro D, Kumar B, Sanchez J, Echavarria Parra L, et al. ImmunoPET, [(64)Cu]Cu-DOTA-Anti-CD33 PET-CT, Imaging of an AML Xenograft Model. Clinical cancer research : an official journal of the American Association for Cancer Research. 2019;25(24):7463-74. Epub 2019/09/25. doi: 10.1158/1078-0432.ccr-19-1106. PubMed PMID: 31548348; PubMed Central PMCID: PMCPMC6911626.
128. Magome T, Froelich J, Holtan SG, Takahashi Y, Verneris MR, Brown K, et al. Whole-Body Distribution of Leukemia and Functional Total Marrow Irradiation Based on FLT-PET and Dual-Energy CT. Molecular imaging. 2017;16:1536012117732203. Epub 2017/09/28. doi: 10.1177/1536012117732203. PubMed PMID: 28948859; PubMed Central PMCID: PMC5624344.
129. Martelli MF, Di Ianni M, Ruggeri L, Falzetti F, Carotti A, Terenzi A, et al. HLA-haploidentical transplantation with regulatory and conventional T-cell adoptive immunotherapy prevents acute leukemia relapse. Blood, The Journal of the American Society of Hematology. 2014;124(4):638-44.
130. Chao C, Bhatia S, Xu L, Cannavale KL, Wong FL, Huang PS, et al. Chronic Comorbidities Among Survivors of Adolescent and Young Adult Cancer. J Clin Oncol. 2020;38(27):3161-74. Epub 2020/07/17. doi: 10.1200/jco.20.00722. PubMed PMID: 32673152; PubMed Central PMCID: PMCPMC7499612.
131. Aristei C, Lancellotta V, Carotti A, Zucchetti C, Pierini A, Saldi S, et al. Total marrow/total lymphoid irradiation as conditioning for haploidentical hematopoietic stem cell transplantation in acute myeloid leukemia patients. International Journal of Radiation Oncology• Biology• Physics. 2018;102(3):e202-e3.

132. Bolanos-Meade J, Fuchs EJ, Luznik L, Lanzkron SM, Gamper CJ, Jones RJ, et al. HLA-haploidentical bone marrow transplantation with posttransplant cyclophosphamide expands the donor pool for patients with sickle cell disease. Blood. 2012;120(22):4285-91. Epub 2012/09/08. doi: 10.1182/blood-2012-07-438408. PubMed PMID: 22955919; PubMed Central PMCID: PMCPMC3507140.
133. Bolanos-Meade J, Cooke KR, Gamper CJ, Ali SA, Ambinder RF, Borrello IM, et al. Effect of increased dose of total body irradiation on graft failure associated with HLA-haploidentical transplantation in patients with severe haemoglobinopathies: a prospective clinical trial. The Lancet Haematology. 2019;6(4):e183-e93. Epub 2019/03/18. doi: 10.1016/s2352-3026(19)30031-6. PubMed PMID: 30878319; PubMed Central PMCID: PMCPMC6506220.
134. van Tuijn CFJ, Schimmel M, van Beers EJ, Nur E, Biemond BJ. Prospective evaluation of chronic organ damage in adult sickle cell patients: A seven-year follow-up study. Am J Hematol. 2017;92(10):E584-e90. Epub 2017/07/13. doi: 10.1002/ajh.24855. PubMed PMID: 28699283.